UNIVERSIDADE D
COIMBRA

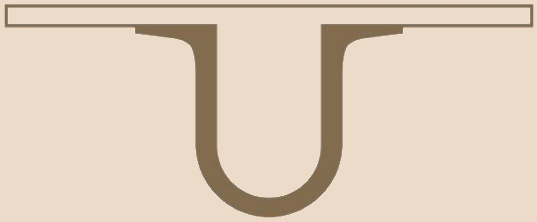

Pedro Miguel De Sá Cunha

COMPUTATIONAL INTELLIGENCE GENERATION OF SUBJECT-SPECIFIC KNEE AND HIP HEALTHY JOINT ANGLES REFERENCE CURVES

Dissertation presented to the University of Coimbra in fulfillment of the requirements necessary for obtain the M.Sc. degree in Electrical and Computer Engineering. Oriented by Professor Doctor António Paulo Mendes Breda Dias Coimbra, Professor Doctor João Paulo Morais Ferreira, Professor Doctor Manuel Marques Crisóstomo, presented to the Electrical and Computer Engineering department of the Faculty of Science and Technology of the University of Coimbra

September 2019

Acknowledgments

"*On the mountains of truth you can never climb in vain: either you will reach a point higher up today, or you will be training your powers so that you will be able to climb higher tomorrow.*"

Friedrich Nietzsche

Firstly, I would like to thank my tutors, Dr. Paulo Coimbra, Dr. João Ferreira, and Dr. Manuel Crisóstomo for the crucial guidance and wisdom necessary for the completion of this project.

To my parents, brother and girlfriend no words would ever be enough to repay the unconditional support, help, and encouragement shown throughout the execution of this work and years of study. Hence, I here express my warm and profound gratitude to them. Without them none of this would be possible.

I am profoundly grateful to all friends, teachers and people who by making part of my life, arouse an unending desire for knowledge and self-improvement that can't ever be dulled.

Resumo

Um procedimento comum na identificação de patologias da marcha é comparar as curvas dos ângulos das articulações do joelho e da anca de pacientes com curvas de referência, contruídas a partir de um grupo de indivíduos saudáveis. No entanto, estas curvas de referência genéricas são usualmente obtidas de uma amostra heterogénea de pessoas saudáveis e não possuem a especificidade necessária para obter resultados precisos. Por estas razões a geração de curvas de referência específicas tendo em conta características como o peso, altura, idade e velocidade de marcha resultarão numa melhor comparação e consequentemente num diagnostico mais preciso. Estas curvas de referência são de grande relevância em áreas como a medicina e a biomédica, na deteção de patologias e/ou reabilitação da marcha. Os métodos de Inteligência Computacional Backpropagation Neural Network (BNN) e Extreme Learning Machine (ELM) são capazes de modelar relações com grande precisão e como tal gerar curvas angulares de referência específicas baseadas em características como altura, peso, idade e velocidade da marcha. Os ciclogramas são curvas paramétricas constituídas pelas curvas de duas articulações, são de fácil visualização e permitem condensar informação pertinente das curvas dos ângulos das articulações do joelho e da anca. Podemos assim obter informação sobre o movimento conjunto das articulações e simetria da marcha do paciente. O principal objetivo do presente trabalho é identificar qual dos dois métodos de inteligência computacional, BNN e ELM, apresentam resultados mais precisos quando usados para gerar curvas de referência especificas do joelho e da anca tendo em conta altura, peso, idade e velocidade da marcha do paciente. No presente trabalho são geradas curvas de referência específicas para um paciente com paralisia cerebral e usadas na construção de ciclogramas para comparação e avaliação da marcha.

Palavras chave: *BNN, Ciclogramas, Curvas de Referência Específicas, ELM, Marcha Humana*.

Abstract

A common procedure used to identify abnormal gait is comparing an individual's knee and hip curves with healthy reference curves. These reference curves are usually obtained from a heterogeneous sample of healthy subjects and might lack the specificity required to obtain accurate results. It is why the generation of reference curves according to an individual's height, weight, age and gait speed should result in a better comparison and diagnosis. These reference profiles are useful in various fields such as biomedical engineering and medicine, for detection of gait pathologies and rehabilitation. Backpropagation Neural Network (BNN) and Extreme Learning Machine (ELM) are Computational Intelligence (CI) methods that can model relations accurately and thus generate subject-specific joint angle reference profiles based on a subject's height, weight, age and walking speed. Cyclograms are parametric curves composed by the curves of two different joints and present a great way of visualizing and condensate information. Furthermore, we can get insights of patient conjoint movement and symmetry. The main objective of the present study is to observe which of the two methods, BNN and ELM, present more accurate results when used to generate reference curve profiles based on subject height, weight, age and gait speed for the knee and hip joint angles. In the present work, subject-specific knee and hip healthy reference curves are generated for a Cerebral Palsy patient. These are used to construct several cyclograms, from which features of importance to patient gait evaluation, can be extracted.

Keywords: *BNN, Cyclograms, ELM, Human Gait, Subject-specific Profiles*.

Index

Figure Index

Table Index

Acronyms

ANN	Artificial Neural Network
BNN	Backpropagation Neural Network
CI	Computational Intelligence
CP	Cerebral Palsy
CS	Cross-Shear
DTW	Dynamic Time Warp
ELM	Extreme Learning Machine
GDI	Gait Deviation Index
GGI	Gillette Gait Index
GPS	Gait Profile Score
GRNN	Generalized Regression Neural Network
GUI	Graphical User Interface
IK	Inverse Kinematics
MoP	Metal-on-polyethylene
MSDs	Musculoskeletal Disorders
NI	Normalcy Index
PCA	Principal Component Analysis
PCs	Principal Components
PD	Parkinson Disease
RMS	Root Mean Square
ROM	Range of Movement
SI	Symmetry Index
SLFNN	Single Layer Feedforward Neural Network
SPO	Swarm Particle Optimization
THA	Total Hip Arthroplasty
VGRF	Vertical Ground Reaction Forces

1 Introduction

Upright walking is one of the most basic, fundamental human characteristics. The way we walk allows us to have mobility and live life as we know it. Nevertheless, some pathologies can arise at an early age, during or towards the end of our life, as a result of mental impairments, physical injuries and/or neurodegenerative diseases [1]–[3]. Gait disorders are associated to aging and become 60% more prevalent in subjects aged over 80 and 10% between 60 to 69 years old [4]. Nevertheless, abnormalities and injuries are recurrent and relevant in other ages. Common severe gait abnormalities result from neurological conditions, among them are hemiplegic cerebral palsy and Parkinson Disease (PD). Hemiplegic cerebral palsy is characterized by the paralysis of one side of the body. A great amount of the cases is resultant of infant strokes, affecting both children and elderly. PD, the second most common neurodegenerative disease, is recognized by its festinating gait and tremors, affecting vastly the elderly population [5], [6]. Another main cause of gait impairment are the Musculoskeletal Disorders (MSDs). According to the World Health Organization (WHO), such conditions are the second largest contributor to disability worldwide affecting joints, bones, muscles and multiple body systems. As a result of MSDs the subjects decrease physical activity which aggravates the state of the patient and explains this disease ubiquity in multi-morbidity [7]. Independently of its cause, gait pathologies can severely affect our quality of life [8], [9]. Even some non-severe gait abnormalities can impose physical limitations and decrease the level of independence. Briggs et al. showed the inherent relation between gait abnormalities and incidence of depression in a cohort of older people [10].

Gait analysis and assessment are used to detect abnormalities in human gait, propose a treatment and observe its effectiveness [11]. Gait analysis and assessment have been relying increasingly on motion capture technologies but is still predominantly based on visual assessment and on the clinical experience of the observer. This gait evaluation is carried out by physicians, biomedical engineers, neurologists, and other specialists who rely on their experience. Furthermore, this approach has the disadvantage of being qualitative and non-repeatable [12]. As previously mentioned a plethora of methods based on the quantitative measurements such as spatiotemporal, kinetic and kinematics have been emerging with motion capture technologies and have been used for the identification and classification of pathological gaits [2], [13]–[15]. This type of analysis shows to be more robust identifying gait abnormalities because it evaluates gait in a quantifiable and repeatable manner over time. Methods for gait analysis based on motion capture have shown to be capable of quantify risk of falls on elderly and predict neurodegenerative diseases before they manifest. Such predictions would be difficult to make, if not impossible, using conventional methods.

A common procedure for gait analysis used by physicians, is the data visualization and comparison, counter-posing the patients kinematic patterns with the control/normal values [16]. This type of approach is usually taken with joint angle curves because is a practical way for the clinician to easily observe deviation patterns. Nevertheless, the generation of the reference healthy joint angle curve is based on very distinct subjects, in such way that it can serve as a standard joint angle curve. Seen that subject specific features such as weight, height and age influence gait pattern, [17]–[20] this curves will lack the specificity necessary for an accurate comparison. Furthermore, such reference profile does not commonly take in consideration the gait speed, which is known to have great impact on joint angle's profile [21],[22]. Using control groups to generate normal joint curves might not always be viable since they need to be a cohort.

The application of Computational Intelligence (CI) methods in broader fields, including biomedical engineering, were made possible because of the fast growth of hardware computational power [23]. CI methods offer the capability of model complex systems such as the human body [24], having by now demonstrated to be capable of identifying and classifying gait pathologies [25], [26].

The main objective of the present work is to assess pros and cons of two CI methods, Backpropagation Neural Network (BNN) and Extreme Learning Machine (ELM), when used to generate specific reference curve profiles for the knee and hip joint angles, based on subject height, weight, age and gait speed. ELM was chosen due to its simplicity and fast results when compared to commonly used regression algorithms, while BNN is the most commonly used CI method [27]. Support Vector Machine (SVM) was not included in the comparison, since results showed to be slower in such applications [14], [28], [29].

2 State of the art

2.1 Human Gait

Walking is an inherent ability to most Humans. Gait is of such trivial semblance that many underestimates the underlying complexity of it. A complete gait cycle can be subdivided in two main phases: Stance and Swing. Stance phase comprises the hell strike to toe-off section of the gait cycle making around 60% of the gait cycle in a healthy subject. Stance phase itself can be subdivided into initial contact (heel strike), loading response, mid-stance, terminal stance and pre-swing. The swing phase which accounts for the remaining 40 % of the gait cycle, is subdivided into initial swing (toe-off), mid-swing (tibia vertical) and terminal swing, terminated by the heel striking the ground [30]. The beginning of the gait cycle is marked by heel strike and the ending with the subsequent heel strike of the same foot. Figure 1 presents, the beginning heel strike, mid-

stance, toe-off, mid-swing, and ending heel strike, respectively. Angle convention is displayed in Figure 2.

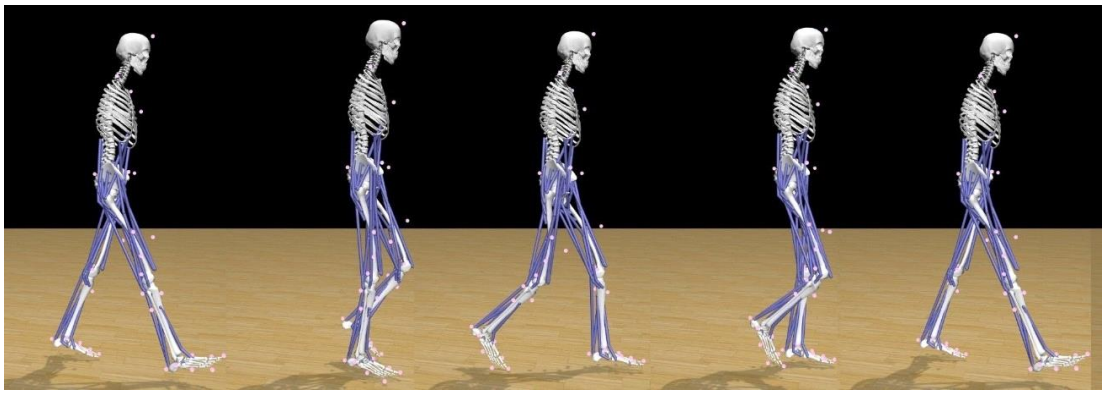

Figure 1. Human Gait Cycle.

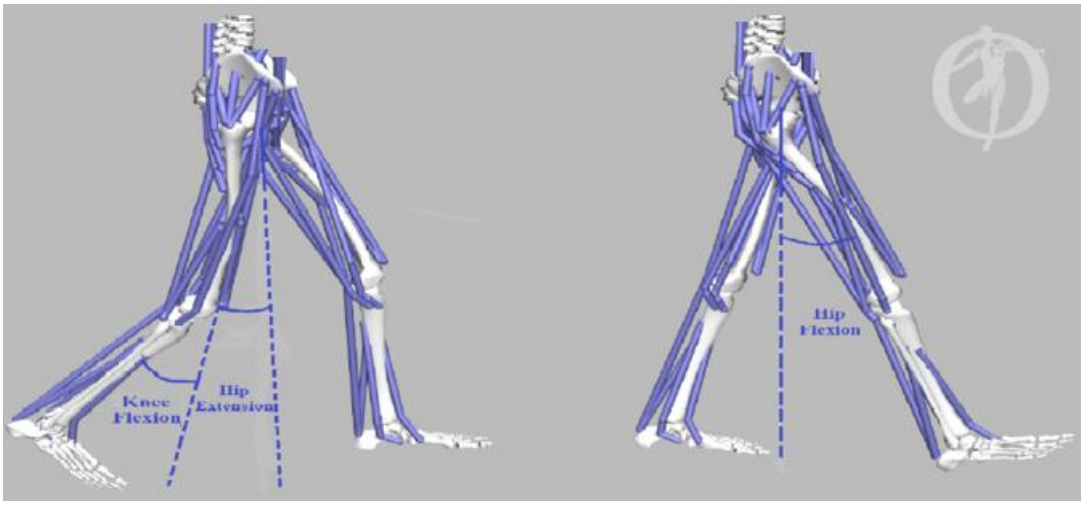

Figure 2. Angle Convention.

Vision systems are emerging and offer data of great value for physicians to detect deviation from normality and asses patient's recovery. Furthermore, the use of this methodology has as objective facilitate physicians and gait experts in analyzing and assessing patients gait and treatments effectiveness. Kinematic data obtained from vision systems is commonly used to evaluate gait. The use of kinetic data obtained through force plates or electromyography is also very used for the effect, being these technologies recurrently used to complement each other. It should be noticed that these technologies require preprocessing of the data before being applied in gait evaluation.

2.1.1 Clinical Gait Analysis

Data acquisition by itself would not be of great value without being of liable interpretation and able to originate concise conclusions. Although computational intelligence has nowadays a strong presence in gait analysis a great part of the work done in this area is still done using statistical methods. Bellow the most commonly used approaches in gait analysis and assessment will be presented.

Moandal et. al [31] made a precise evaluation of distinct l-DOPA-sensitive and l-DOPA-resistant gait profiles of PD patients in a cross-sectional study. l-DOPA is a commonly used drug in PD patients that has shown to improve bradykinesia and rigidity in mild stages of the disease. Spatiotemporal parameters were obtained using a long electronic walkway containing pressure sensors embedded in a carpet. The patients were evaluated in their OFF and ON phases of l-DOPA medication. The gait parameters of PD patients were compared to age and gender-matched healthy participants using independent sample t-test for parametric data and Mann–Whitney U test for nonparametric data.

A commonly applied statistical analysis technique is the Principal Components Analysis (PCA). This multivariate technique permits data dimensionality reduction by projecting it in a lower dimension. The eigenvectors and eigenvalues of the covariance matrix are used for this effect. These represent, respectively, the direction where most variance occurred, and the amount of variation associated to each eigenvector. This way PCA is able to reduce dimensionality conserving the maximum amount of variance [32]. Peng et. al [33] used PCA for analyses of variations in the distribution of sliding distance and Cross-Shear (CS) ratio among Total Hip Arthroplasty (THA) patients. Metal-on-Polyethylene (MoP) is the most commonly used bearing surface in THA. The microscopic particles produced by friction between articulating surfaces is a major concern. PCA has been used for analyses of variations in the distribution of sliding distance or CS ratio. It has also detected two principal components (PCs) of the sliding distance that together contribute to 94.8% of the total variation and four PCs that together contribute to 86% of the total variation of the cross-shear ratio.

The effects of orthopedic walking boots were tested by Gulgin et. al [34] using 3D gait analysis vision system (Vicon, Oxford, UK) and two force Advanced Mechanical Technology plates (AMTI Inc., Watertown, MA). Peak values for kinematic and kinetic variables were tested for significance ($p < 0.05$) across conditions using one-way repeated ANOVA with the Bonferoni procedure. Followed-up paired t-tests were performed to test from right to left differences. Significant differences in joint angles and moments were found when using orthopedic walking boots.

When comparing PD subjects with age-matched controls Castagna et. al [35] used the Mann-Whitney U test, while the Wilcoxon test was used for comparison of the *ON* and *OFF* states in PD patients. The study was based in spatiotemporal, kinematic, and kinetic gait parameters. Furthermore, Wald test was used to correct for possible influence of different gait speeds between the *OFF* and the *ON* state. The nonparametric correlation analysis, Spearman Rank test, was used to correlate instrumented gait measures with demographic and clinical data.

The application of CI methods in the medical area dates to the early 1970s [36]. Up to these days a plethora of applications of methods have been applied, solving problems with medical interest. Regardless of a lot of questions still lacking answer, such haven't stopped the fast proliferation of CI's.

CI's are capable of generating healthy joint angle curves based on subject specific parameters. Luu et al. [37] used anthropometric data and gait parameters of subjects to feed a Generalized Regression Neural Network (GRNN) which was trained to target Fourier coefficients of joint angle's waveform. Posteriorly, inverse Fourier transform can be applied to obtain the lower limb joint angle waveform.

H. Alaskar et al. [38] used signals from force sensitive resistors of a continuous walk of subjects with PD and healthy subjects. Multilayer neural network, trained with backpropagation using the Levenberg-Marquardt optimization, was used to classify the presence of PD. Classification was performed using statistical and frequency features from data, clinical information (age, height, gait speed, weight and gender), and both previous type of features, resulting in the classification accuracies of 64%, 81% and 91% respectively.

Rani M. P. et al. [14] used ELM in multicategory classification of gait abnormalities in children, obtaining accuracies of 97.98% when using PCA and 99.21% accuracy using T-Test.

Utomo C. P. et al. [39] showed that ELM performed better as a generalization classifier model, when compared with BNN in diagnosing breast cancer. ELM resulted in sensitivity, specificity and accuracy of 94.8%, 97.4%, 96.4% respectively. Meanwhile, BNN showed considerably lower sensitivity (84.3%) and accuracy (92.1%) and slightly higher specificity (98%).

Ma X. et al. [27] used Swarm Particle Optimization (SPO) to choose input bias, weights and number of neurons of hidden layer and trained the ELM algorithm to identify falls out of low-cost Kinect depth camera. This strategy, denominated by the author as variable-length SPO, was able to achieve up to 86.83% fall detection accuracy.

Blażkiewicz et. al [40] trained an Artificial Neural Network (ANN) to simulate the sagittal plane angle of the knee when the hip and ankle sagittal plane angular curve are given as input. The hip and ankle angles were increasingly reduced by 20%. The results for the several combinations of the two joints angles reductions were compared with targets using the correlation

coefficient. The lowest correlation obtained was of 0.70. A quasi-Newton optimization method was used for the learning.

In Kutilek et. al [41] a neural network was trained with segments of a cyclogram in order to predict the missing values of the parametric curve. The neural network received as inputs the angles of the cyclogram segment, the angular accelerations of the joint, and subject's weight and age. This procedure was done for knee-hip and knee-ankle cyclograms. In a subsequent article Kutilek et. al [42] displayed bilateral synchronized cyclograms properties in gait symmetry evaluation. Similar procedures were used by Sobral et. al [43] with Vertical Ground Reaction Forces (VGRF). A synchronized bilateral cyclogram was created for the VGRF and a Symmetry Index (SI) was obtained through percentual relative difference of the slope that fits the cyclogram and the ideal symmetrical gait gradient (45º Degrees).

Some of the most relevant and accepted measurements in clinical gait analysis for gait normality deviation are based on kinematic and spatial temporal measurements. Nevertheless, gait symmetry measurements [42]–[44] and indexes as GDI-Kinetic [45], based on kinetic data, are also commonly used. The Normalcy Index (NI) or Gillette Gait Index (GGI) stand out as being one of the oldest most accepted indices in gait assessment. It serves as a measure of the severity and normality deviation of the patient pathological gait. Furthermore, GGI allows the analysis of treatments effectiveness by quantifying the changes on the pathological gait. This index makes use of the PCA applied to 16 independent discrete variables [46]. From the 16 variables, 3 are temporal-spatial parameters, (time of toe off, walking speed, cadence) and 13 are kinematic variables (mean pelvic tilt, range of pelvic tilt, mean pelvic rotation, minimum hip flexion, range of hip flexion, peak hip abduction in swing, mean hip rotation in stance, knee flexion of initial contact, time of peak knee flexion, range of knee flexion, peak of ankle dorsiflexion in stance, peak of ankle dorsiflexion in swing, mean foot progression angle). GGI has been extensively used and validated in both clinical and scientific environments, predominantly in children with CP. Despite the common use in children with CP, GGI has also been used for other pathologies such as PD, Multiple sclerosis and strokes. One of the limitations of this index it's the lack of evidence in the choice of the 16 discrete variables as being the most adequate ones. As well as GGI, indexes such Gait Deviation Index (GDI), and Gait Profile Score (GPS) make use of kinematic variables such as the pelvis and hip in the three planes and the knee and ankle in the sagittal plane as well as the foot progression.

Symmetry is a main feature of gait. Asymmetric gait is correlated with gait pathologies [47], [48] and an evaluation of it can bring great insights of the patient state and situation. Despite the importance, up to date there is no standard for SI, neither for the calculation nor the parameters to use [44]. Some commonly used approaches are based on bilateral cyclograms, i.e., graphs of dominant vs non-dominant limb. In the present work, bilateral cyclograms will be used for

symmetry evaluation, as well as some features of hip vs knee cyclograms will be used to show the potential of such approaches.

2.1.1.1 Gait Analysis using Cyclograms

Cyclograms, commonly referred as angle-angle graphs, are far from being a novelty in gait analysis and assessment. This type of parametric curve is generated by plotting the angle of different markers, such as hip and knee, or the same marker for both dominant and non-dominant limb, being the former named bilateral cyclogram. By creating such plots, we can get clear insights of the gait symmetry and quality. The generated geometries of such plots enable us to distinguish a normal from an abnormal gait pattern and condenses information such as range of motion that might be important for gait evaluation [46]. Cyclograms fall in one of two categories regarding their construction: synchronized and unsynchronized. In order to understand such differentiation, it should be noticed that in a gait cycle the angles of both limbs are nearly complementary, i.e., legs move approximately out-of-phase. In order to synchronize a cyclogram the moment of heel strike for both limbs need to be found before plot one gait cycle against the other. In a synchronized cyclogram the angle of the right knee, when the right heel touches the ground, corresponds to the angle of the left knee when left heel touches the ground. An example of a synchronized knee cyclogram is presented in Figure 3 at left and unsynchronized knee cyclogram at right.

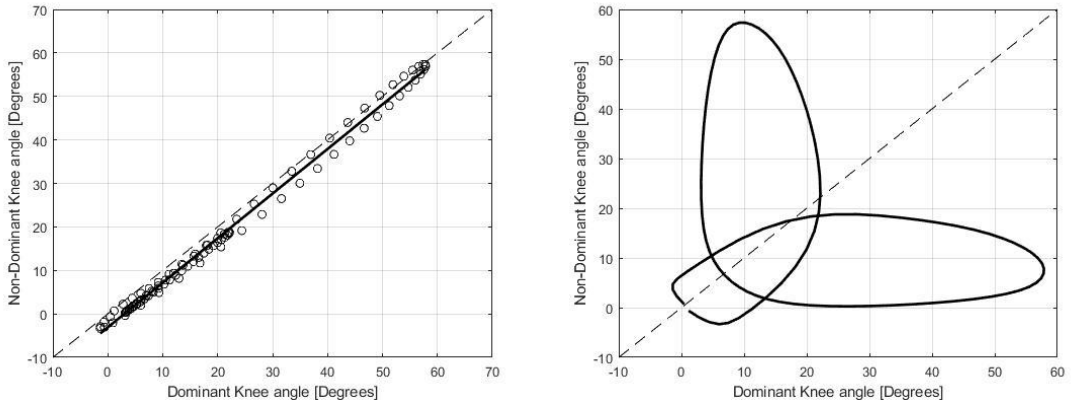

Figure 3. Synchronized and Unsynchronized knee cyclograms.

Both bilateral and regular cyclograms present features of interest for gait analysis and assessment. The most relevant aspects are presented below along with the insights they can provide in a subject's gait evaluation.

A) Area: The enclosed area of the cyclogram is a direct repercussion of the range of movement of both joints in analysis. This feature encodes all possible pair of angles during the gait cycle. When evaluated in sections the diagram permits the identification of phases where conjoint movements happen, and area is naturally more expressive.

B) Perimeter: While the area reflects changes based on conjoint movement, increasing one joint angle solely might keep the area unchanged while drastically modifying the cyclogram. The perimeter of the cyclogram, would nevertheless, reflect this change making the evaluation based on this characteristic more robust. This property permits to identify uncoordinated movements in the gait.

C) $\boldsymbol{P_A = \frac{Perimeter}{\sqrt{Area}}}$**:** This dimensionless ratio presents a relation with the cyclogram shape, although the value by itself cannot ensure a unique specific shape. If the diagram shape remains the same P_A will remain the same even if the area changes drastically [49]–[51].

The previous referred characteristics are of interest mainly for the hip vs knee cyclograms since the conjoint movement of two different markers is of interest. Nevertheless, when using bilateral cyclograms the focus is shifted for a symmetry evaluation and the perimeter and P_A ratio are no longer of such importance. With bilateral cyclograms the deviation from both limbs to the perfect symmetry line (45º degrees line) can be noticed at several moments of the gait cycle. This comparison is done since the expected cyclogram of a perfectly symmetrical gait would be a line that crosses the origin of unitary slope and zero area, being the angular deviation and area of these cyclograms the main features of such evaluation.

A different approach for symmetry evaluation can be done with unsynchronized cyclograms. Besides bringing a different visualization, perhaps more intuitive of the patient limb conjoint movement, this approach takes into account the phase shift occurring between joints of both limbs [44]. Both methodologies based on cyclograms used in this work are explained with greater detail in section 3.2.1.

2.2 Computational Intelligence

Computers can perform a task by being programmed to respond in a given way for a certain scenario. It is the programmer's responsibility to provide the necessary instruction for the proper functioning of the application over several situations. However, common tasks that humans perform, depend on previous learning experience, and many of them are too complex for a programmer to provide a specific set of instructions that could, for every case, result in a satisfactory outcome. CI general interest is the solving of problems that require intelligence. Such intelligence resembles human and animal intelligence. It is many times used to englobe Artificial

Neural Networks, Fuzzy Logic Systems, Genetic Algorithms, and many others used interchangeably with Artificial Intelligence. Although boundaries are not yet defined CI presents itself as a broader field majorly concerned in problems such as object recognition, signal analysis, discovery of structures in data, simple associations and control [52], [53]. CI provides applications, the capability to adapt, i.e., improve with experience and extract patterns, sometimes too complex for a human to try to model

There are three major common categorizations of CI methods named as supervised, unsupervised and reinforcement learning (see Figure 5). The difference between these groups rely in the way they learn and how information is provided to the algorithm for the learning procedure.

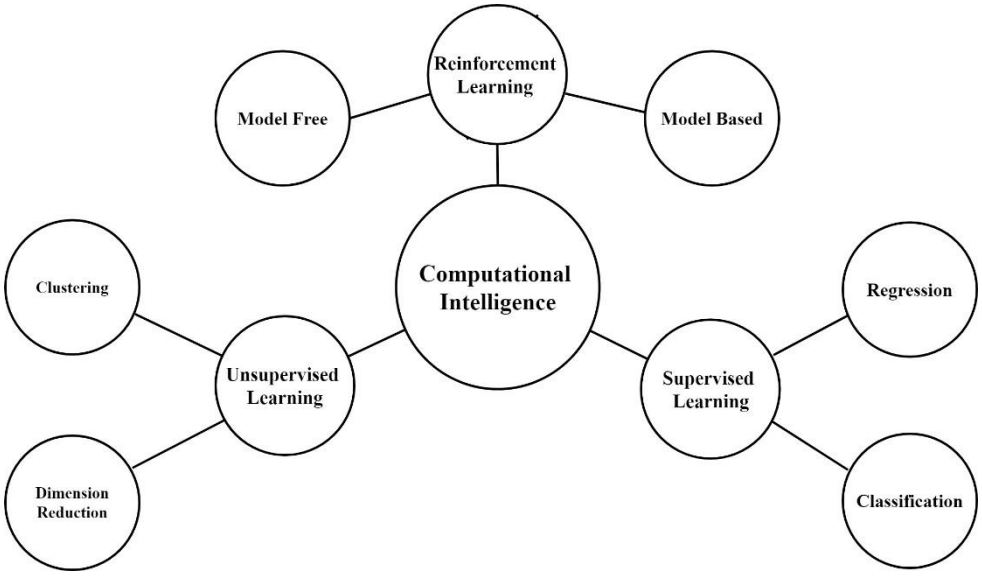

Figure 4. Computational Intelligence Categories.

In supervised learning, feature identification is done by an expert that also provides to the algorithm the correct outcome for the several training cases. This information can be a label or a continuous value. Being referred as a classification and regression respectively. In the classification supervised case, the algorithm could be trained to identify one of many categories, while for the regression a concrete continuous value is intended. Independently of being a regression or classification problem, an algorithm fits the supervised category when the given the expected output, also commonly referred as target, is given.

The unsupervised learning is mostly used to cluster data, but no data labelling is used. There is no given information and it is up to the algorithm to find a structure or a feature out of data. Such algorithms can also be used for dimension reduction. Typically, the algorithm would identify common features between two groups and discard them since they bring no value in distinguishing them.

Reinforcement learning is based on a system of punishment and reward where the algorithm adapts its own behavior based on the consequences of his actions. The algorithm is like an agent whose actions are based on the feedback state given by the environment. Model-based algorithm is able to model the problem accurately and understand the decision making behind it, whereas model-free approach is not to learn the model and simply find a good policy on the run.

2.2.1 Neural Networks

Artificial neural networks are by now the reference algorithm inside the CI field. Due to its appealing apparent simplicity and high performances obtained in the immensities of applications and fields, neural networks became commonly used in our nowadays technology background. Several types of networks exist. Each one with its strength and purpose, among them the most common are the feed-forward, convolutional and recurrent neural network.

Feed-Forward neural networks can be either fully connected or sparse. They contain an input, output and hidden layer and flow occurs from the input to the output layer. These algorithms use backpropagation to update the bias and weights of the several layers and in this way train the network. For this reason, the term backpropagation neural network is recurrently used in the literature and will also be applied in the present work.

2.2.1.1 Backpropagation Neural Network

An artificial neural network is composed of several layers containing multiple neurons per layer. Deep Neural Network (DNN) comprises a more extended number of hidden layers and neurons. This type of network can learn more complex data relations than BNNs. However, they require higher processing power and memory [54]. Nevertheless, single hidden layer neural networks, with sufficient hidden units, can attain high accuracies and model complex problems [55], [56].

Every neuron has a weight, bias and chosen activation function. The weights and bias are used to calculate a weighted sum of the input of the neuron, which is then applied to the activation function, like shown in Figure.6.

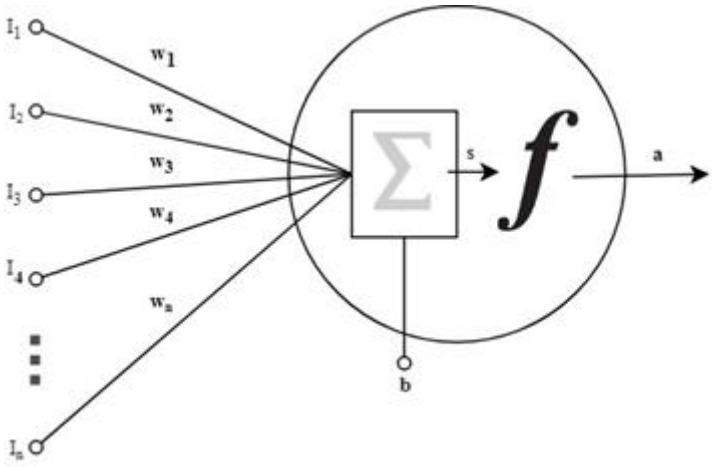

Figure 5. Neuron structure.

For the one neuron example, $w_1 \ldots w_n$ represent the weights of the several connections, $I_1 \ldots I_n$ represent the inputs of the neuron, b is the neuron bias or threshold value, f is the activation function, a the value output from the neuron that will be feedforward to the several neurons of the next layer, and s is the input of the activation function of the neuron and will then be given by:

$$s = \sum_{i=1}^{n} \omega_i I_i + b \tag{1}$$

It should be noticed that a layer usually contains several neurons and in order to distinguish among the connections the $w_{i,j}$ notation will be used further in this work. Where i represents the connection to ith neuron and j the source.

The hidden layer neurons have commonly non-linear activation functions while input and output are usually chosen linear ($f(n) = n$), as is the case. The hidden layer activation function used in the present work is the sigmoid function, defined as:

$$f(n) = \sigma(n) = \frac{1}{1 + e^{-n}} \tag{2}$$

The Sigmoid curve resembles an ‘s’ shape and is presented in Figure.6.

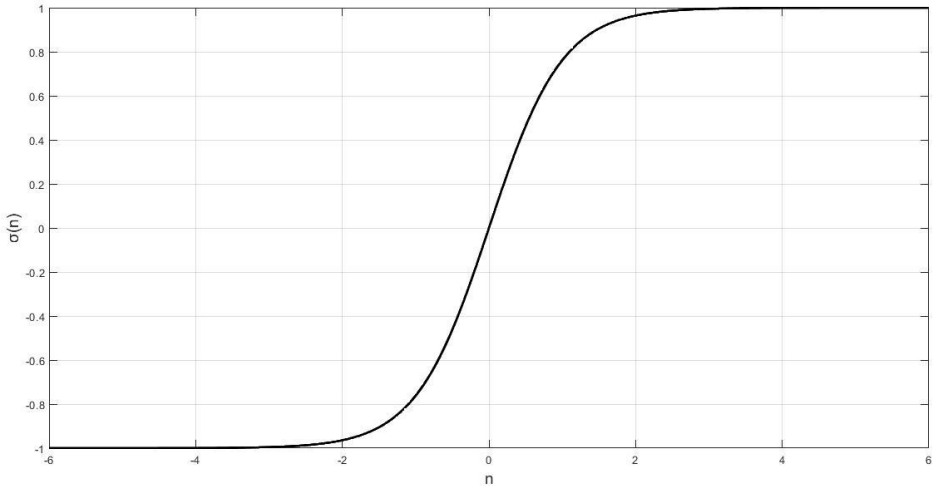

Figure.6 Sigmoid Function.

As mentioned before, previous layer output will be feedforward as input to the next layer, except for the input and the output layer. The former receives external inputs while the latter one outputs the prediction results. For a *M* layers neural network, it can be written:

$$a^{m+1} = \sigma^{m+1}(W^{m+1}a^m + b^{m+1}) \text{ for } m = 0, 1, \dots, M - 1 \quad (3)$$

Where W is matrix of weights of the layer and σ^{m+1} the activation function of the next layer. Initially the weights, as well as the bias of the neurons are attributed randomly. The error of every iteration is used to change the weights for the next iteration in trying to improve results. This procedure is referred as backpropagation and consists of a gradient descendent optimization algorithm [57], [58]. In this case, the backpropagation algorithm used for networks was the Marquardt-Levenberg.

If the supervised learning paradigm consists of given an input, finding the weights and bias for which prediction best matches real target, a cost function can be defined for the purpose. This will serve of indication of whether such goal is being achieved. In the present work this cost function is simply the Mean Squared Error of the prediction to the target and can be defined as:

$$\mathrm{F(x)} = \frac{1}{\mathrm{n}}\sum_{\mathrm{I=1}}^{\mathrm{n}} (\mathrm{t_I} - \mathrm{a_I})^2 \quad (4)$$

Being x the vector containing the network weights and bias, n the overall number of training inputs and t_I and a_I, respectively, the target and network prediction for the I input.

Considering the MSE for the *k* iteration and extending the previous formula for a network with several outputs.

$$\hat{F}(x) = \big(t(k) - a(k)\big)^T \big(t(k) - a(k)\big) \tag{5}$$

In steepest descent algorithm the weights and bias of the *m* layer are updated in the following manner:

$$w_{i,j}{}^m(k+1) = w_{i,j}{}^m(k) - \eta \frac{\partial \hat{F}}{\partial w_{i,j}{}^m} \tag{6}$$

$$b_i{}^m(k+1) = b_i{}^m(k) - \eta \frac{\partial \hat{F}}{\partial b_i{}^m} \tag{7}$$

The *i,j* represent the rows and columns of the weights matrix and correspond to the weight of the connection between the *jth* neuron of the current layer (*m*) to the *ith* neuron of the next layer (*m+1*). The learning rate is here denoted as η.

The Marquardt-Levenberg algorithm applied in the present work, differs, in certain situations, from previously shown steepest descent algorithm and approximates the Newton's method.

Rewriting eq. (5) in a matrixial form for a several output network:

$$\mathrm{F(x)} = \frac{1}{\mathrm{n}} \sum_{\mathrm{I}=1}^{\mathrm{n}} (\mathrm{t_I} - \mathrm{a_I})^T (\mathrm{t_I} - \mathrm{a_I}) \tag{8}$$

Or,

$$\mathrm{F(x)} = \frac{1}{\mathrm{n}} \sum_{\mathrm{I}=1}^{\mathrm{n}} e^T e \tag{9}$$

To minimize such function with respect to the weights and bias vector x, Newtons method would be computed in the following manner:

$$\nabla(\mathrm{x}) = [-\nabla^2 F(x)]^{-1} \nabla F(x) \tag{10}$$

Being $\nabla^2 F(x)$ and $\nabla F(x)$ the Hessian matrix and the gradient of the cost function, respectively.

Considering $\mathrm{F(x)}$ the sum of all squares function, i.e.:

$$\mathrm{F(x)} = \frac{1}{\mathrm{n}}\sum_{\mathrm{I=1}}^{\mathrm{n}} e_I^2(x) \tag{11}$$

The gradient and the Hessian matrix can be defined as:

$$\nabla F(x) = \mathrm{J^T}(x)\mathrm{e}(x) \tag{12}$$

$$\nabla^2 F(x) = \mathrm{J^T}(x)\mathrm{J}(x) + S(x) \tag{13}$$

Where $\mathrm{J}(x)$ is the Jacobian matrix given by:

$$\mathrm{J}(x) = \begin{bmatrix} \frac{\partial e_1(x)}{\partial x_1} & \frac{\partial e_1(x)}{\partial x_2} & \cdots & \frac{\partial e_1(x)}{\partial x_n} \\ \frac{\partial e_2(x)}{\partial x_1} & \frac{\partial e_2(x)}{\partial x_2} & \cdots & \frac{\partial e_2(x)}{\partial x_n} \\ \vdots & \vdots & \ddots & \vdots \\ \frac{\partial e_n(x)}{\partial x_1} & \frac{\partial e_n(x)}{\partial x_2} & \cdots & \frac{\partial e_n(x)}{\partial x_n} \end{bmatrix} \tag{14}$$

And

$$S(x) = \sum_{\mathrm{I=1}}^{\mathrm{n}} e_I(x)\nabla^2 e_I(x) \tag{15}$$

The update using Marquardt-Levenberg is then:

$$\nabla\mathrm{(x)} = [J(x)^T J(x) + \mu\mathrm{I}]^{-1} J(x)^T e(x) \tag{16}$$

Where *I* is the entity matrix and should not be confused with *I* used previously as subscript. It can be noted that for large values of μ the algorithm becomes the steepest descendent while for small values it becomes the Gauss-Newton.

2.2.1.2 ELM

ELM algorithm consists of a Single-hidden Layer Feedforward Network (SLFN), where the input layer neurons, weights, and bias are attributed randomly and kept fixed. After, the SLFN can be considered as a simple linear system. This algorithm uses the least squares method and the

Moore-Penrose generalized inverse matrix to obtain the weights between the hidden layer and the output (see Eq.(25)). These two concepts will be briefly explained ahead, as well as their use in the ELM algorithm.

It can be stated that for a given matrix A of order $n \times m$, a unique Moore–Penrose generalized inverse of A, $H^{\dagger}$, of order $m \times n$, satisfies the following properties:

$$AH^{\dagger}A = A \tag{17}$$

$$H^{\dagger}AH^{\dagger} = H^{\dagger} \tag{18}$$

$$\left(AH^{\dagger}\right)^{T} = AH^{\dagger} \tag{19}$$

$$\left(H^{\dagger}A\right)^{T} = H^{\dagger}A \tag{20}$$

The great advantage of the Moore-Penrose generalized matrix is the ability to solve easily a linear system $Ax = y$ where $A \epsilon R^{m \times n}$ and $y \epsilon R^{m \times n}$, for the case where A may be singular and not even squared [59].

For N distinct samples (x_i, y_i) where $x_i = [x_{i1}, x_{i2}, \dots, x_{in}]^T \epsilon R^n$ and $y_i = [y_{i1}, y_{i2}, \dots, y_{in}]^T \epsilon R^m$, considering an SLFN with h hidden neurons so that, $h \leq N$. A standard SLFN can be describe mathematically as:

$$\sum_{\mathrm{i}=1}^{\mathrm{h}} \omega_{oi} f\left(\omega_i . x_j + b_i\right) = a_j, \ j = 1, \dots, N \tag{21}$$

Where ω_i is the vector of weights connecting the *ith* hidden layer neuron to the several inputs and ω_{oi} is the vector of weights connecting the hidden layer to the output, b_i is the bias of the ith hidden neuron and $\omega_i . x_j$ the inner product of ω_i and x .

The N cases can then be grouped in a hidden layer output matrix, H.

$$\mathrm{H} = \begin{bmatrix} \mathrm{f}(\omega_1 . \mathrm{x}_1 + \mathrm{b}_1) & \mathrm{f}(\omega_2 . \mathrm{x}_1 + \mathrm{b}_2) & \cdots & \mathrm{f}(\omega_\mathrm{h} . \mathrm{x}_1 + \mathrm{b}_\mathrm{h}) \\ \mathrm{f}(\omega_1 . \mathrm{x}_2 + \mathrm{b}_1) & \mathrm{f}(\omega_2 . \mathrm{x}_2 + \mathrm{b}_2) & \cdots & \mathrm{f}(\omega_\mathrm{h} . \mathrm{x}_2 + \mathrm{b}_\mathrm{h}) \\ \vdots & \vdots & \ddots & \vdots \\ \mathrm{f}(\omega_1 . \mathrm{x}_\mathrm{N} + \mathrm{b}_1) & \mathrm{f}(\omega_2 . \mathrm{x}_\mathrm{N} + \mathrm{b}_2) & \cdots & \mathrm{f}(\omega_\mathrm{h} . \mathrm{x}_\mathrm{N} + \mathrm{b}_\mathrm{h}) \end{bmatrix} \tag{22}$$

And then rewrite the equation as:

$$H\omega = T \tag{23}$$

Where

$$\omega_o = \begin{bmatrix} {\omega_{o1}}^T \\ {\omega_{o2}}^T \\ \vdots \\ {\omega_{oh}}^T \end{bmatrix} \text{ and } T = \begin{bmatrix} {t_1}^T \\ {t_2}^T \\ \vdots \\ {t_N}^T \end{bmatrix} \tag{24}$$

The Minimum Least-Squares method can now be applied to the previous linear system.

$$\hat{\omega}_o = H^{\dagger}T \tag{25}$$

With $\hat{\omega}_o$ being the smallest least square solution of the linear system, $H\omega_o = T$, and represents the output weights. T represent the targets and $H^{\dagger}$the Moore-Penrose generalized inverse of the hidden layer output matrix [59].

ELM can be used for classification and regression achieving the smallest training error, being a clear advantage when comparing with back-propagation algorithms that stop at local minimums. Besides its simplicity, applications in several areas have shown that ELM is much faster when compared with gradient based algorithms and produces good generalization [59]–[62].

3 Methodology

This work is oriented to the application in the clinical area in order to facilitate physicians and gait experts in analyzing and assessing patients gait and treatments effectiveness. Among the several factors that difficult the proliferation of such systems for the clinical area are the cost of the systems, the need of expertise for setting these systems, being able to understand their results, and the difficulty to obtain or generate patient-oriented normative data. In order to culminate some of the enunciated roadblocks, the approaches presented make use of knee and hip sagittal angles that can be obtained by every vision system that possesses two cameras. Furthermore, CIs are used to generate subject-specific joint angle reference profiles and cyclograms are generated to facilitate visualization and obtain quantifiable measurements of interest to gait analysis. We can view this work as two steps:

1) **Creation and training of the CI methods to generate subject-specific joint angle profiles→** BNN and ELM algorithms are compared when generating subject-specific joint angle reference profiles for the knee and hip. Furthermore, these methods are compared to standard reference curves present in the literature.

2) **Gait analysis and assessment of subject with cerebral palsy using cyclograms and the CI generated curves→** Knee and hip angle curves are generated using a CI method according to the characteristics and trial speed of a cerebral palsy patient. These healthy specific reference curves of the patient are then used to generate a cyclogram that can be compared to the real patient cyclogram. In other words, CI is used to generate angle curves as if the patient was healthy. This curve and its features permit a comparison and assessment of a patient gait.

3.1 CI Considerations

The present work used a public dataset from the Laboratory of Biomechanics and Motor Control at the Federal University of ABC, Brazil [63]. The dataset contains pre-processed lower-body kinematic data of 42 healthy volunteers. It was one of the most complete datasets found with such characteristics. To train the BNN and ELM, the knee and hip angles of the male's subjects (young and old), on over-ground walking at three different speeds (slow, comfortable and fast) were used as targets. This data consists, for the young group, of a target matrix composed by 42 columns (14 young male's × 3 strides) and 101 rows (marker angles normalized to 101 points) and for the old group of 30 columns (10 male's x 3 strides) by 101 rows. The inputs fed to the CI's were age, height, weight and speed of the subject trial, all normalized between 0 and 1. The target amplitudes of the joint angles were also normalized for improved results in CI methods and a reliable comparison.

The accuracy was measured in terms of Mean Squared Error (MSE) for both algorithms which consists in the average squared error between the BNN output and the target. Since both network output and target are angular curves, MSE will be the mean of the angular distance between BNN results and targets and is given by:

$$MSE = \frac{1}{N}\sum_{i=1}^{N}\left(\frac{1}{101}\sum_{k=0}^{100}\left(\theta_{t,k} - \theta_{CI,k}\right)^2\right) \quad (26)$$

Where N is the number of train/test samples and $\theta_{t,k}$ and $\theta_{CI,k}$ are respectively, the target value and the CI output at $k\%$ of the gait cycle.

Table 1 shows the data division used for the two methods and normalization range used.

Table 1. Data Normalization Ranges.

Method	Input Range	Target Range		Accuracy	Data Division		
		Knee	Hip	Measurement	Train (%)	Test (%)	Validation (%)
BNN	[0,1]	[0,1]	[-1,1]	MSE	70	25	5
ELM	[0,1]	[0,1]	[-1,1]	MSE	75	25	-

Different networks were generated for dominant/non-dominant limb and young/old group for both knee and hip angles.

The CI's were implemented using Matlab in a computer with an Intel i7-6700, 2.90 GHz processor and 16,0 GB RAM. The Deep Learning Toolbox™ was used for the neural networks and a self-written script for ELM.

The criteria for validation was based on generating realistic accurate and smooth curves for two subjects out of the training set. For this reason, and because of the lack of data, ELM validation data was assigned to the training set. In the BNN case the validation data percentage was kept at the lowest permitted by the Deep Learning Toolbox™.

For BNN, the number of hidden units was iterated from 4 to 50 and each network topology was trained and tested 3 times. For ELM, the number of hidden neurons were iterated from 4 to 50 and trained/tested 50 times.

The activation function of the hidden layer neurons used in both algorithms was the sigmoid and the output activation functions were kept linear.

Figure 7 shows the structure of the single hidden layer neural network were θ_0 to θ_{100} represent the angle values from 0% to 100% of the gait cycle. An example of an joint curve is represented in Figure 9.

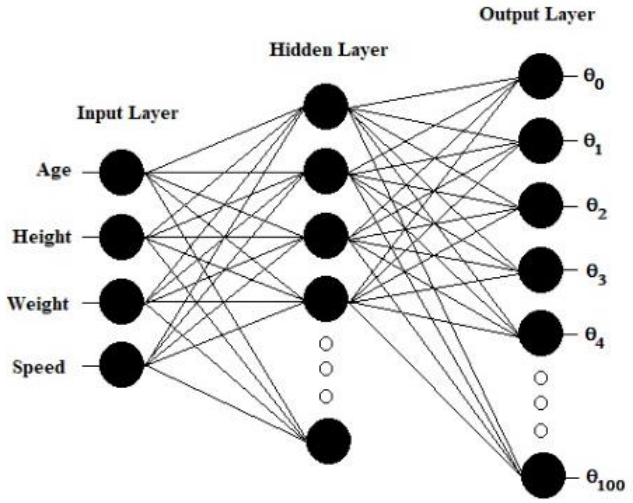

Figure 7. Single hidden layer neural network structure.

3.2 Cerebral Palsy gait assessment using cyclograms

Data from a cerebral palsy patient with 23 years was obtained and made publicly available by authors [64]. This data contains anthropometric data of the patient, EMG and force plate data, and kinematic data. This kinematic file contains the displacement of 15 markers of the patient lower body in the x, y and z coordinates. It was recorded using Vicon motion analysis system (Vicon Motion Systems, Inc., Lake Forest, CA) at 50Hz for the duration of 1.50 seconds. All files types given were only compatible with Gaitlab software, which is currently deprecated. OpenSim was the chosen software for this purpose. Using excel and Matlab, the kinematic file (.kin) was read and organized into a matrix. The columns contained the several markers coordinates and the lines correspond to the value of that coordinate for the respective time of sampling. Every marker displacement data was filtered using an 4ºth order zero-phase-shift Butterworth filter. The cut-off frequency was 6 Hz and was chosen by residual analysis [65] rather than Fourier Transform because such analysis is as reliable due to the presuppose that the filters and their cut-off frequency are ideal [66]. Residual analysis explanation and results are presented further ahead in the present chapter. Once again, Excel was used to create a trace (.trc) file required to visualize the experiment in OpenSim software. OpenSim GUI rotation method was used to match data orientation with OpenSim coordinate system. Furthermore, OpenSim was used to solve the Inverse Kinematics (IK) problem that yield both knee and hip angles. This open source software contains several human body models that can be scaled using anthropometric information and

markers displacement data emulating the recorded patient trial. Detailed information about OpenSim software and procedures previously mentioned can be found in Section 3.2.3.

Force plate information was used to extract heel strike and toe off moments for both limbs and is displayed in Figure 8.

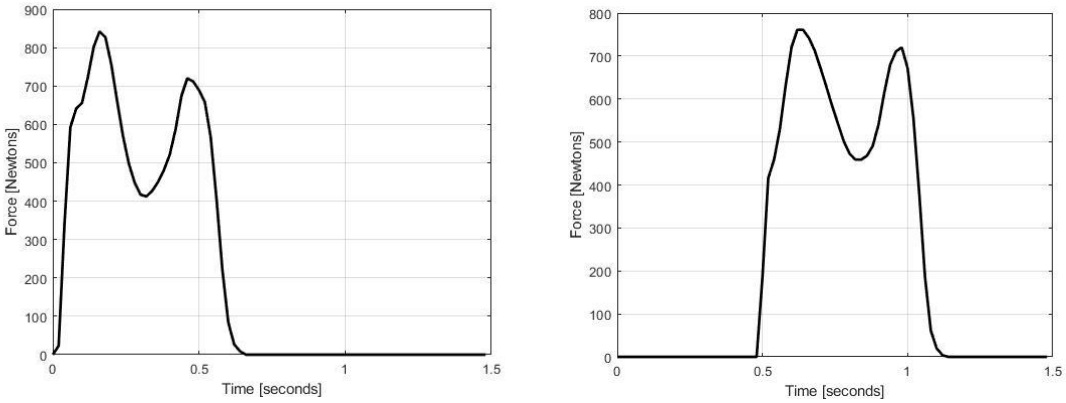

Figure 8. Force Plate Information.

The available force plate information contains only one step of each limb, since a complete gait cycle encloses the moment of heel strike up to the subsequent moment of the same limb heel strike. OpenSim was used to visually obtain such events times and confirm force plate information.

With these events times, the knee and hip angles were reduced to one gait cycle and interpolated to 100% in order to allow comparisons. Results of the right hip and knee angles for the patient are presented in Figure 9.

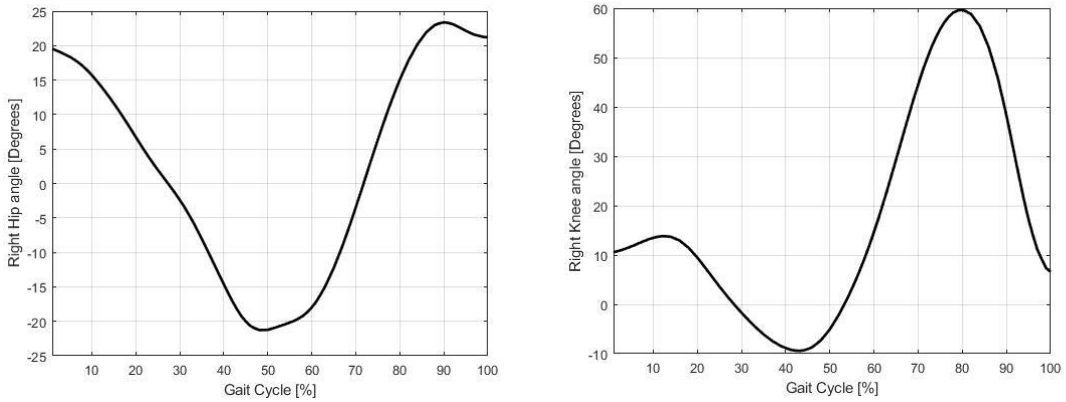

Figure 9. Right hip and knee angle curve for cerebral palsy patient.

The authors from where displacement data was obtained, present an entire chapter dedicated to this patient [64], from the medical history to the kinematic and kinetic evaluation. Even though, only the right limb curves are presented. A very close match was obtained for knee angle curve when comparing the obtained with presented results. Nevertheless, right hip angle curve results needed an offset correction. It is common for authors to consider neutral position as a pelvic tilt of 12º to 13º degrees, nevertheless, OpenSim model Gait2354 considers 0º degrees pelvic tilt with respect to the ground. This will then reflect in an offset in hip flexion that needs to be corrected. A 10º degrees offset was added to the hip flexion. This is a typical tilt value and is recommended in OpenSim user manual when comparing curves [67].

3.2.1 Symmetry Analysis Using Bilateral Cyclograms

When using bilateral cyclograms the synchronized plot of left against right limb were created and the enclosed area of the cyclograms was calculated. Furthermore, a linear regression is used to fit the coordinates x and y that correspond, respectively, to the right and left limb angles for the several moments that constitute the gait cycle. Considering $(x_0, y_0), (x_1, y_1), \ldots, (x_{100}, y_{100})$ the pair of angles of right and left limb for the entire gait cycle and using linear regression relation present in Equation (27).

$$y = \beta_1 x + \beta_0 + \varepsilon \tag{27}$$

Where β_0 is the value for the y axis interception, β_1 is the slope and ε the error term. The following system of equation is created and can be solved in Matlab.

$$\begin{bmatrix} y_0 \\ y_1 \\ \vdots \\ y_{100} \end{bmatrix} = \begin{bmatrix} 1 & x_0 \\ 1 & x_1 \\ \vdots & \vdots \\ 1 & x_{100} \end{bmatrix} \begin{bmatrix} \beta_0 \\ \beta_1 \end{bmatrix} \tag{28}$$

The slope of the regression is then used to calculate the inclination angle θ.

$$tan(\beta) = \theta \tag{29}$$

The angular distance θ_{45} is obtain by subtracting θ by 45º to yield the cyclogram deviation from the perfect symmetry. More precisely $\theta_{45º} = |45º - \theta|$. For an ideal gait the area of such cyclogram would be 0 $degrees^2$ and the line would align perfectly with the 45º degrees line.

Nevertheless, such results are not possible even for perfectly healthy subjects. SI was, in a first approach, calculated as the ratio of ROM of the non-dominant limb to ROM of the dominant limb.

$$SI = \frac{ROM_{Non-Dominant}}{ROM_{Dominant}} \tag{30}$$

In order to improve the analysis, the same methodology was applied to the ELM generated curves, permitting this way a comparison of the patient results to what would be expected if such subject was healthy (ELM generated curve). The difference of the SI of patient and the SI of ELM is represented and calculated as:

$$\Delta SI = SI_{Patient} - SI_{ELM} \tag{31}$$

The same comparison philosophy was applied to the unsynchronized cyclograms. Similar methodology to the one used in [44] was applied to make a more accurate alternative of the symmetry evaluation with unsynchronized cyclograms.

The unsynchronized cyclograms are built by plotting right versus left limb like shown in Figure 10.

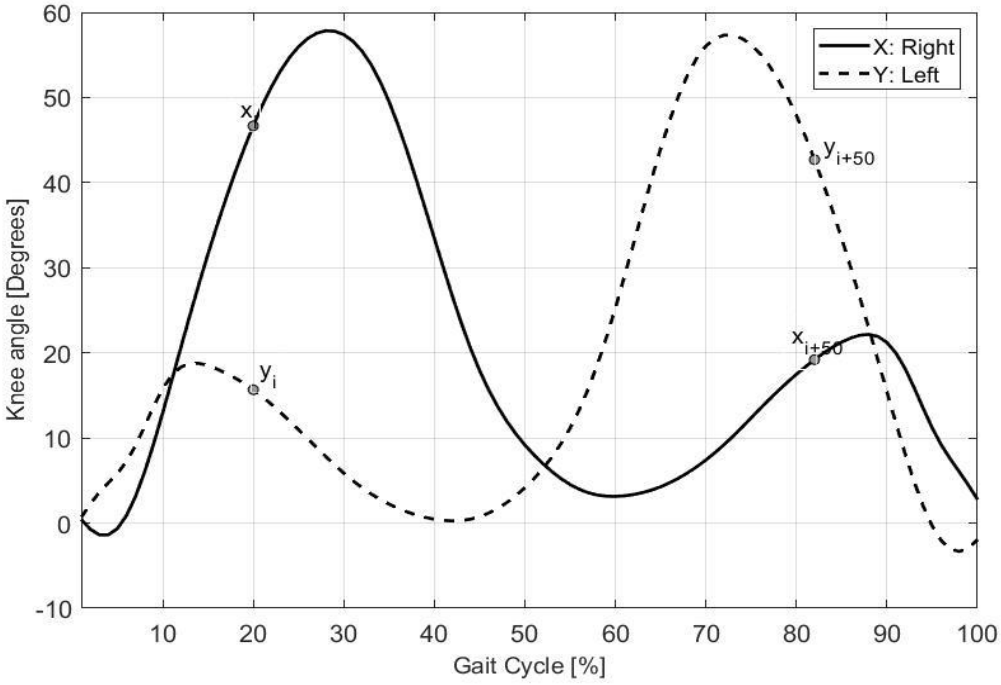

Figure 10. Right and left knee unsynchronized angle curve.

For each pair moment of the gait cycle, i.e., (x_i, y_i) for the right limb and (x_{i+50}, y_{i+50}) for the left limb (see Figure 10 and Figure 11), the Euclidean distance to 45º degrees line is calculated (c_j *and* d_j respectively). Furthermore, the ratio of the distance from (x_i, y_i) and (x_{i+50}, y_{i+50}) to the origin (a_j *and* b_j respectively) is taken into account yielding the symmetry equation for both hip and knee marker.

$$S_{Marker} = \frac{\sum_{j=0}^{50} \left(\frac{a_j}{b_j} + \frac{c_j}{d_j} \right)}{N} \tag{32}$$

Where *j* represent every instance of the gait cycle and *N* is 101, the total number of instances.

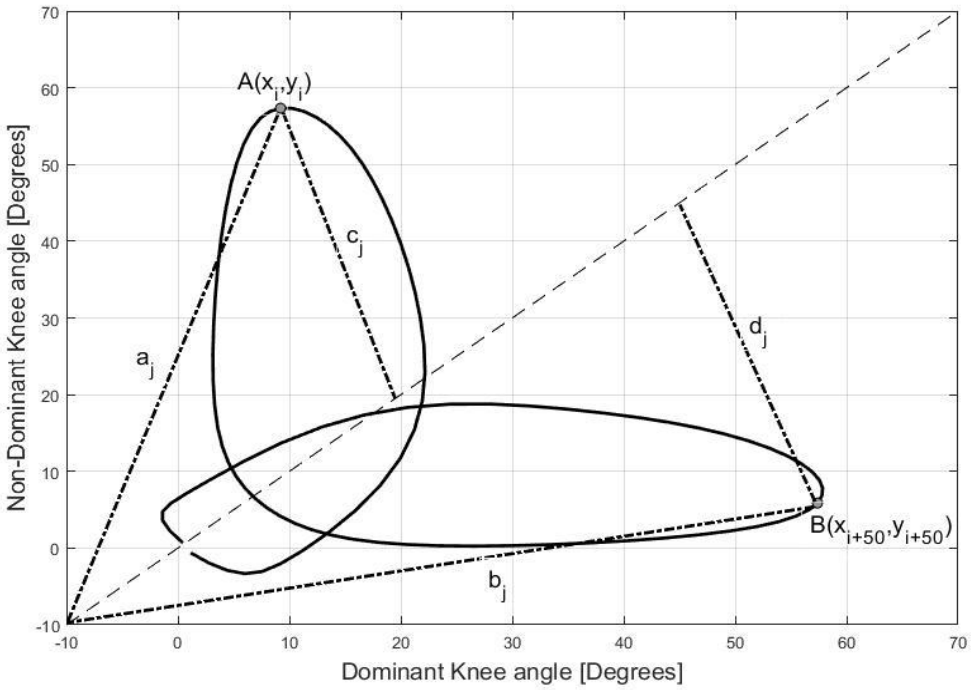

Figure 11. Ratios for SI calculation using unsynchronized bilateral cyclogram.

Overall symmetry was visualized in polar coordinate system [44]. The adapted equation used to calculate the overall symmetry is the following.

$$S = \frac{\sqrt{S_{Knee} + S_{Hip}}}{1.41} \tag{33}$$

Where 1.41 is the normalization factor so that *S* is a value between 0 and 1. When using SI together with unsynchronized cyclograms in such way, it can be considered the phase shift occurring between joints of both limbs. Furthermore, this approach is sensitive to variations of the right and left limb range of motion because of the point-by-point comparison. Later, when analyzing the results, it becomes clear the importance of such characteristics in making an accurate evaluation of the patient symmetry.

3.2.2 Residual Analysis and Experimental Data Filtering

As previously mentioned, residual analysis was made in order to choose cutoff frequency of the 4ºth order zero-phase-shift Butterworth filter (see Section 3.2). In this section the procedures associated to residual analysis and the cerebral palsy patient raw data filtering are described. Such analysis presents an alternative to the commonly used spectral analysis in frequency domain using Fourier transform. Typically, in spectral analysis, cutoff frequency is chosen for the frequency at which 95 to 99% of the signal power lays underneath. Whereas in residual analysis the cutoff frequency is chosen based on the residual, i.e., the difference of the filtered data at several frequencies to the original unfiltered data. In this way, there is a better understanding and control of the trade-off between the signal attenuation and the noise allowed to pass. Furthermore, spectral analysis cutoff frequency selection assumes that the filter is ideal and has infinitely sharp cutoff [65], [66].

The procedure for the residual analysis consists in creating the residual of the marker and fitting a linear regression to the linear segment of the residual. Using the y-interception value of the regression, a horizontal line with same value is traced (Y line). The election cutoff frequency is made by identifying the frequency for which the Y line intersects the residual, for an equal amount of signal distortion and amount of noise to pass. An example of the residual for the Great Trochanter right marker is presented in Figure 12.

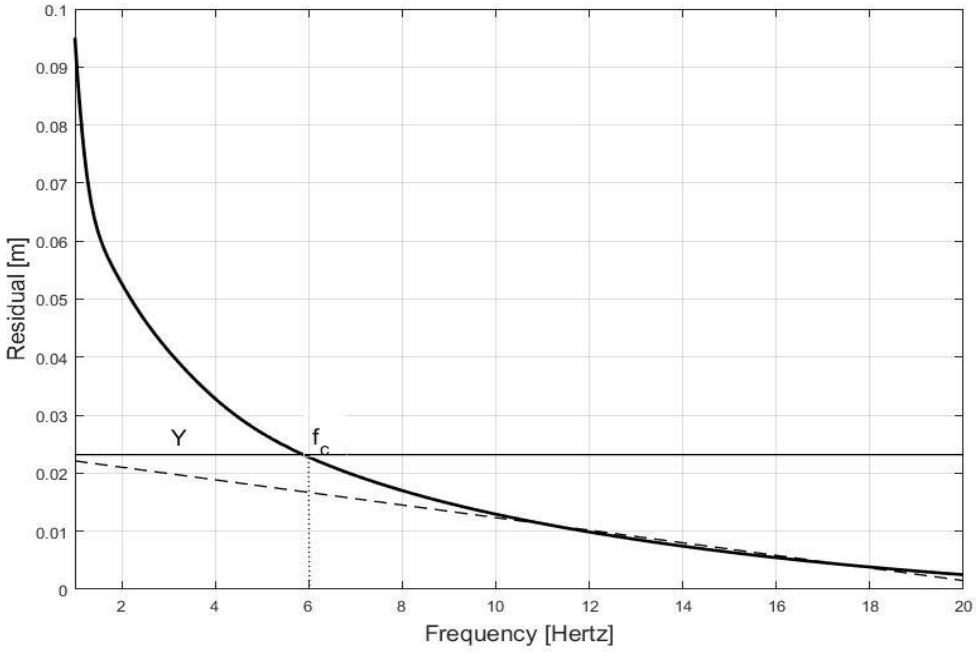

Figure 12. Residual Analysis for Great Trochanter Right Marker.

This procedure can be better understood by thinking in the case where signal is only constituted by random noise. The residual of random noise is a straight line with negative slope with an intersection for 0 Hz and the horizontal axis intersection at the Nyquist frequency ($\frac{f_s}{2}$). Our best estimation of the noise its then the regression to the linear section of the residual and the y-intersection of the fitted regression line is the Root Mean Square (RMS) of the noise. Due to the signal distortion of the filtering, when data is constituted of signal plus noise, the residual magnitude will surpass the linear line for increasingly smaller cutoff frequencies [65], [66].

For the data filtering a 2th order Butterworth filter was used. Nevertheless, data is again filtered in the inverse direction to correct the phase lag introduced by the filter. It creates in this way a 4th order zero-phase-shift Butterworth filter.

3.2.3 OpenSim Scaling and Inverse Kinematics

OpenSim is an open source software developed by the National Institute of Health (NIH) from Stanford University. Among many features, it permits to analyze musculoskeletal models and gait simulations. It was used in this work to visualize and obtain knee and hip angles for the subject diagnosed with CP. For this purpose, two main steps involving the software were taken. The first was scaling a generic musculoskeletal model. Starting with the generic musculoskeletal model available, one can scale in order to match subject-specific anthropometric characteristics.

The second step was to use the scaled model together with experimental marker positions and solve the inverse kinematic problem in order to obtain knee and hip sagittal angles.

3.2.3.1 Scaling

In order to scale the generic model, the marker placement used by Fukuchi et. al [63] had to be replicated in the model. These markers, named virtual markers, are used to compare the model body segment size to the subject body segments extracted out of the experimental marker position of the trial in order to determine the scaling factors.

3.2.3.2 Inverse Kinematics

OpenSim IK tool uses the experimental data of the subject trial at each frame and computes the set of joint angles that yield the closest result to the experimental data. For this purpose, OpenSim solves the weighted least squares optimization problem to minimize the distance between the virtual marker and the experimental markers. For every frame of the trial the IK problem is solved, originating a vector of joint angles that minimizes the weighted sum for all markers (see eq.(34)).

$$\min_{q}\left[\sum_{i\,\in\, markers}\omega_i\left\|x_i^{exp}-x_i(q)\right\|^2\right] \tag{34}$$

Where q is the vector of joint angles, x_i^{exp} the position of the experimental marker i, $x_i(q)$ the position of the corresponding virtual marker, and ω_i is the weight attributed to the error of the *ith* marker and represents the importance of that marker error for the least squares problem. In the present work such weights were kept to 1 for all markers, which can be seen as giving the same level of concern for all marker errors in the problem. The IK accuracy is shown in the message window of OpenSim for every frame and serves as good guidance for the adjustment of the virtual marker, since the misplacement of these, in relation to experimental data will result in bigger joint angle error [68].

4 Data Description

The used dataset is composed of raw and processed lower-body kinematic data of 24 young adults and 18 old adults obtained through a motion-capture system with 12 cameras (Raptor-4; Motion Analysis Corporation, Santa Rosa, CA, USA) on 10 meter over-ground walk and using a dual-belt, instrumented treadmill (FIT; Bertec, Columbus, OH, USA).

Overground trials were made at 3 different speeds: self-selected comfortable speed, slow (30% slower) and fast (30% faster). Each participant's comfortable speed was determined during the 10-meter over-ground walking familiarization period. The 45 healthy subjects' characteristics (age, height, weight) are displayed in Table 2 and further detailed in Annex A. The Young/Old group division was done by dataset authors and comprises the ranges of 27-37 and 50-84 years old.

Table 2. Dataset characteristics.

Age Group	Gender	Number of Persons	Mean Age	Mean Height (cm)	Mean Weight (kg)
Old	F	8	60.1	154.8	61.09
Old	M	10	64.8	167.4	71.58
Young	F	10	25.9	162.9	58.92
Young	M	14	28.8	176.9	75.17

Figure 13 shows the anatomical markers used for obtaining kinematic data.

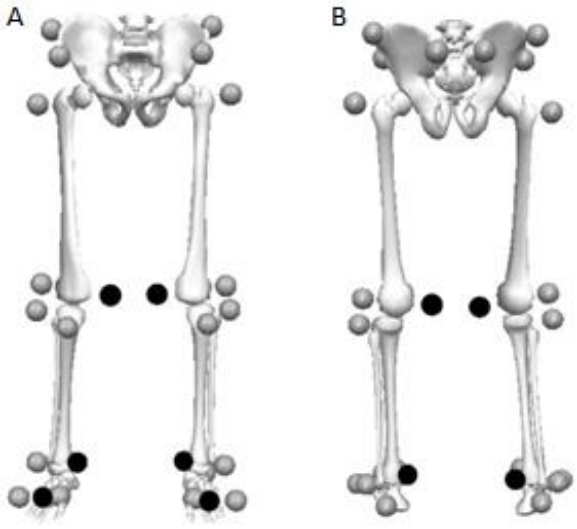

Figure 13. Markers protocol. Anterior (A) and posterior (B) views. Markers shown black are removed during the trial recording. Image from [63].

5 Results and Discussion

5.1 Computational Intelligence

The main objective of the present study was to observe which of the two Computational Intelligence (CI) methods, BNN and ELM, present more accurate results when used to generate reference curve profiles based on subject height, weight, age, and gait speed for the knee and hip joint angles. The best accuracy results for the BNN and ELM are shown in Table 3 and Table 4, for young and old man dominant limb and young and old man non-dominant limb respectively.

Table 3. CI's best accuracies for young and old men dominant limb.

Limb	Method	Age Group	Train Accuracy MSE	Test Accuracy MSE	Validation Accuracy MSE
Knee	BNN	Young	**0.0001**	**0.0022**	0.0009
		Old	**0.0010**	**0.0022**	0.0027
	ELM	Young	0.0036	0.0061	-
		Old	0.0045	0.0089	-
Hip	BNN	Young	**0.0015**	**0.0069**	0.0023
		Old	**0.0025**	0.0784	0.0027
	ELM	Young	0.0463	0.0215	-
		Old	0.0330	**0.0349**	-

Table 4. CI's best accuracies for young and old men non-dominant limb.

Limb	Method	Age Group	Train Accuracy MSE	Test Accuracy MSE	Validation Accuracy MSE
Knee	BNN	Young	**0.00004**	**0.0010**	0.0006
		Old	**0.00008**	**0.0011**	0.0013
	ELM	Young	0.0037	0.0078	-
		Old	0.0034	0.0094	-
Hip	BNN	Young	**0.0010**	**0.0021**	0.0029
		Old	**0.0002**	**0.0030**	0.0038
	ELM	Young	0.0394	0.0330	-
		Old	0.0378	0.0544	-

BNN's test results proved to be better for dominant knee and hip networks except for the old group hip, where ELM performed slightly better. BNN presented better results in every situation for non-dominant hip and knee. Nevertheless, in both dominant and non-dominant cases, similar test performances were obtained. Difference in accuracies were never superior to 0.0084, except for the hip results from young subjects. ELM test accuracies were lower for the young and old hip case in both dominant and non-dominant limbs.

BNN high accuracies also happened to decrease for the hip of the old dominant limb but not for the non-dominant. By contrasting such results, it was hypothesized that such decrease might be related to the misrepresentation of the test subjects' characteristics and trial speed in the

training set. Furthermore, the reduction of hidden units for the BNN in hip old dominant case should have had compensated generalization accuracy (see Table 5), but such did not happen. This could be attributed to the lack of data for certain characteristics in the training set, i.e., since data division is randomly assigned it might choose fewer cases representative of a certain trial speed or a conjugation of subjects' characteristics and speed. This will translate in a predominance of the existing cases and a poorer modeling capacity. For every case, an independent network is generated with randomly attributed weights and bias, making it difficult to analyze such discrepancies, since these might be the cause of the modeling capability of the network [69]. The same procedures were performed for the treadmill data and accuracies results can be found in Annex C.

Table 5 presents the number of hidden neurons that resulted in the best accuracies for several BNNs and ELMs.

Table 5. CI's topologies for best test accuracies

Limb	Age Group	Dominant/Non-Dominant	Nº Hidden Neurons	
			BNN	ELM
Knee	Young	D	16	5
		ND	17	4
	Old	D	8	4
		ND	20	6
Hip	Young	D	20	4
		ND	11	4
	Old	D	9	4
		ND	15	4

For every BNN and ELM created, two subjects outside of the training and validation set were used to test CI's capabilities of generating accurate and smooth subject-adapted joint angle curves. The selection of these two subjects for every network was based on the overall difference (largest and smallest) of his characteristics (age, height, weight, gait speed) and the mean characteristics of the subjects used for training. The test subject that showed to have lower difference between his characteristics and the train subjects mean characteristics will be referred as the "closer to the mean subject" and the subject who showed greater difference, the "further from mean subject".

Table 6 contains the MSE of the joint angle curves generated by the CI's to the real test subject joint angle curve for the subject closer to the mean and

Table 7 contains the MSE for the subject further from the mean.

Table 6. Error for test subject further from subject's mean characteristics.

Network Information			Subject Input Information				CI's MSE	
Limb	Age Group	D/ND	Age	Height (cm)	Weight (kg)	Gait Speed (m/s)	BNN	ELM
Knee	Young	D	30	171.0	95.4	1.27	0.0053	**0.0028**
		ND	24	184.0	61.1	1.65	**0.0004**	0.0028
	Old	D	55	165.6	79.1	0.89	0.0044	**0.0006**
		ND	84	155.5	66.4	1.00	0.0009	**0.0008**
Hip	Young	D	36	182.5	64.0	1.34	0.027	**0.0021**
		ND	37	155.0	69.6	0.69	**0.001**	0.031
	Old	D	84	155.5	66.4	1.00	**0.0009**	0.043
		ND	84	155.5	66.4	1.00	**0.002**	0.003

Table 7. Error for test subject closer from subject's mean characteristics.

Network Information			Subject Input Information				CI's MSE	
Limb	Age Group	D/ND	Age	Height (cm)	Weight (kg)	Gait Speed (m/s)	BNN	ELM
Knee	Young	D	33	179.3	75.9	0.96	**0.0003**	0.003
		ND	33	179.3	75.9	0.96	**0.0007**	0.002
	Old	D	68	167.0	70.3	1.30	0.029	**0.005**
		ND	68	167.0	70.3	1.30	**0.0001**	0.0016
Hip	Young	D	31	172.9	77.9	1.48	**0.001**	0.014
		ND	33	179.3	75.9	0.68	**0.005**	0.024
	Old	D	68	167.0	70.3	1.58	**0.001**	0.023
		ND	62	164.5	70.5	0.78	**0.005**	0.094

Figure 14 and Figure 15 shows the real and CI generated flexion/extension joint angle curves for dominant knee and hip of the test subject further from the mean. Figure 16 and Figure 17 present the same data for the test subject closer to the mean.

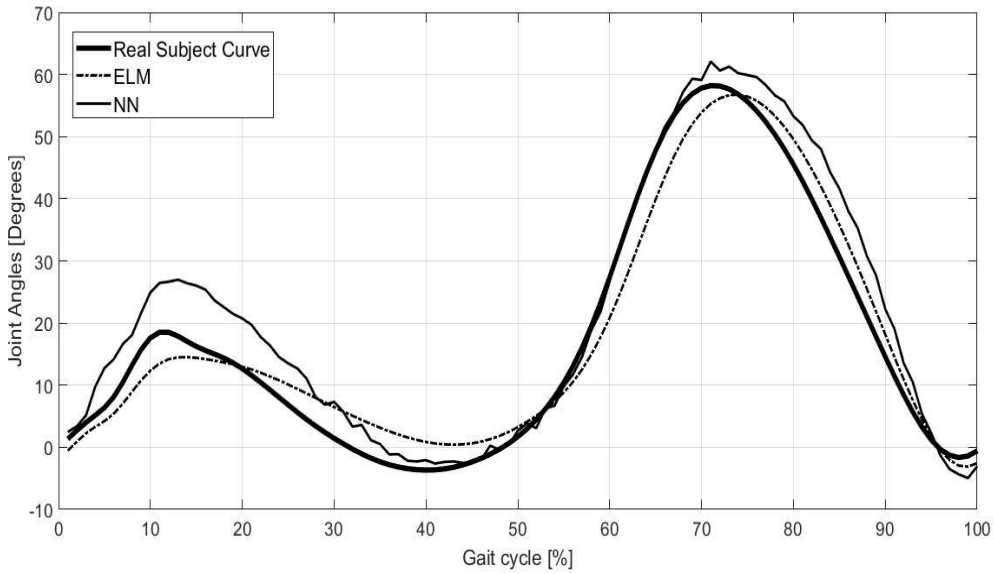

Figure 14. Dominant joint angle knee curves (generated and real) for young subject further from the mean.

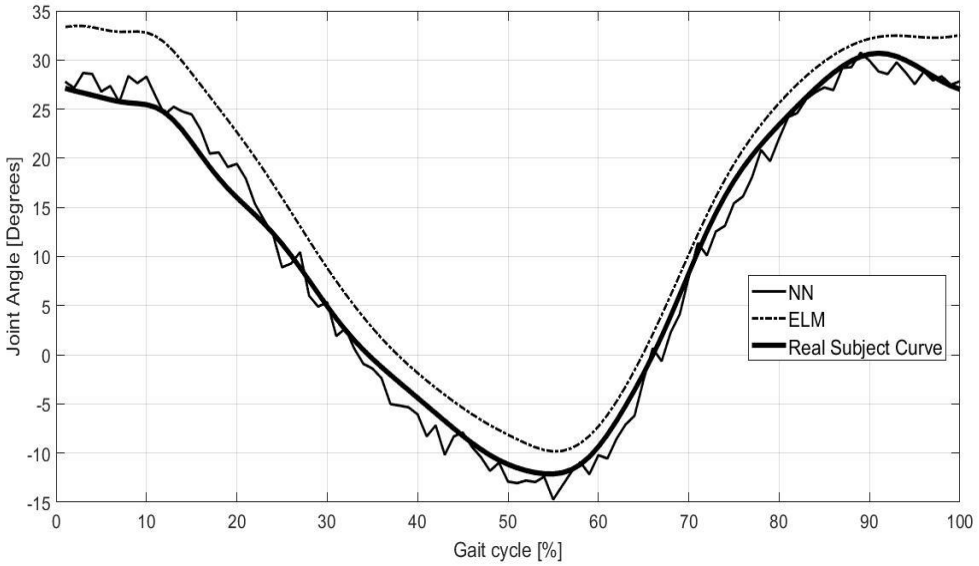

Figure 15. Dominant joint angle hip curves (generated and real) for young subject further from the mean.

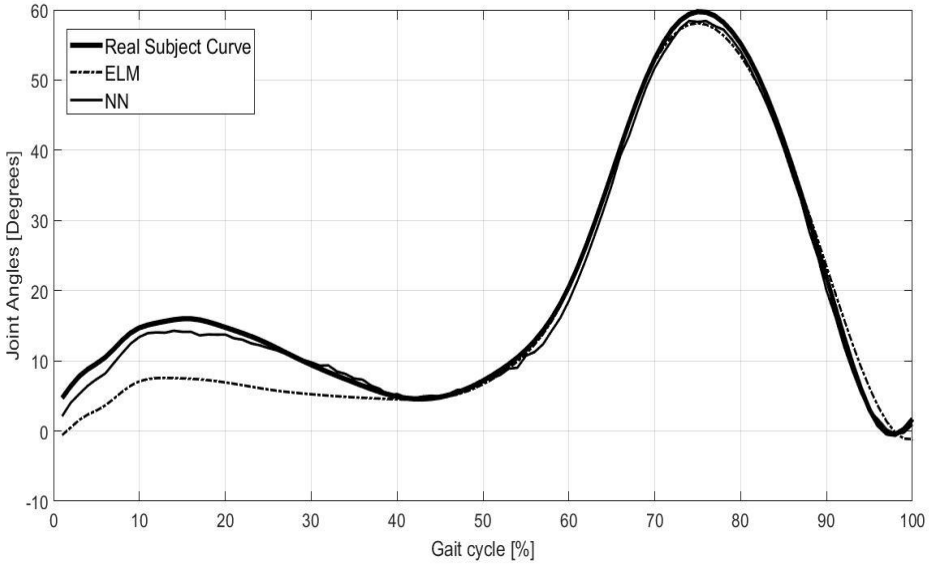

Figure 16. Dominant joint angle knee curves (generated and real) for young subject closer to the mean.

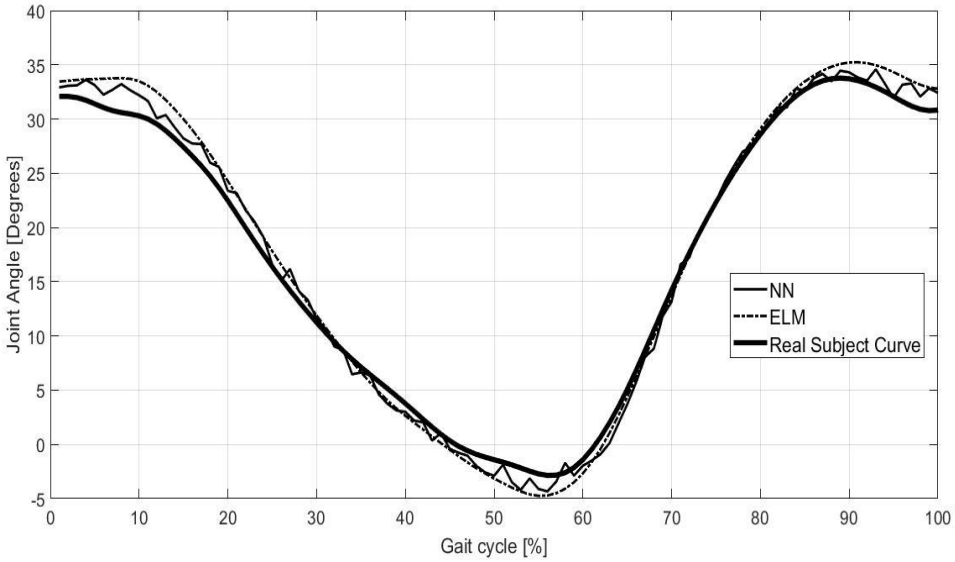

Figure 17. Dominant joint angle hip curves (generated and real) for young subject closer to the mean.

For the case of the test subject further from subjects mean characteristics, knee ELM accuracies are better or very similar to knee BNN accuracies. Accuracies for hip show a better performance of the BNN. For the closer to the mean test subject accuracies are predominantly favorable to the BNN. Nevertheless, BNNs are not capable of generating smooth joint angle curves either for the knee nor for the hip (see Figure 14 to Figure 17). On the contrary, ELMs present in every case smooth joint angle curves. Test MSE's obtained for the best male subject when generating knee angular reference profiles were similar to the ones presented by Ferreira et.

al [29]. There were not found any publications with the generation of hip reference joint profiles that could be compared with the results obtained in the present dissertation.

Figure 18 to Figure 21 show the joint angles prediction for test subjects (For the knee: age 33, height 179 cm, weight 75 kg; For the hip: age 25, height 174 cm, weight 83 kg) at the three distinct speeds (slow, comfortable, fast) together with the literature reference joint angle curve. CIs predictions and the literature joint angle curve were both compared to the real subject joint curves.

Table 8 contains the MSE results as well as the trials concrete speeds.

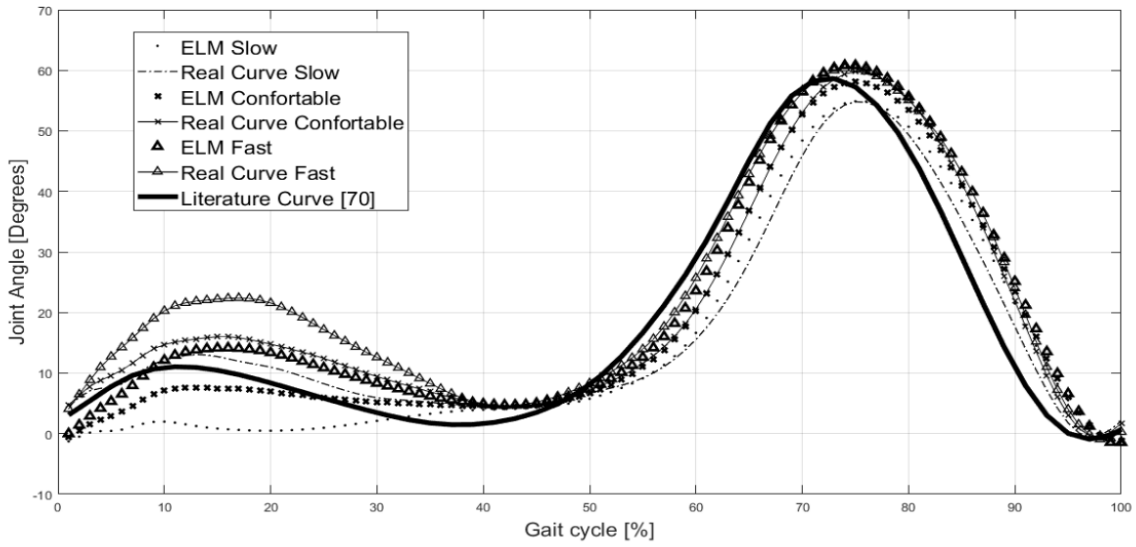

Figure 18. Dominant joint angle knee curve generation for young subject at several speeds and literature reference curve.

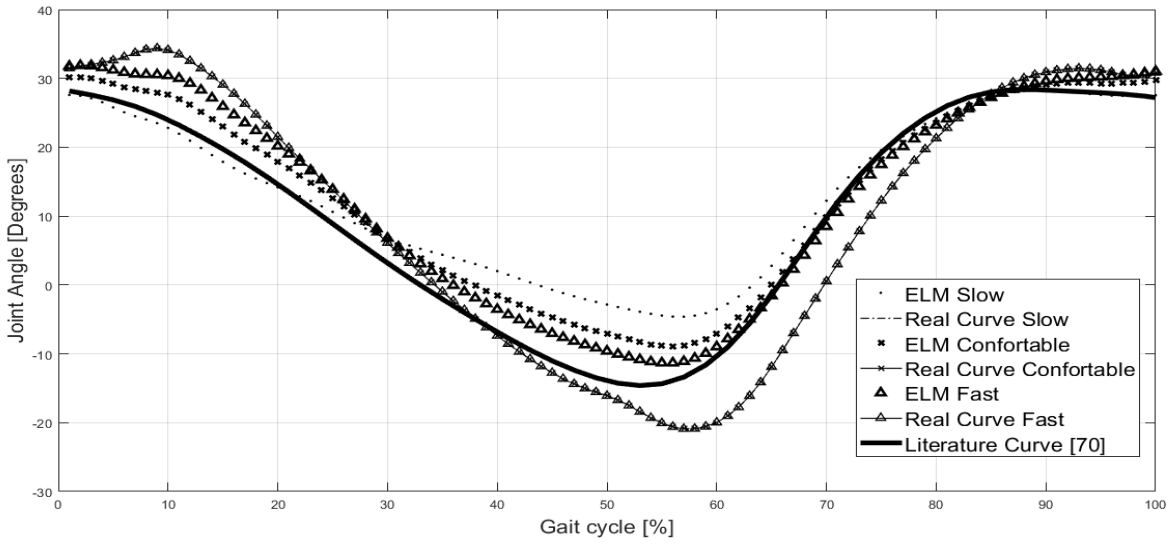

Figure 19. Dominant joint angle hip curve generation for young subject at several speeds and literature reference curve.

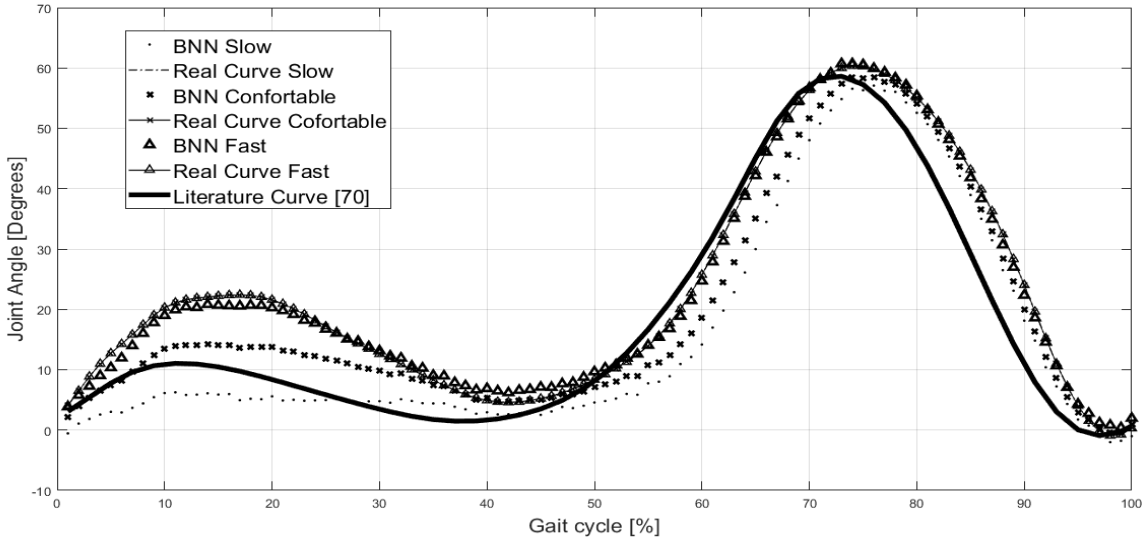

Figure 20. Dominant joint angle knee curve generation for young subject at several speeds and literature reference curve.

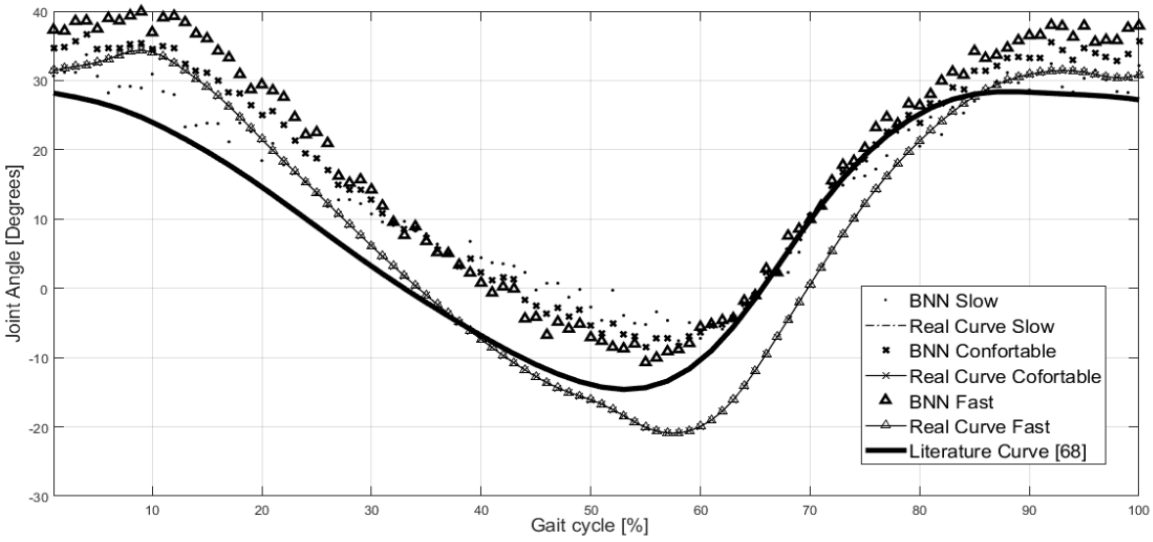

Figure 21. Dominant joint angle hip curve generation for young subject at several speeds and literature reference curve.

Table 8. CI's and literature MSE at different gait speeds for young subjects.

Limb	Gait Speed (m/s)	Literature [70] MSE	CI's MSE	
			BNN	ELM
Knee	0.68	0.017	0.014	0.005
	0.96	0.016	0.004	0.003
	1.29	0.021	0.0002	0.003
Hip	0.92	0.16	0.024	0.011
	1.32	0.12	0.004	0.022
	1.56	0.11	0.004	0.026

For the test subject used, BNN and ELM presented significant improvements when compared with the literature curve. The literature MSE increased for faster gait speeds, for the case of the knee. BNN showed better results specifically for the knee, with MSE decreasing for faster gait speeds. Nevertheless, joint angle curves originated were not smooth. ELM presented better or similar results as the BNN for knee, as already shown in [29], and slightly worse results for the hip. The knee and hip curves of all the test subjects can be found in Annex B.

Table 9 presents the mean train time for ELM and BNN for the number of neurons of the networks which originated the best accuracies.

Table 9. Training Time for ELM and BNN.

Network Information			CI's Training Times (seconds)	
Limb	Age Group	D/ND	BNN	ELM
Knee	Young	D	7.1438	**0.0003**
		ND	9.4813	**0.0003**
	Old	D	1.6235	**0.0001**
		ND	8.5998	**0.0001**
Hip	Young	D	32.0725	**0.0007**
		ND	5.6565	**0.0003**
	Old	D	2.0	**0.0002**
		ND	4.8022	**0.0003**

ELM learning speed was 10,000 times faster than BNN for every case. In Huan et. al [71] ELM learning speed surpassed BNN by more than a 1,000 times. The discrepancy in the speedup between these two works might reside in the training set size used, which was considerably smaller for the case of the present work. The number of hidden layer neuron was always smaller for ELM and training times obtained for the same number of hidden units still put ELM ahead by 10,000 times with neglectable loss of generalization (lost generalization < 0.004 for the knee and < 0.03 for the hip).

Based on obtained results both methods outperformed literature reference curve. ELM was able to generate smooth subject-specific joint angle curves and presented similar generalization accuracy to BNN, reason why it was chosen for the continuation of this work.

5.2 Hip-Knee Cyclogram analysis using ELM

The patient and ELM hip-knee cyclograms were compared using Dynamic Time Warp (DTW). Furthermore, the standard curves of the hip and knee used in [64] were used to generate the standard cyclogram and to evaluate the results of a comparison using subject-specific curves counterposed to a standard curve.

When comparing DTW results between ELM and the patient curve to standard curve, DTW's for the knee show a difference of 592.48º degrees, being both ELM and literature reference curve very similar in shape. The hip results show a substantial difference of 545.74º degrees. ELM learned correctly the influence of speed on hip range of motion. The increase of speed seems to accentuate hip flexion and decrease/narrow extension. On the other hand, the

standard curve used in [64] from Winter et. al [66] was age matched, but did not take into account the several other parameters that influence gait and thus does not constitute a reliable curve for comparison. Results from the DTW comparison are presented in Table 10. Hip-knee cyclograms for the right/dominant limbs are presented in Figure 22 for ELM, Figure 24 for the reference cyclogram from literature, and Figure 24 for CP patient. Area of the dominant limb cyclogram for the patient was bigger than the ELM cyclogram. This might be due to the fact that patient presented a knee extension of approximately 10º degrees together with greater amounts of hip extension. One should notice that knee recurvatum is a sign of pathological gait. These two factors might have led to a bigger conjoint movement since knee recurvatum happens nearly at the same time that hip achieves minimum angle, translating in this way, in a bigger area and the stretched look of the cyclogram (see Figure 9 and Figure 24).

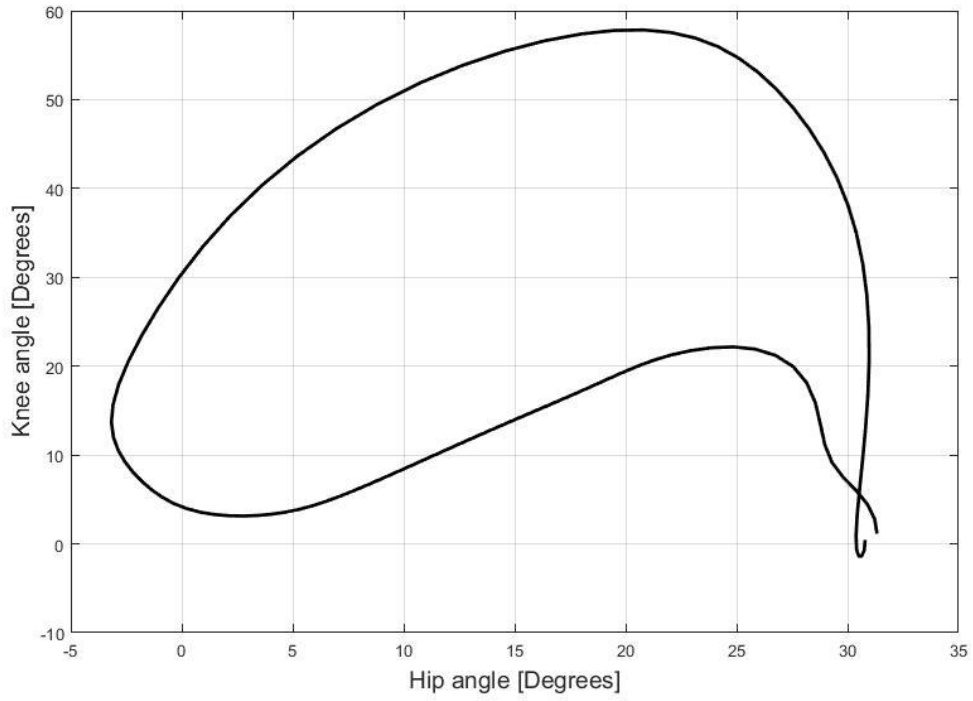

Figure 22. Dominant Hip-Knee Cyclogram Generated using ELM.

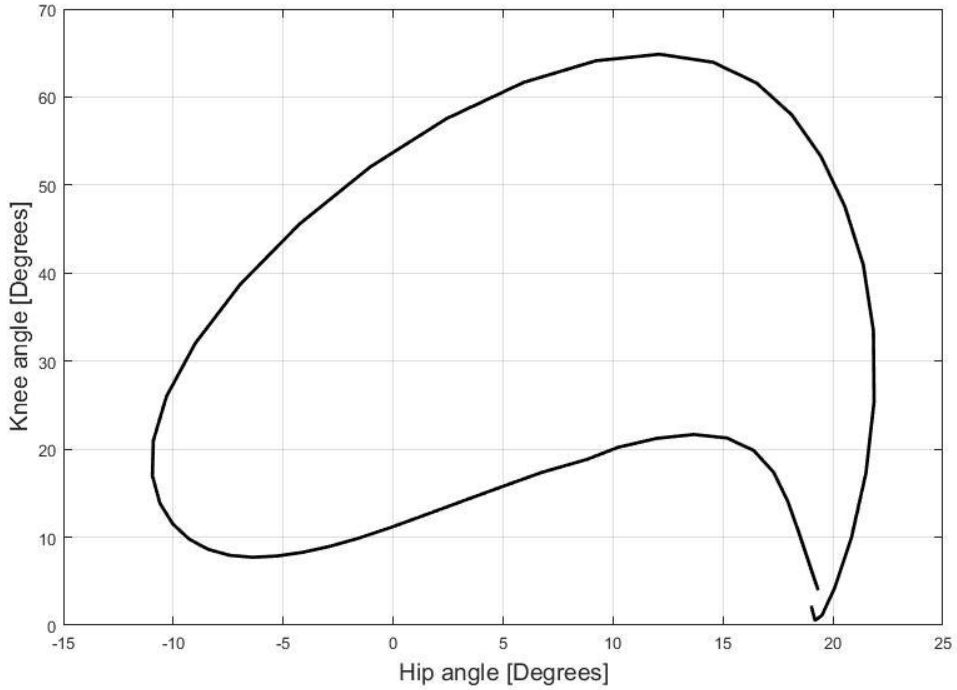

Figure 23. Dominant Hip-Knee Literature Reference Cyclogram.

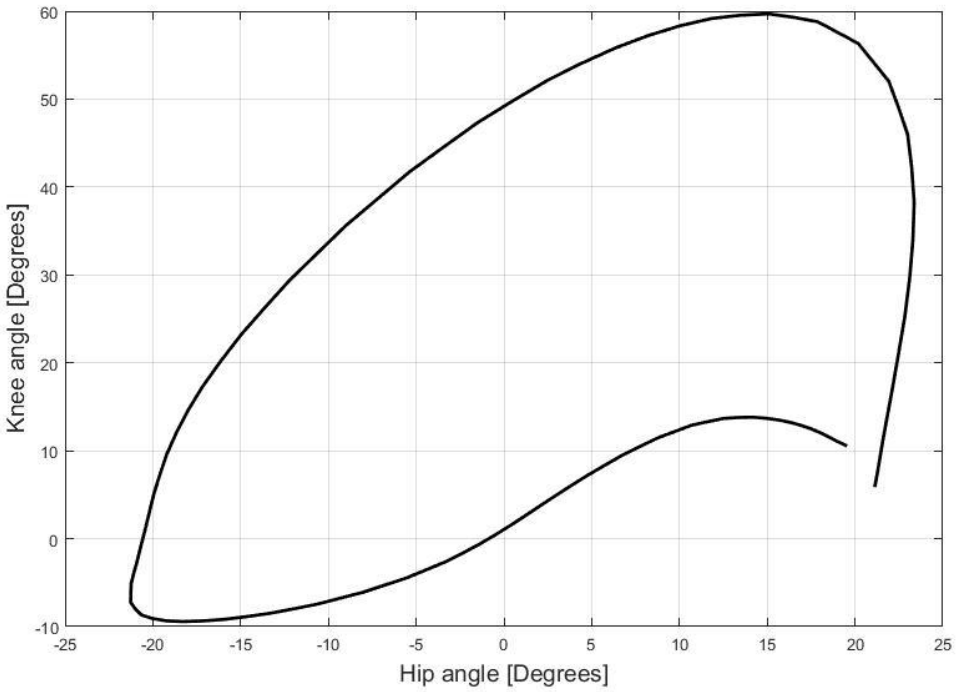

Figure 24. Dominant Hip-Knee Cyclogram Of Cerebral Palsy Patient.

Patient knee and ELM curve are similar and hip curves, although very distinct, present similar ROM. Due to the fact that perimeter is more sensitive to individual joint changes than area, the differences between patient and ELM generated cyclogram perimeter weren't so accentuated. Nevertheless, patient cyclogram displayed a bigger perimeter than his healthy expected equivalent generated using ELM.

Table 10. Dynamic Time Warp Right Limb Cyclograms.

Joint	ELM- CP Patient	Literature Reference- CP Patient
Knee	454.5	651.5
Hip	794.6	308.0

Table 11. Right Limb Area, Perimeter and P_A of Hip-Knee Cyclograms.

Feature	ELM	Literature Reference Curve	Patient
Area	1197.2	1292.0	1828.5
Perimeter	184.7	182.5	194.4
P_A	5.3	5.0	4.5

The P_A ratio, as mentioned previously, gives an indication of the shape. It can be seen that ELM healthy expected profile has a ratio closer to the literature reference curve than to the patient curve. The shape of the patient is difference from a healthy expected cyclogram, and such reflects slightly in the P_A ratio.

5.3 Symmetry Analysis Using Bilateral Cyclograms

In the present section results of bilateral Cyclograms, namely hip-hip and knee-knee, are displayed. The synchronized cyclogram were used to get insights of patient gait symmetry. The subject specific synchronized cyclogram created using ELM are also displayed and serve as support for patient evaluation. Synchronized cyclogram of a perfectly symmetrical gait would

correspond to a line that crosses the origin of unitary slope and zero area. Furthermore, the orientation of such line would be 45º degrees. This property can serve us to evaluate the symmetry state of patient knee and hip joints. Since even among healthy subjects there is no perfect symmetry, ELM generated cyclograms give us support in discerning what is an acceptable deviation from perfect symmetry. SI presented in Table 12 and Table 13 is based on [42] and is calculated as the ratio between ROM of non-dominant limb and ROM of dominant limb. Furthermore, difference of patient SI to ELM generated cyclogram SI is calculated for comparison (see Equations (30) and (31)) replacing the previous comparison measure, the ideal symmetry (SI = 1).

Table 12. Area and $\theta_{45º}$ for Hip-Hip Synchronized Cyclograms.

Feature	ELM	Patient
Area	11.9266	314.1163
$\theta_{45º}$	3.2330	0.4609
SI	1.1115	1.0063

Table 13. Area and $\theta_{45º}$ for Knee-Knee Synchronized Cyclograms.

Feature	ELM	Patient
Area	220.9088	477.4071
$\theta_{45º}$	0.7071	1.2104
SI	1.0243	0.9591

As can be seen by the results in Table 12 and Table 13 patient has a great deviation from the perfect symmetry expected area (Ideal area, A = 0) and when compared to ELM areas which stand as the expected area for a subject of such characteristics, it still presents differences of more than double for the knee 256.4983 $dgrees^2$ and 302.1897 $degrees^2$ of difference for the hip area. The ΔSI was of 0.0652 for the knee and 0.1052 for the hip. Naturally, greater the difference, greater will be the asymmetry. It can be noticed that for a comparison with the ideal symmetry (SI=1) results would be more symmetrical. In the following figures are displayed the unsynchronized cyclograms of both patient and ELM.

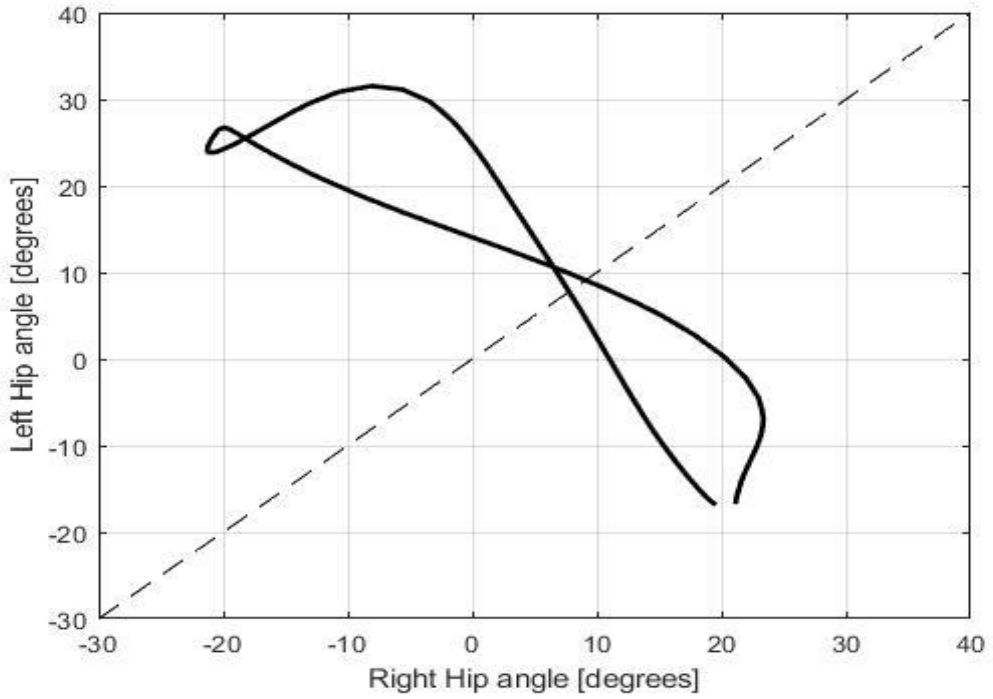

Figure 25. Unsynchronized Hip Cyclogram Of Cerebral Palsy Patient.

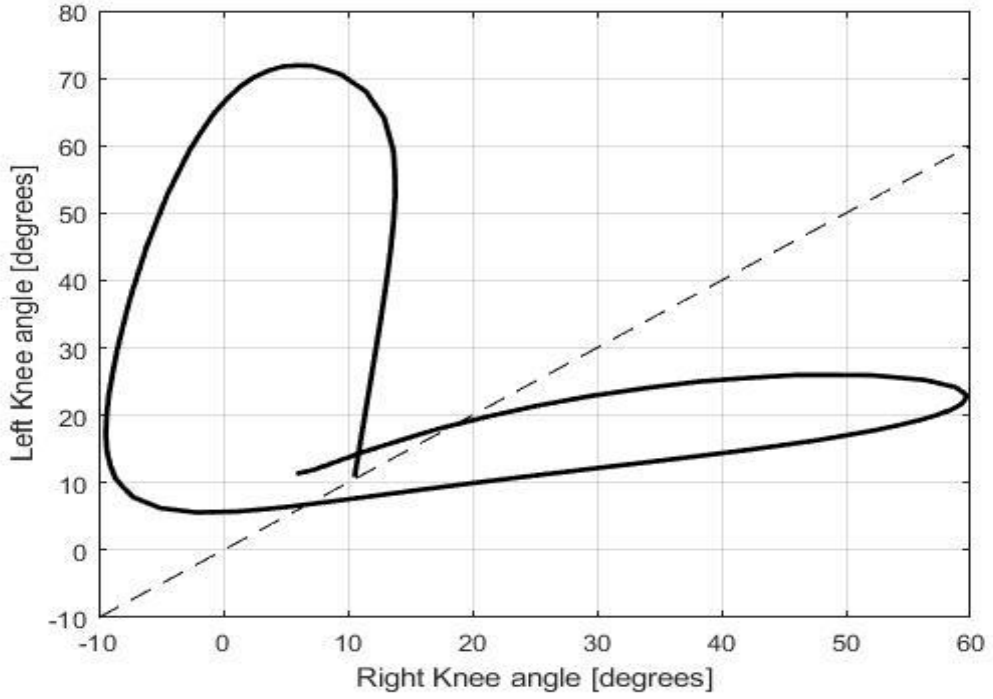

Figure 26. Unsynchronized Knee Cyclogram Of Cerebral Palsy Patient.

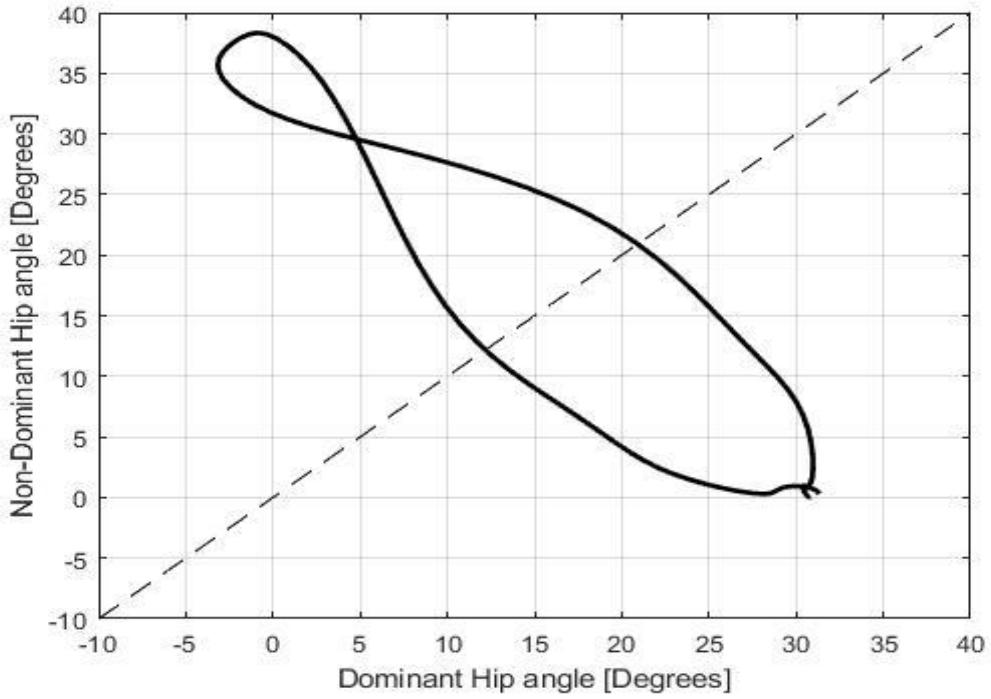

Figure 27. Unsynchronized Hip Cyclogram Generated Using ELM.

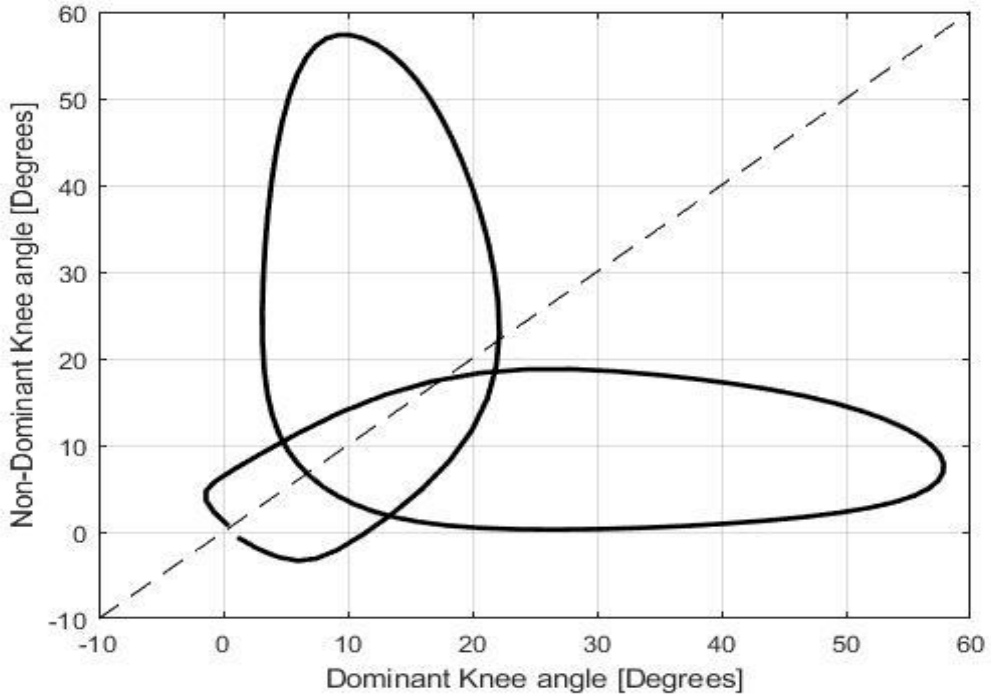

Figure 28. Unsynchronized Knee Cyclogram Generated Using ELM.

By visualizing both Cyclograms together with the 45º degrees perfect symmetry line, we can have a better understanding of the differences between the pathological and correspondent healthy. When using synchronized cyclograms, area is a good indicator of abnormally, nevertheless, by visualizing the unsynchronized cyclogram we can easily identify the discrepancy between right and left limb. SI based on unsynchronized cyclograms will penalize the abnormal knee negative extension since it contributes to a bigger range of movement of the right limb while left limb remain fairly normal. SI of the hip values were almost the same for ELM and patient, nevertheless, knee symmetry was 1.6 times lower for the patient, emphasizing the presence of some abnormality. The enclosed area of the synchronized cyclograms reinforce such results with a significant difference to the expected healthy curve, nevertheless cyclogram orientation did not shown conclusive results. By using unsynchronized cyclogram anomaly can be clearly visualize and quantified by comparison to the expected healthy results. The results for overall SI for both ELM generated curve and patient are present in Table 14.

Table 14. Overall SI for ELM and Patient.

	ELM	Patient
SI	0.67	0.57

SI results are considerably different using unsynchronized cyclograms than when ROM's are used. When unsynchronized cyclograms were used, ΔSI of the knee was of 0.2410 and 0.0699 for the hip. Overall ΔSI is then of 0.1 which is a much less symmetrical gait than ROM's based SI indication. This results seem to be coherent with patient gait evaluation present in [64], furthermore, Pilkar et. al [44] results were also shown to be lower when using such approach.

6 Conclusion and future work

For test subjects (For the knee: age 33, height 179 cm, weight 75 kg; For the hip: age 25, height 174 cm, weight 83 kg) at the three distinct speeds (slow, comfortable, fast), both CIs generated reference curves closer to a patient real curves than the literature standard curve. The capability of generation of this healthy profile for specific subject characteristics and gait speed permit the use of this methodology in gait assessment in a broad range of impairments. Such results were reinforced for increasing gait speeds.

For the BNN, the lack of smoothness of the curves for subjects at the edge of the train data set was a recurrent issue, although accuracies were higher than with ELM, for most cases. For the case of the test subject further from subjects mean characteristics, knee ELM results are better or similar to BNN, nevertheless, hip accuracies were higher for the BNN. Furthermore, curves generated with ELM were always smooth, suggesting that this CI method is the indicated CI to generate knee and hip, subject-specific, healthy joint angle curves for both dominant and non-dominant limbs. BNN was better suited for subjects closer to the mean characteristics of the data set, although generated curves need to be smoothed.

The use of the several types of cyclograms implied in the work permitted the visualization and extraction of data of relevancy for the gait analysis and assessment. The use of bilateral cyclograms and the Symmetry Index (SI) extracted allowed the comparison between the patient and subject-specific curves generated by ELM. This analysis brought insights on patient symmetry and its distance to his healthy expected results instead of the ideal unattainable symmetry. Furthermore, the SI obtained by unsynchronized cyclograms shown to be more sensitive to variations of the right and left limb range of movement (ROM) due to the point-by-point comparison. The SI based on unsynchronized cyclograms takes into consideration the phase shift occurring between joints of both limbs that is not considered in the SI based on ROM.

In the future would be of interest the creation or acquisition of a much bigger dataset, as well as the application of the methodology to women. Regularization should be applied to CI's in the future.

Further validation should be done when using unsynchronized cyclograms based SI and in using ELM healthy expected generated cyclograms as reference for comparison. Also, would be of interest to do a selection of main cyclograms features that would allow a deviation index out of ELM generated cyclograms, originating this way a subject-specific gait deviation measure.

The present work resulted in the article *Pedro S. Cunha, João P. Ferreira, A. Paulo Coimbra, Manuel Crisóstomo, "Computational Intelligence Generation of Subject-Specific Knee and Hip Healthy Joint Angles Reference Curves"*. Presented at the *15th Mediterranean Conference on Medical and Biological Engineering and Computing*, MEDICON2019.

Bibliography

[1] C. Buckley *et al.*, “The role of movement analysis in diagnosing and monitoring neurodegenerative conditions: Insights from gait and postural control,” *Brain Sci.*, vol. 9, no. 2, pp. 1–21, 2019.

[2] W. Zeng and C. Wang, “Classification of neurodegenerative diseases using gait dynamics via deterministic learning,” *Inf. Sci. (Ny).*, vol. 317, pp. 246–258, 2015.

[3] R. Morris, S. Lord, J. Bunce, D. Burn, and L. Rochester, “Gait and cognition: Mapping the global and discrete relationships in ageing and neurodegenerative disease,” *Neurosci. Biobehav. Rev.*, vol. 64, pp. 326–345, 2016.

[4] P. Mahlknecht *et al.*, “Prevalence and Burden of Gait Disorders in Elderly Men and Women Aged 60-97 Years: A Population-Based Study,” *PLoS One*, vol. 8, no. 7, Jul. 2013.

[5] T. R. Mhyre, J. T. Boyd, R. W. Hamill, and K. A. Maguire-Zeiss, “Parkinson’s Disease HHS Public Access,” *Subcell Biochem*, 2012.

[6] Ivan E. Danhof. "Role of N-2-Hydroxy-Ethyl-Piperazine-N-2 Ethane Sulfonic Acid in pain controlo and reversal of Demyelinization injury.” U.S. Patent, Nov. 11, 2014.

[7] S. J. Duffield *et al.*, “The contribution of musculoskeletal disorders in multimorbidity: Implications for practice and policy.,” *Best Pract. Res. Clin. Rheumatol.*, vol. 31, no. 2, pp. 129–144, 2017.

[8] G. Minakaki *et al.*, “Treadmill exercise intervention improves gait and postural control in alpha-synuclein mouse models without inducing cerebral autophagy,” *Behav. Brain Res.*, vol. 363, pp. 199–215, 2019.

[9] A. Santamato *et al.*, “Postural and Balance Disorders in Patients with Parkinson’s Disease: A Prospective Open-Label Feasibility Study with Two Months of Action Observation Treatment,” *Parkinsons. Dis.*, vol. 2015, pp. 1–7, 2015.

[10] R. Briggs, D. Carey, R. A. Kenny, S. P. Kennelly, “What is the longitudinal relationship between gait abnormalities and depression in a cohort of community-dwelling older people? Data from the Irish Longitudinal Study on Ageing,” *The American Journal of Geriatric Psychiatry*, vol. 26, no. 1, pp. 75–86, 2018.

[11] T. R. Ham, M. Farrag, A. M. Soltisz, E. H. Lakes, K. D. Allen, and N. D. Leipzig, “Automated Gait Analysis Detects Improvements after Intracellular σ Peptide Administration in a Rat Hemisection Model of Spinal Cord Injury,” *Ann. Biomed. Eng.*,

vol. 47, no. 3, pp. 744–753, 2019.

[12] M. Alaqtash, T. Sarkodie-Gyan, H. Yu, O. Fuentes, R. Brower, and A. Abdelgawad, "Automatic classification of pathological gait patterns using ground reaction forces and machine learning algorithms," *Proc. Annu. Int. Conf. IEEE Eng. Med. Biol. Soc. EMBS*, pp. 453–457, 2011.

[13] H. Alaskar, A. Hussain, "Prediction of Parkinson Disease Using Gait Signals," *International Conference on Developments in eSystems Engineering*, pp. 23–26, 2018.

[14] M. P. R. Rani and G. Arumugam, "Children Abnormal GAIT Classification Using Extreme Learning Machine," *Glob. J. Comput. Sci. Technol.*, vol. 10, no. 13, pp. 66–72, 2010.

[15] S. Joshi, D. Shenoy, G. G. Vibhudendra Simha, P. L. Rrashmi, K. R. Venugopal, and L. M. Patnaik, "Classification of Alzheimer's disease and Parkinson's disease by using machine learning and neural network methods," *ICMLC 2010 - 2nd Int. Conf. Mach. Learn. Comput.*, pp. 218–222, 2010.

[16] K. Manal and S. J. Stanhope, "A novel method for displaying gait and clinical movement analysis data," *Gait Posture*, vol. 20, no. 2, pp. 222–226, 2004.

[17] S. Summa *et al.*, "Gait changes after weight loss on adolescent with severe obesity after sleeve gastrectomy," *Surg. Obes. Relat. Dis.*, no. xxxx, pp. 1–8, 2019.

[18] R. Begg and J. Kamruzzaman, "A machine learning approach for automated recognition of movement patterns using basic, kinetic and kinematic gait data," *J. Biomech.*, 2005.

[19] F. Horst, M. Mildner, and W. I. Schöllhorn, "One-year persistence of individual gait patterns identified in a follow-up study – A call for individualised diagnose and therapy," *Gait Posture*, vol. 58, no. August, pp. 476–480, 2017.

[20] S. Shameem, F. Smh, and W. B. Rsd, "Abnormal walk identification for systems using gait patterns," *Biomedical Research-India* , vol. 27, 2016.

[21] M. H. Schwartz, A. Rozumalski, and J. P. Trost, "The effect of walking speed on the gait of typically developing children," *J. Biomech.*, vol. 41, no. 8, pp. 1639–1650, 2008.

[22] H. G. Kang and J. B. Dingwell, "Separating the effects of age and walking speed on gait variability," *Gait Posture*, vol. 27, no. 4, pp. 572–577, 2008.

[23] Xue-Wen Chen and Xiaotong Lin, "Big Data Deep Learning: Challenges and Perspectives," *IEEE Access*, vol. 2, pp. 514–525, 2014.

[24] D. T. H. Lai, R. K. Begg, and S. Member, “Computational Intelligence in Electromyography Analysis - A Perspective on Current Applications and Future Challenges,” *Comput. Intell. Electromyogr. Anal. - A Perspect. Curr. Appl. Futur. Challenges*, vol. 13, no. 5, pp. 687–702, 2012.

[25] J. H. Yoo, K. Y. Moon, D. Hwang, and M. S. Nixon, “Automated human recognition by gait using neural network,” in *2008 1st International Workshops on Image Processing Theory, Tools and Applications, IPTA 2008*, 2008.

[26] C. P. Utomo, A. Kardiana, and R. Yuliwulandari, “Breast Cancer Diagnosis using Artificial Neural Networks with Extreme Learning Techniques,” 2014.

[27] X. Ma, H. Wang, B. Xue, M. Zhou, B. Ji, and Y. Li, “Depth-based human fall detection via shape features and improved extreme learning machine,” *IEEE J. Biomed. Heal. Informatics*, vol. 18, no. 6, pp. 1915–1922, 2014.

[28] A. Vieira *et al.*, “Dynamic Human Gait VGRF Reference Profile Generation via Extreme Learning Machine,” *Proc. Int. Jt. Conf. Neural Networks*, vol. 2018-July, 2018.

[29] J. P. Ferreira, A. Vieira, P. Ferreira, M. Crisóstomo, and A. P. Coimbra, “Human knee joint walking pattern generation using computational intelligence techniques,” *Neural Comput. Appl.*, vol. 30, no. 6, pp. 1701–1713, 2018.

[30] W. Pirker and R. Katzenschlager, “Gait disorders in adults and the elderly: A clinical guide,” *Wiener Klinische Wochenschrift*, vol. 129, no. 3–4. Springer-Verlag Wien, pp. 81–95, 01-Feb-2017.

[31] B. Mondal *et al.*, “Analysis of gait in Parkinson’s disease reflecting the effect of l-DOPA,” *Annals of Movement Disorders*, p. 21, 2019.

[32] I. T. Jollife and J. Cadima, “Principal component analysis: A review and recent developments,” *Philosophical Transactions of the Royal Society A: Mathematical, Physical and Engineering Sciences*, vol. 374, no. 2065. Royal Society of London, 13-Apr-2016.

[33] Y. Peng, P. Arauz, S. An, and Y. M. Kwon, “In vivo sliding distance on the metal-on-polyethylene total hip arthroplasty articulation using patient-specific gait analysis,” *J. Orthop. Res.*, 2018.

[34] H. Gulgin, K. Hall, A. Luzadre, and E. Kayfish, “3D gait analysis with and without an orthopedic walking boot,” *Gait Posture*, vol. 59, pp. 76–82, Jan. 2018.

[35] A. Castagna *et al.*, “Quantitative gait analysis in parkin disease: Possible role of

dystonia," *Mov. Disord.*, vol. 31, no. 11, pp. 1720–1728, Nov. 2016.

[36] V. L. Patel *et al.*, "The coming of age of artificial intelligence in medicine," *Artif. Intell. Med.*, vol. 46, no. 1, pp. 5–17, May 2009.

[37] T. P. Luu, K. H. Low, X. Qu, H. B. Lim, and K. H. Hoon, "An individual-specific gait pattern prediction model based on generalized regression neural networks," *Gait Posture*, vol. 39, no. 1, pp. 443–448, 2014.

[38] H. Alaskar and A. Hussain, "Prediction of Parkinson disease using gait signals," in *Proceedings - International Conference on Developments in eSystems Engineering, DeSE*, 2019.

[39] C. Prasetyo, A. Kardiana, and R. Yuliwulandari, "Breast Cancer Diagnosis using Artificial Neural Networks with Extreme Learning Techniques," *Int. J. Adv. Res. Artif. Intell.*, vol. 3, no. 7, pp. 10–14, 2014.

[40] M. Błażkiewicz and A. Wit, "Artificial neural network simulation of lower limb joint angles in normal and impaired human gait," *Acta Bioeng. Biomech.*, vol. 20, no. 3, pp. 43–49, 2018.

[41] P. Kutilek and B. Farkasova, "Prediction of lower extremities' movement by angle-angle diagrams and neural networks," 2011.

[42] P. Kutilek, S. Viteckova, Z. Svoboda, and P. Smrcka, "Kinematic quantification of gait asymmetry in patients with peroneal nerve palsy based on bilateral cyclograms," *J. Musculoskelet. Neuronal Interact.*, vol. 13, no. 2, pp. 244–250, 2013.

[43] H. Sobral *et al.*, "Two New Indices to Assess Gait Disturbances Applied to Anterior Cruciate Ligament Reconstructed Knees," *8th Annu. IEEE Int. Conf. Cyber Technol. Autom. Control Intell. Syst. CYBER 2018*, pp. 701–706, 2019.

[44] R. Pilkar, A. Ramanujam, K. Chervin, G. F. Forrest, and K. J. Nolan, "Cyclogram-Based Joint Symmetry Assessment After Utilization of a Foot Drop Stimulator During Post-stroke Hemiplegic Gait," *J. Biomech. Eng.*, vol. 140, no. 12, p. 121005, Sep. 2018.

[45] A. Rozumalski and M. H. Schwartz, "The GDI-Kinetic: A new index for quantifying kinetic deviations from normal gait," *Gait Posture*, vol. 33, no. 4, pp. 730–732, Apr. 2011.

[46] M. L. McMulkin and B. A. MacWilliams, "Application of the Gillette Gait Index, Gait Deviation Index and Gait Profile Score to multiple clinical pediatric populations," *Gait Posture*, vol. 41, no. 2, pp. 608–612, 2015.

[47] G. Yogev, M. Plotnik, C. Peretz, N. Giladi, and J. M. Hausdorff, “Gait asymmetry in patients with Parkinson’s disease and elderly fallers: When does the bilateral coordination of gait require attention?,” *Exp. Brain Res.*, vol. 177, no. 3, pp. 336–346, Mar. 2007.

[48] L. Wafai, A. Zayegh, J. Woulfe, S. Mahfuzul, and R. Begg, “Identification of foot pathologies based on plantar pressure asymmetry,” *Sensors (Switzerland)*, vol. 15, no. 8, pp. 20392–20408, Aug. 2015.

[49] C. Hershler and M. Milner, “Angle--angle diagrams in the assessment of locomotion.,” *Am. J. Phys. Med.*, vol. 59, no. 3, pp. 109–25, Jun. 1980.

[50] C. Hershler and M. Milner, “Angle-angle diagrams in above-knee amputee and cerebral palsy gait.,” *Am. J. Phys. Med.*, vol. 59, no. 4, pp. 165–83, Aug. 1980.

[51] K. Oberg, H. Lanshammar, “An Investigation of Kinematic and Kinetic Variables for the Description of Prosthetic Gait using the ENOCH System,” *Prosthetics and orthotics international*, vol. 6, no. 1, pp. 43-47, 2009.

[52] W. Duch, “What is Computational Intelligence and what could it become?”, 2003.

[53] K. Wang, “Computational Intelligence in Agile Manufacturing Engineering,” in *Agile Manufacturing: The 21st Century Competitive Strategy*, Elsevier, 2001, pp. 297–315.

[54] A. M. Abdelsalam, F. Boulet, G. Demers, J. M. Pierre Langlois, and F. Cheriet, “An Efficient FPGA-based Overlay Inference Architecture for Fully Connected DNNs,” *2018 Int. Conf. ReConFigurable Comput. FPGAs*, pp. 1–6, 2018.

[55] G. E. Hinton, N. Srivastava, A. Krizhevsky, I. Sutskever, and R. R. Salakhutdinov, “Improving neural networks by preventing co-adaptation of feature detectors,” pp. 1–18, 2012.

[56] A. Osmanovi, S. Halilovi, L. A. Ilah, A. Fojnica, and Z. Gromili, “WC 2003-World Congress on Medical Physics and Biomedical Engineering,” *Med. Eng. Phys.*, vol. 24, no. 6, p. II, 2002.

[57] H. Li, Z. Zhang, and Z. Liu, “Application of Artificial Neural Networks for Catalysis: A Review,” *Catalysts*, vol. 7, no. 10, p. 306, 2017.

[58] C. Mair *et al.*, “An Investigation of machine learning based prediction systems,” *J. Syst. Softw.*, vol. 53, no. 1, pp. 23–29, 2000.

[59] G. Bin Huang, Q. Y. Zhu, and C. K. Siew, “Extreme learning machine: A new learning scheme of feedforward neural networks,” *IEEE Int. Conf. Neural Networks - Conf.*

Proc., vol. 2, no. February 2014, pp. 985–990, 2004.

[60] T. Matias, F. Souza, R. Araújo, and C. H. Antunes, "Learning of a single-hidden layer feedforward neural network using an optimized extreme learning machine," *Neurocomputing*, vol. 129, pp. 428–436, 2014.

[61] J. Tang, C. Deng, and G. Bin Huang, "Extreme Learning Machine for Multilayer Perceptron," *IEEE Trans. Neural Networks Learn. Syst.*, vol. 27, no. 4, pp. 809–821, 2016.

[62] C. Karakuzu and U. Yüzgeç, "A Simple Heuristic Approach to Improve Performance of Extreme Learning Machine," no. May, pp. 212–217, 2018.

[63] C. A. Fukuchi, R. K. Fukuchi, and M. Duarte, "A public dataset of overground and treadmill walking kinematics and kinetics in healthy individuals," *PeerJ*, vol. 6, p. e4640, 2018.

[64] C. L. Vaughan, B. L. Davis, and J. C. OConnor, *Dynamics of human gait*, vol. 2. Leeds (England): Human Kinetics Publishers, 1992.

[65] J. Sinclair, P. John Taylor, and S. Jane Hobbs, "Digital filtering of three-dimensional lower extremity kinematics: An assessment," *J. Hum. Kinet.*, vol. 39, no. 1, pp. 25–36, 2013.

[66] D. A. Winter, *Biomechanics and motor control of human movement*, 4th ed. Hoboken (NJ): Wiley, 2009.

[67] Simtk-confluence.stanford.edu. (2019). *Gait 2392 and 2354 Models - OpenSim Documentation*. [online] Available at: https://simtk-confluence.stanford.edu:8443 /display/OpenSim/Gait+2392+and+2354+Models [Accessed 25 Aug. 2019].

[68] Simtk-confluence.stanford.edu. (2019). *Scaling - OpenSim Documentation*. [online] Available at: https://simtk-confluence.stanford.edu:8443/display/OpenSim/Scaling [Accessed 25 Aug. 2019].

[69] J. Frankle and M. Carbin, "The Lottery Ticket Hypothesis: Finding Sparse, Trainable Neural Networks," Mar. 2018.

[70] Sites.google.com. (2019). *Download Files - Gait Analysis ADplot*. [online] Available at: https://sites.google.com/site/gaitanalysisadplot/file-cabinet [Accessed 26 Jan. 2019].

[71] G. Bin Huang, Q. Y. Zhu, and C. K. Siew, "Extreme learning machine: A new learning scheme of feedforward neural networks," in *IEEE International Conference on Neural Networks - Conference Proceedings*, 2004, vol. 2, pp. 985–990.

Annex A

Table 15. Healthy Subjects Input Observations Information.

Subject Number	Age	Height (cm)	Weight (kg)	Gait Speed (m/s)
1	25	172.50	74.30	0.85
2	33	179.30	75.85	0.68
3	24	184	61.05	0.90
4	28	170.90	77.55	0.87
5	25	174.20	83.15	0.92
6	36	182.50	64	1.00
7	32	192	77.55	0.93
8	30	171	95.40	0.74
9	23	180.60	89.30	1.09
10	31	172.90	77.90	0.77
11	28	185.50	79.05	0.99
12	29	175.80	66.25	0.84
13	22	180.70	61.50	0.97
14	37	155	69.55	0.68
1	25	172.50	74.30	1.22
2	33	179.30	75.850	0.96
3	24	184	61.05	1.28
4	28	170.90	77.55	1.25
5	25	174.20	83.15	1.32
6	36	182.50	64	1.33
7	32	192	77.55	1.34
8	30	171	95.40	1.08
9	23	180.60	89.30	1.48
10	31	172.90	77.90	1.12
11	28	185.50	79.05	1.32
12	29	175.80	66.25	1.17
13	22	180.70	61.50	1.42
14	37	155	69.55	1.00

1	25	172.50	74.30	1.62
2	33	179.30	75.85	1.28
3	24	184	61.05	1.64
4	28	170.90	77.55	1.60
5	25	174.20	83.15	1.56
6	36	182.50	64	1.76
7	32	192	77.55	1.61
8	30	171	95.40	1.26
9	23	180.60	89.30	1.96
10	31	172.90	77.90	1.48
11	28	185.50	79.05	1.67
12	29	175.80	66.25	1.59
13	22	180.70	61.50	1.71
14	37	155	69.55	1.26

Table 16. CP Patient Information.

Age	Height (cm)	Weight (kg)	Gait Speed (m/s)
23	170	69.5	1.24

Annex B

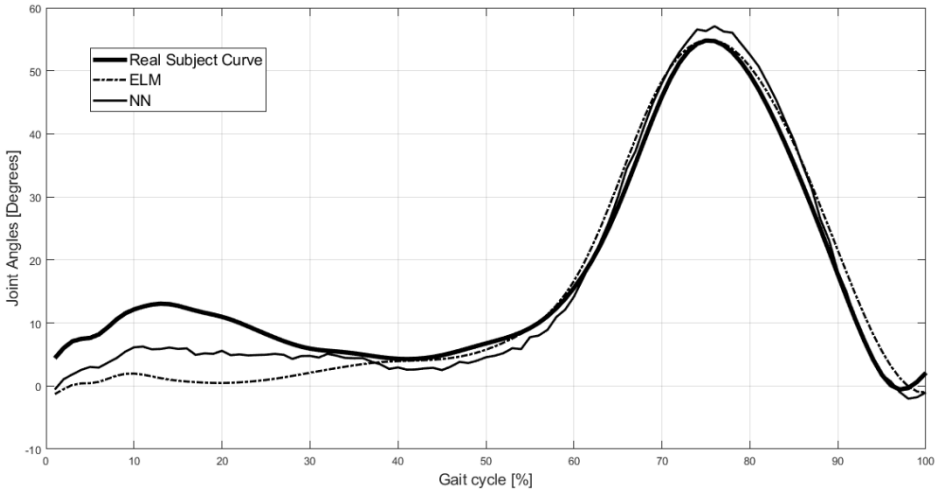

Figure 29. Young Dominant Knee Test Subject 1 Results.

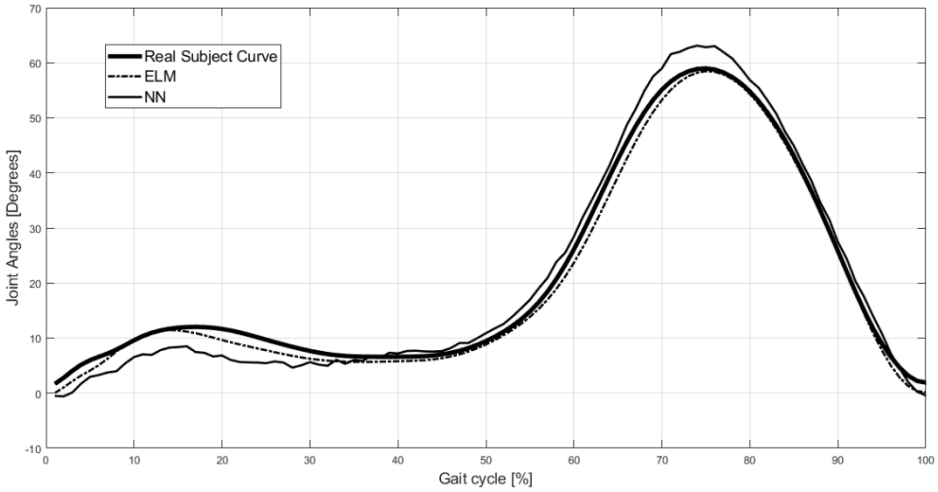

Figure 30. Young Dominant Knee Test Subject 2 Results.

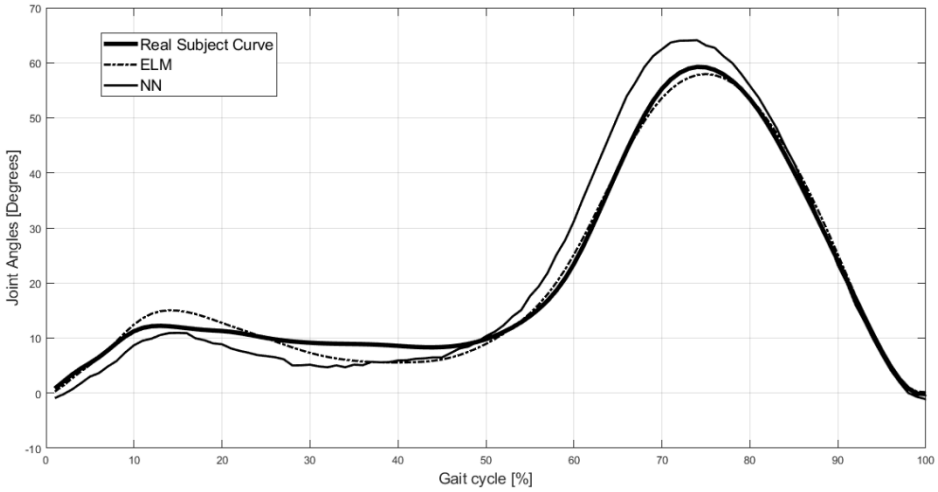

Figure 31. Young Dominant Knee Test Subject 3 Results.

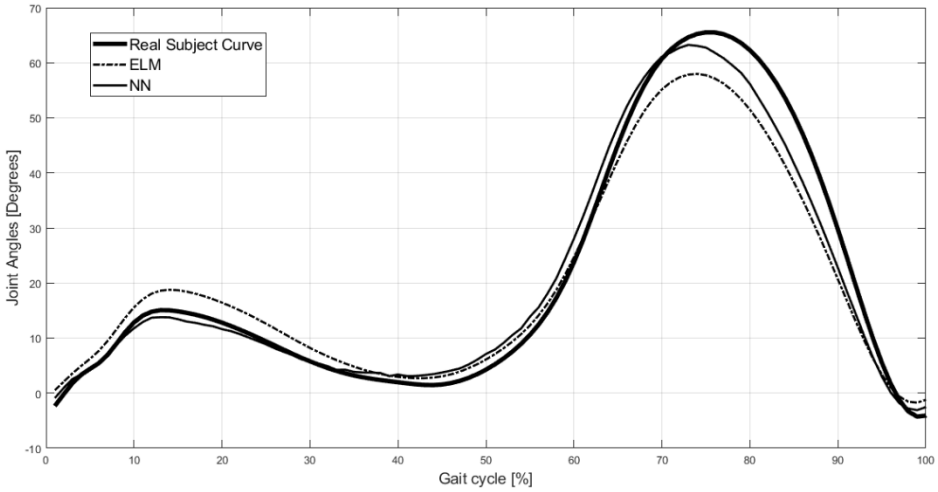

Figure 32. Young Dominant Knee Test Subject 4 Results.

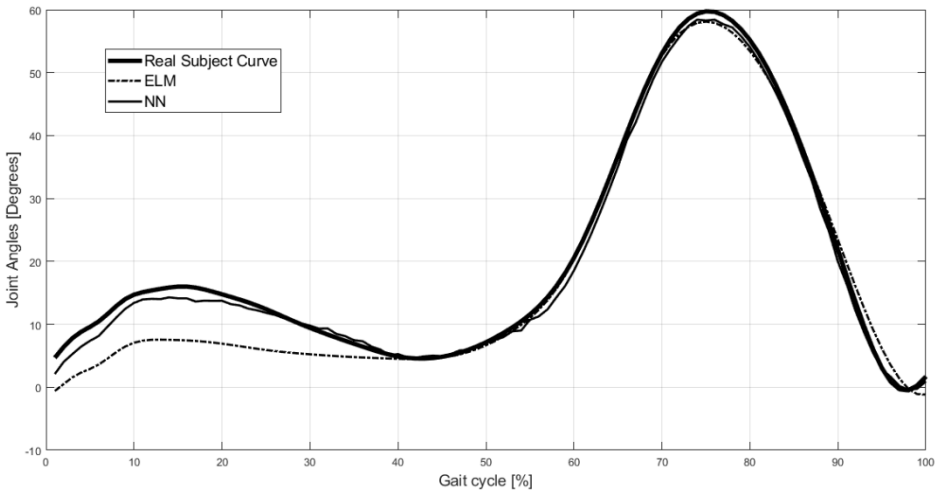

Figure 33. Young Dominant Knee Test Subject 5 Results.

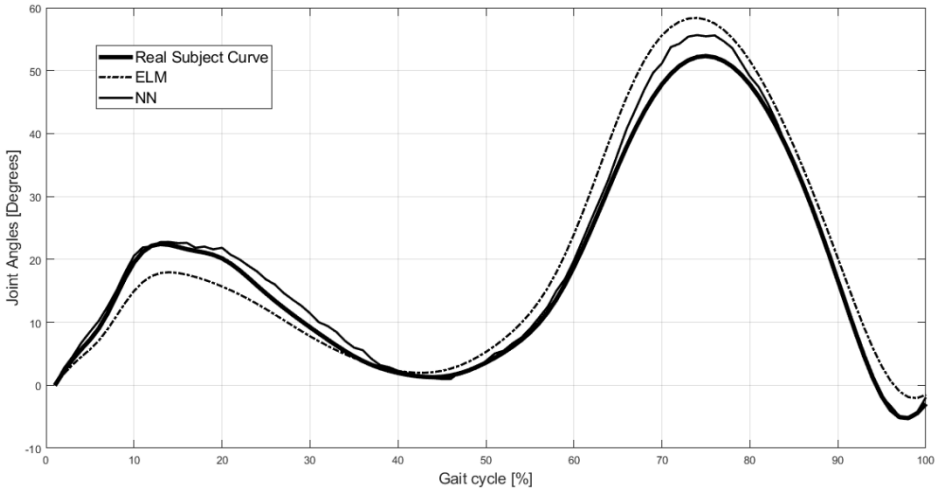

Figure 34. Young Dominant Knee Test Subject 6 Results.

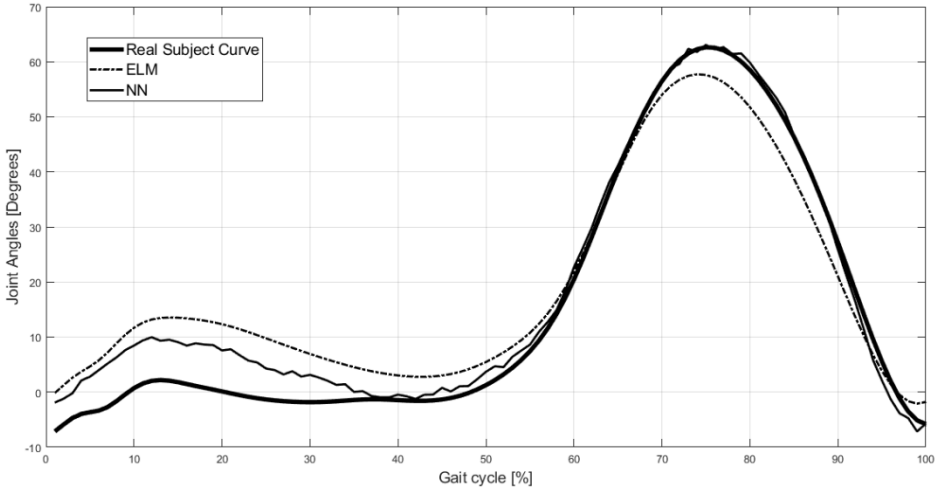

Figure 35. Young Dominant Knee Test Subject 7 Results.

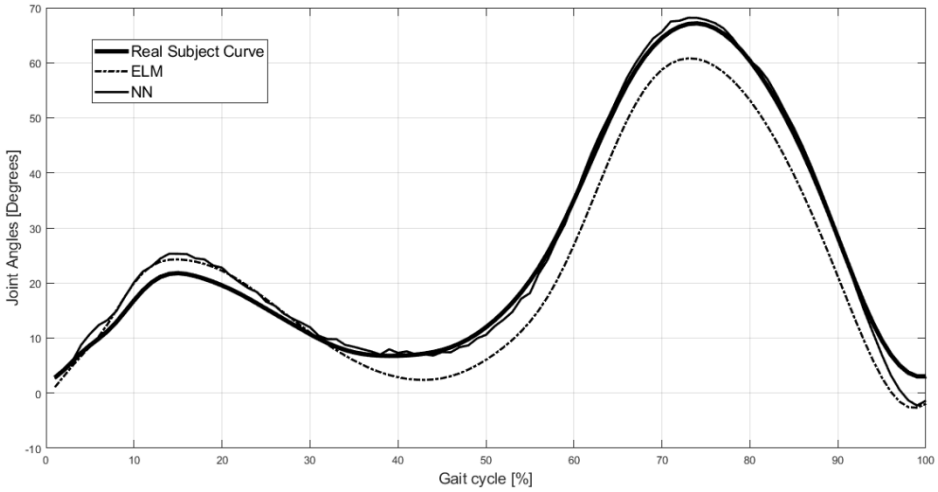

Figure 36. Young Dominant Knee Test Subject 8 Results.

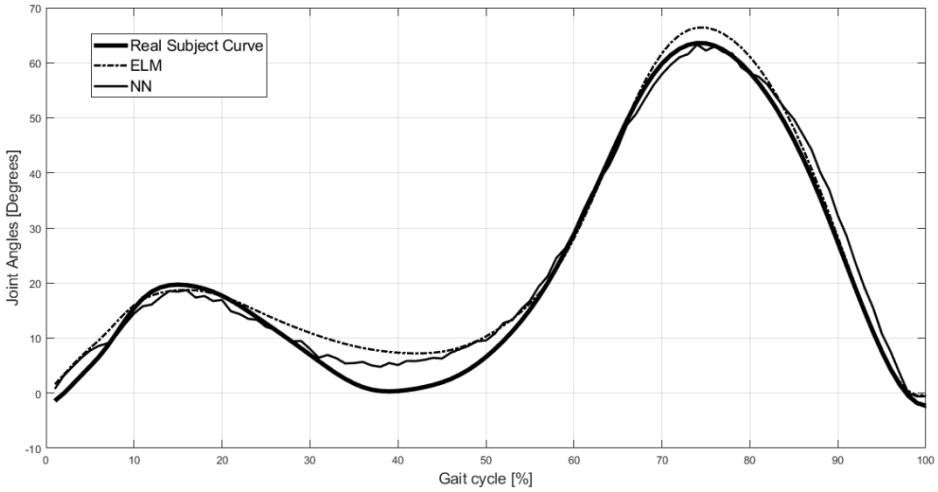

Figure 37. Young Dominant Knee Test Subject 9 Results.

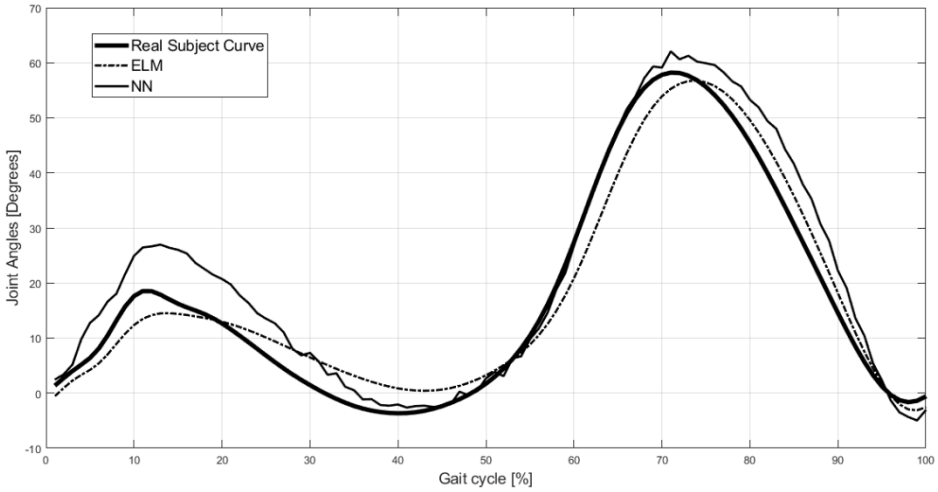

Figure 38. Young Dominant Knee Test Subject 10 Results.

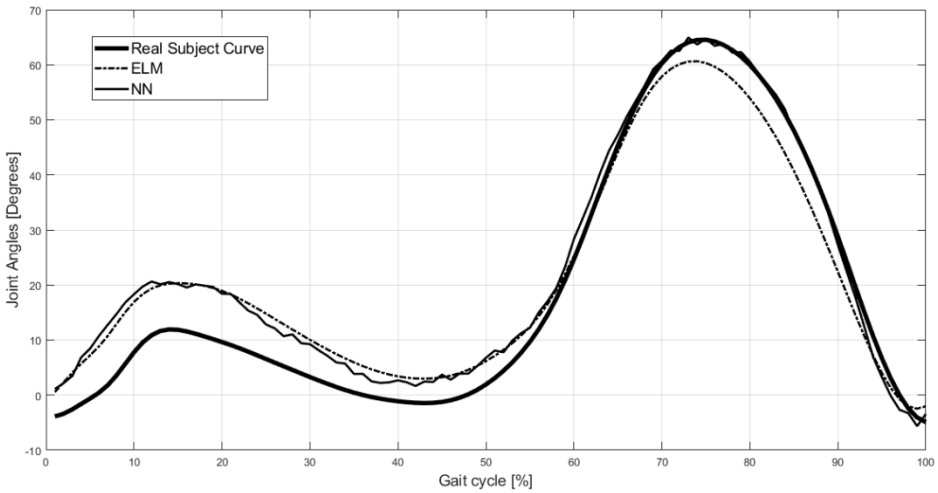

Figure 39. Young Dominant Knee Test Subject 11 Results.

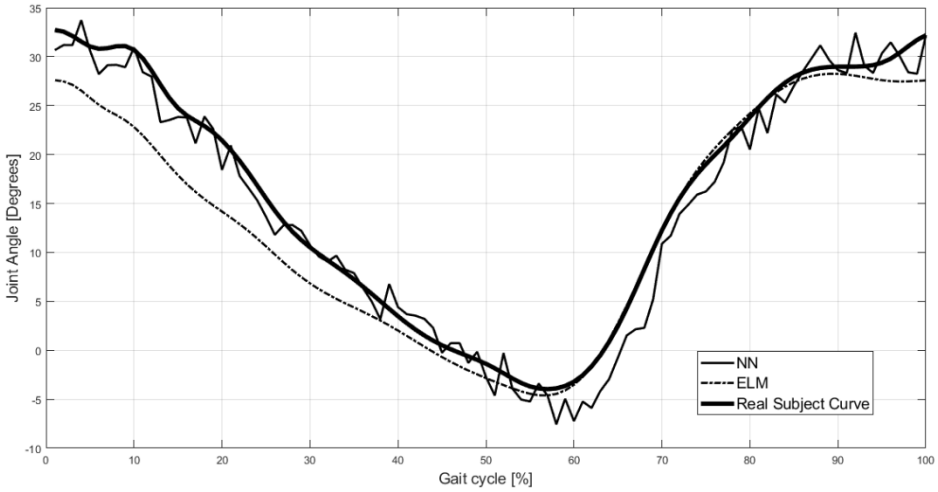

Figure 40. Young Dominant Hip Test Subject 1 Results.

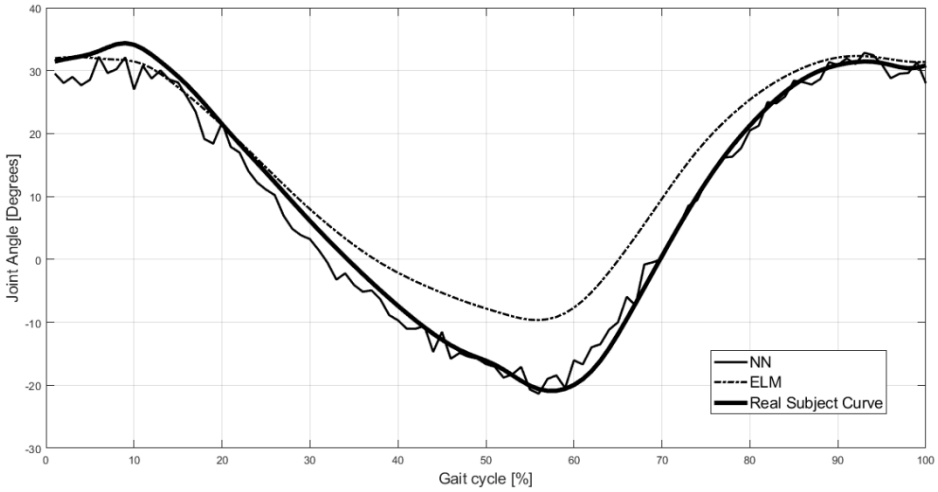

Figure 41. Young Dominant Hip Test Subject 2 Results.

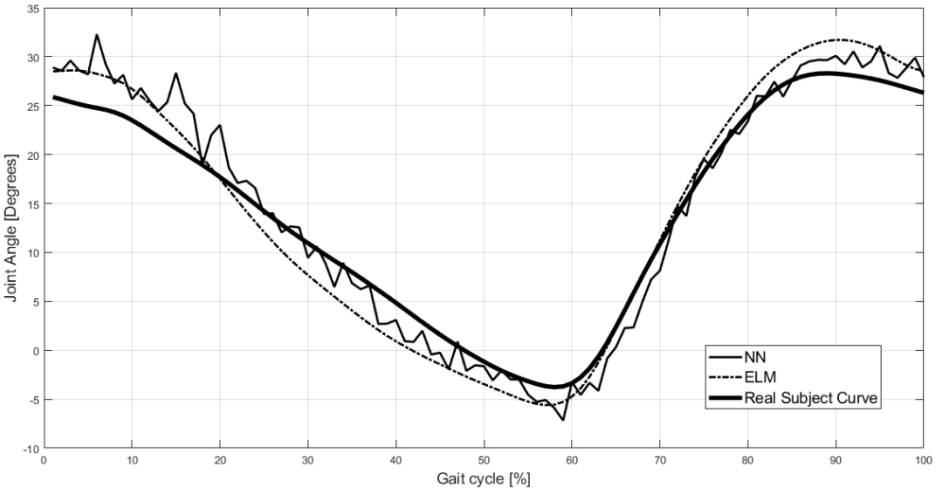

Figure 42. Young Dominant Hip Test Subject 3 Results.

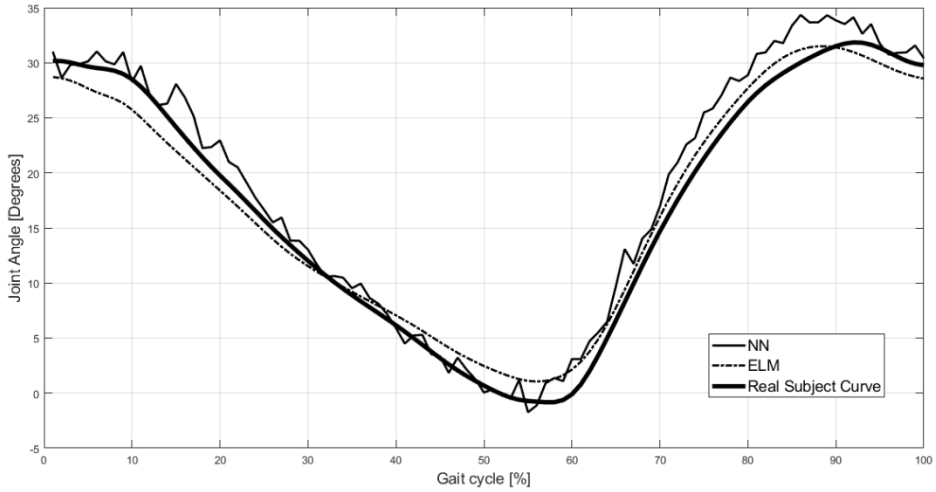

Figure 43. Young Dominant Hip Test Subject 4 Results.

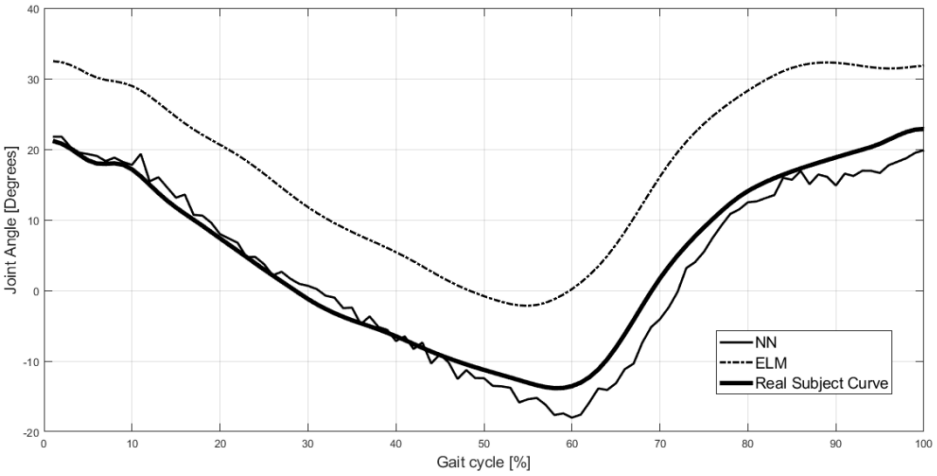

Figure 44. Young Dominant Hip Test Subject 5 Results.

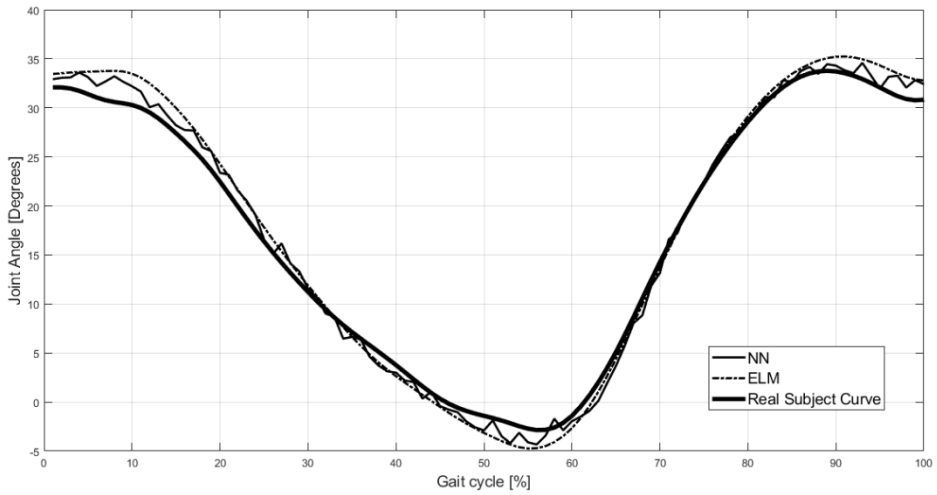

Figure 45. Young Dominant Hip Test Subject 6 Results.

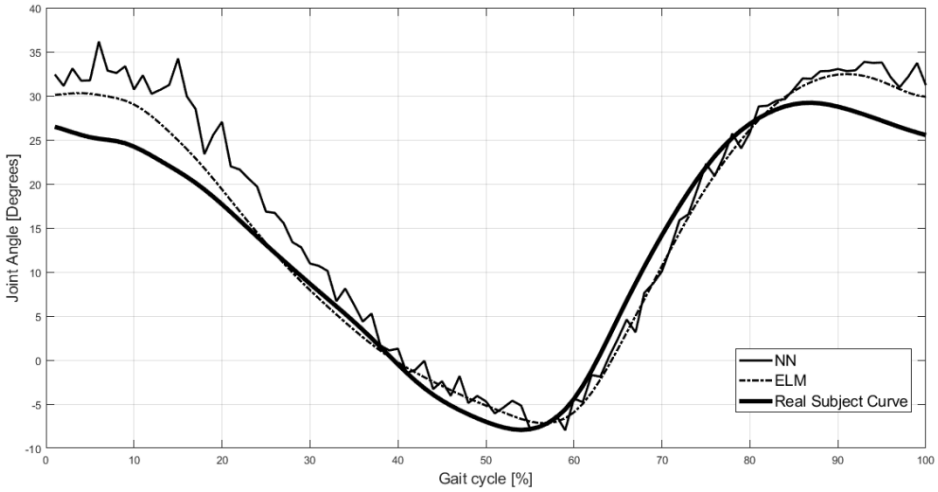

Figure 46. Young Dominant Hip Test Subject 7 Results.

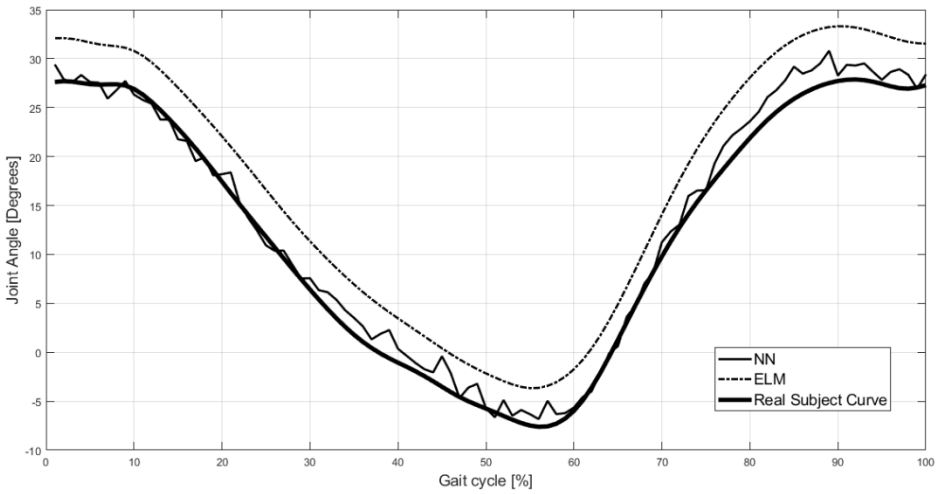

Figure 47. Young Dominant Hip Test Subject 8 Results.

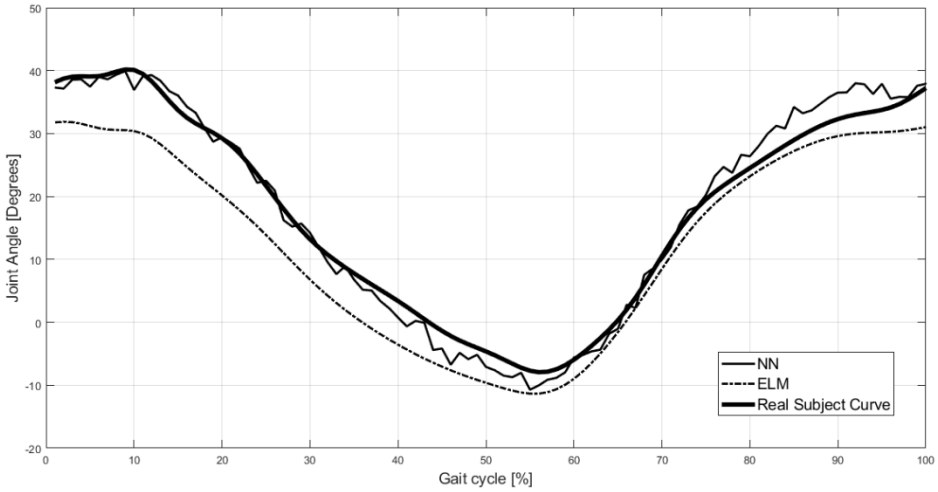

Figure 48. Young Dominant Hip Test Subject 9 Results.

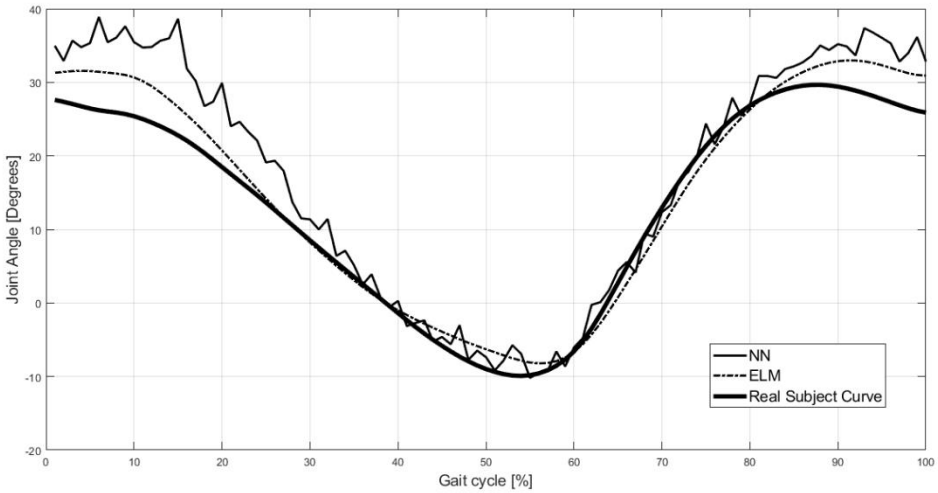

Figure 49. Young Dominant Hip Test Subject 10 Results.

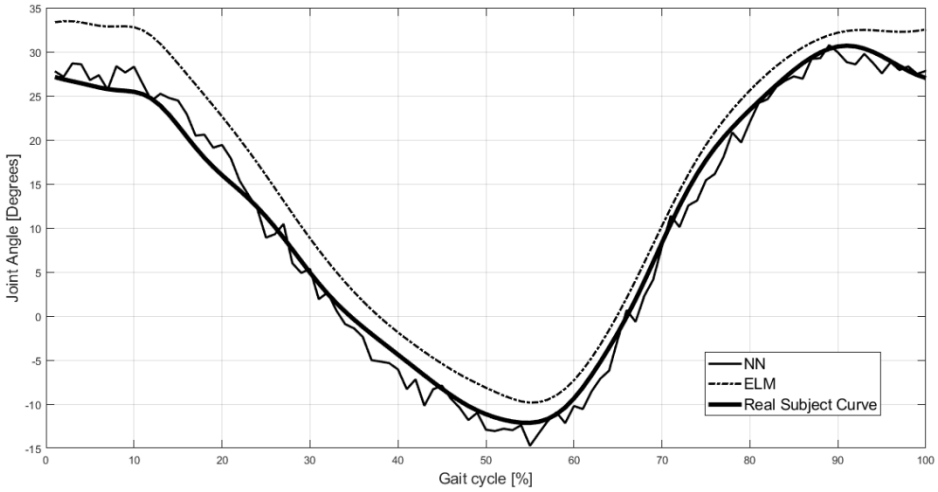

Figure 50. Young Dominant Hip Test Subject 11 Results.

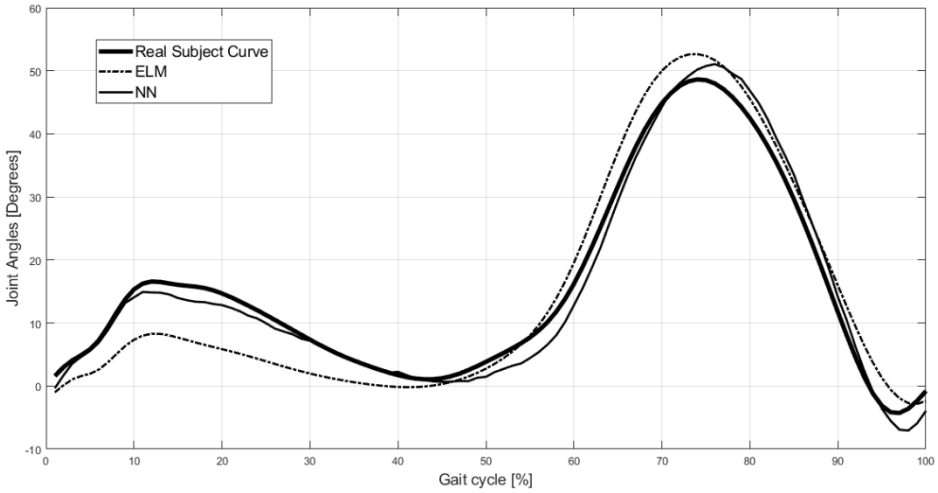

Figure 51. Young Non-Dominant Knee Test Subject 1 Results.

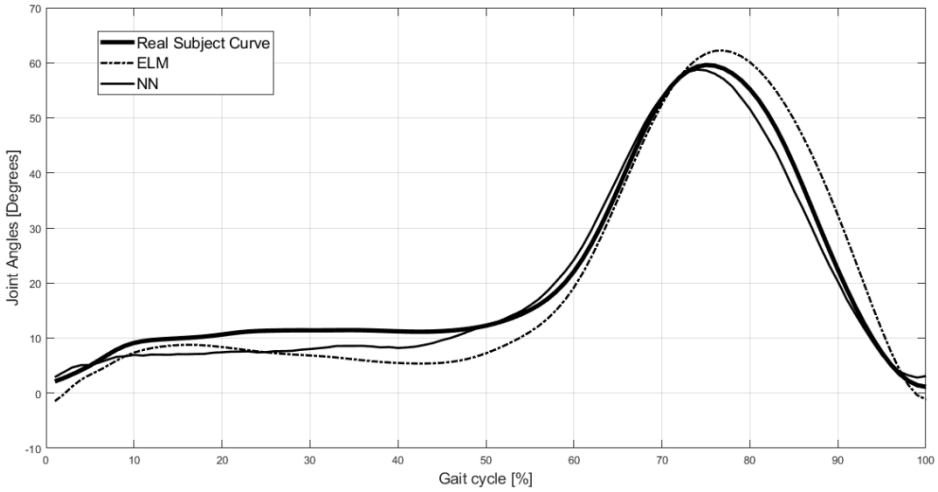

Figure 52. Young Non-Dominant Knee Test Subject 2 Results.

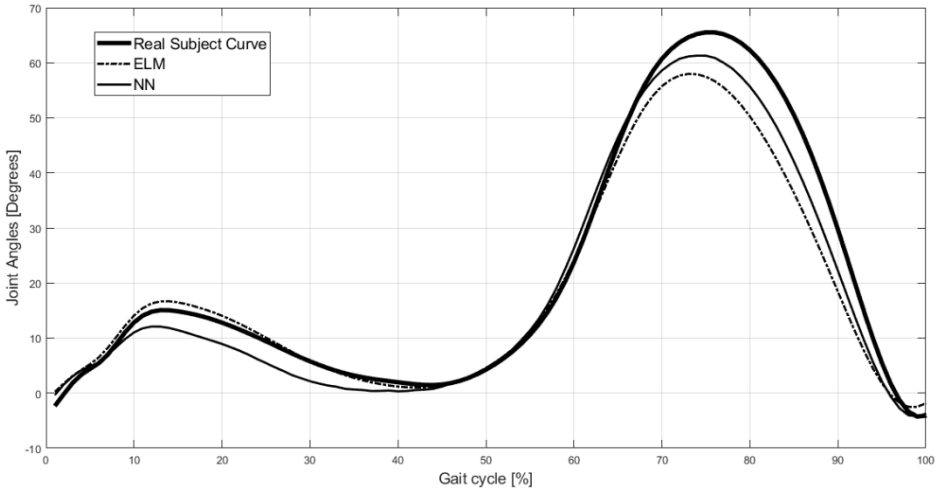

Figure 53. Young Non-Dominant Knee Test Subject 3 Results.

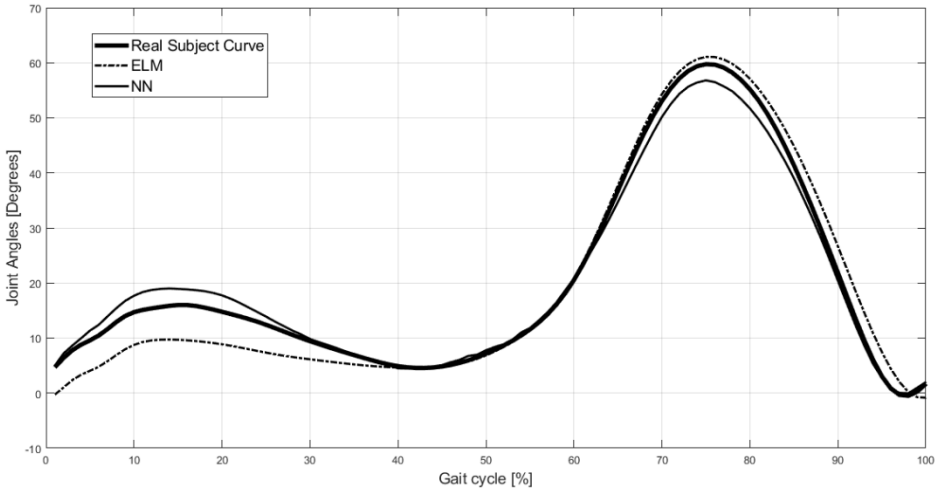

Figure 54. Young Non-Dominant Knee Test Subject 4 Results.

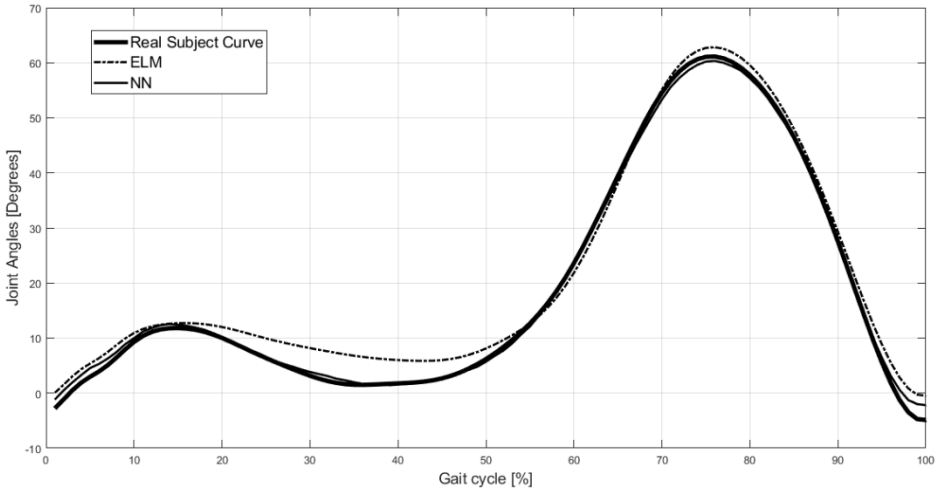

Figure 55. Young Non-Dominant Knee Test Subject 5 Results.

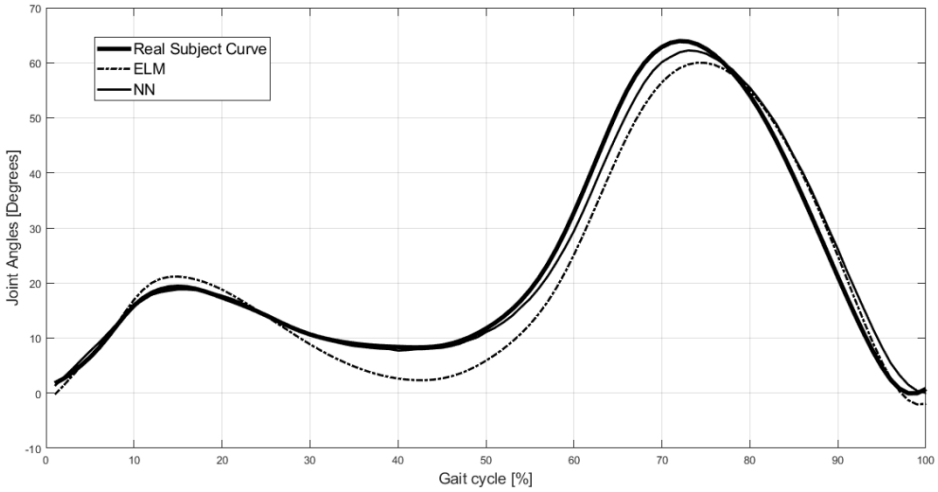

Figure 56. Young Non-Dominant Knee Test Subject 6 Results.

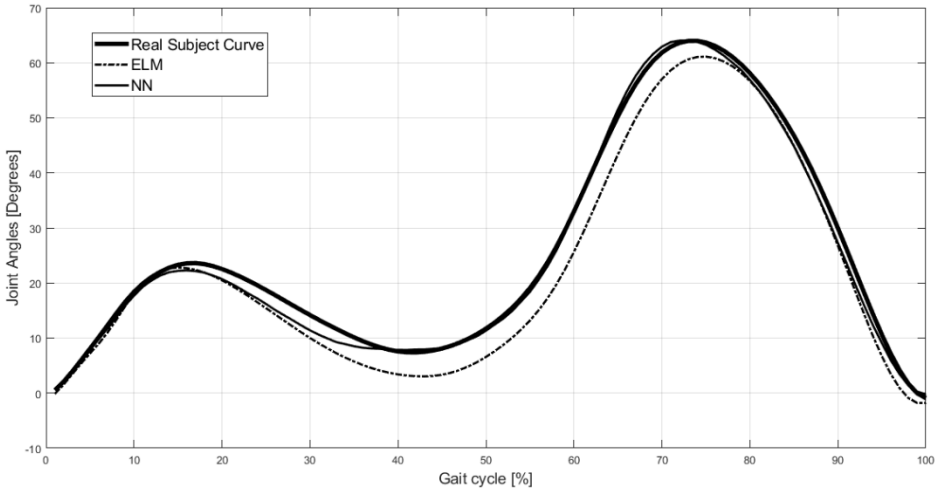

Figure 57. Young Non-Dominant Knee Test Subject 7 Results.

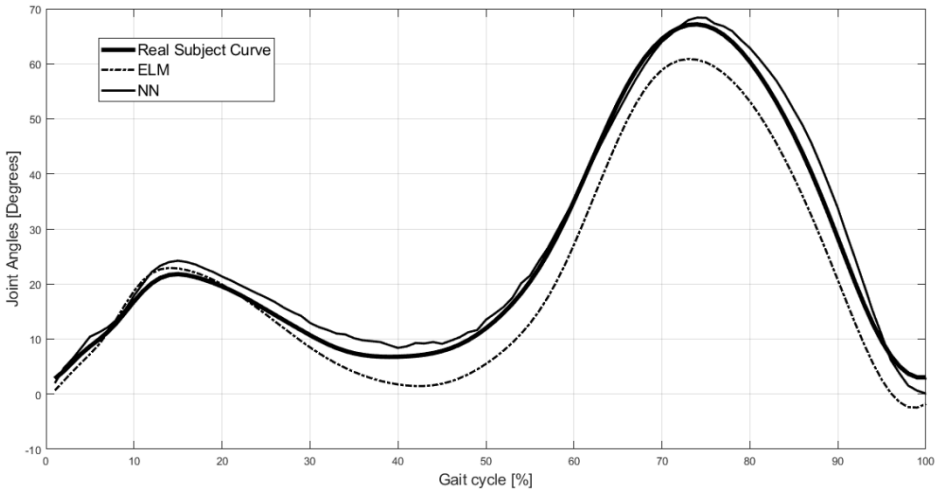

Figure 58. Young Non-Dominant Knee Test Subject 8 Results.

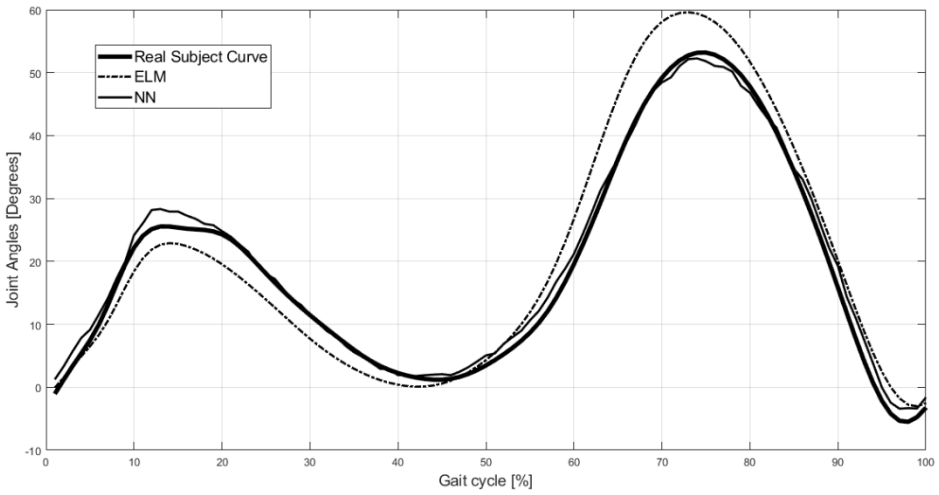

Figure 59. Young Non-Dominant Knee Test Subject 9 Results.

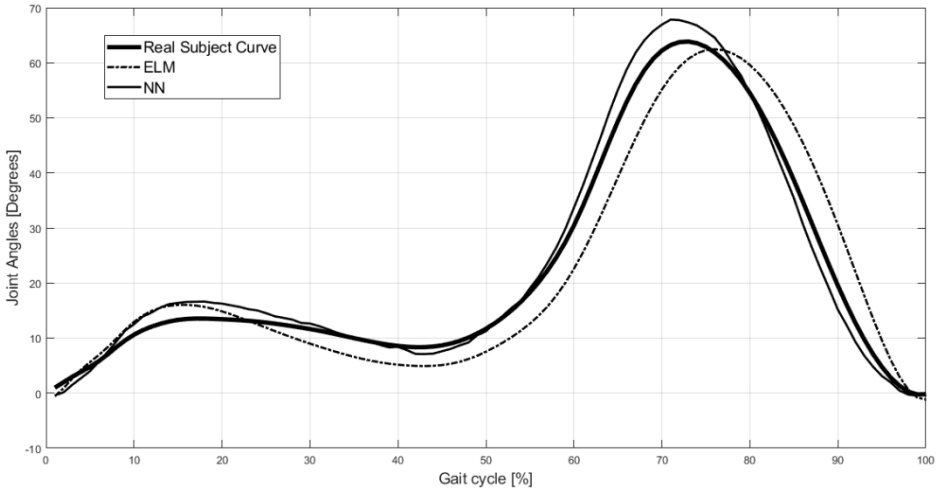

Figure 60. Young Non-Dominant Knee Test Subject 10 Results.

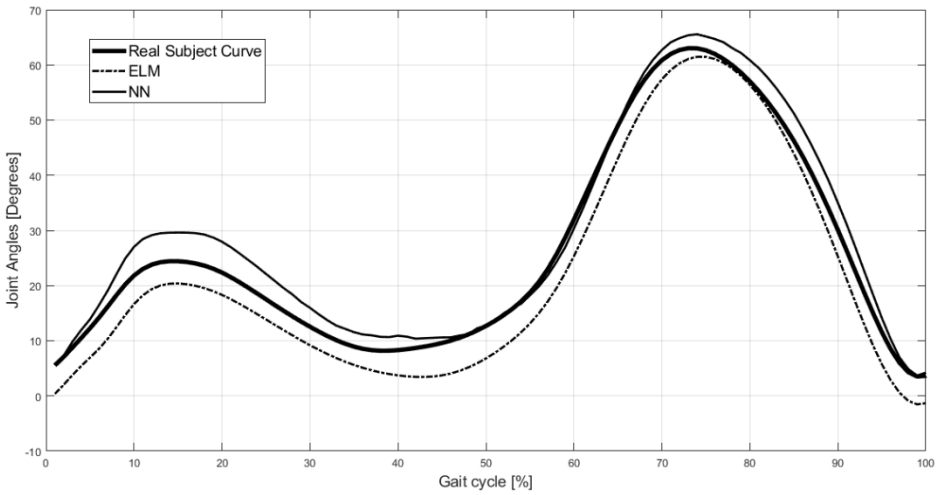

Figure 61. Young Non-Dominant Knee Test Subject 11 Results.

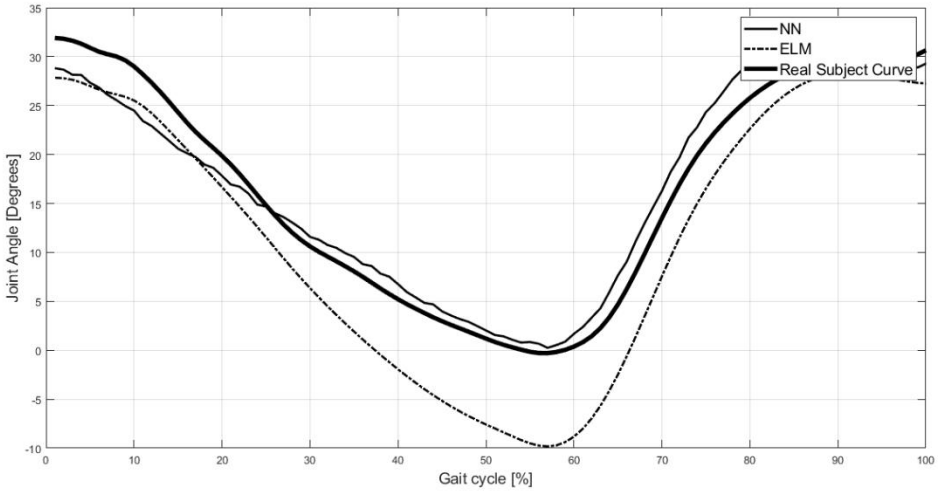

Figure 62. Young Non-Dominant Hip Test Subject 1 Results.

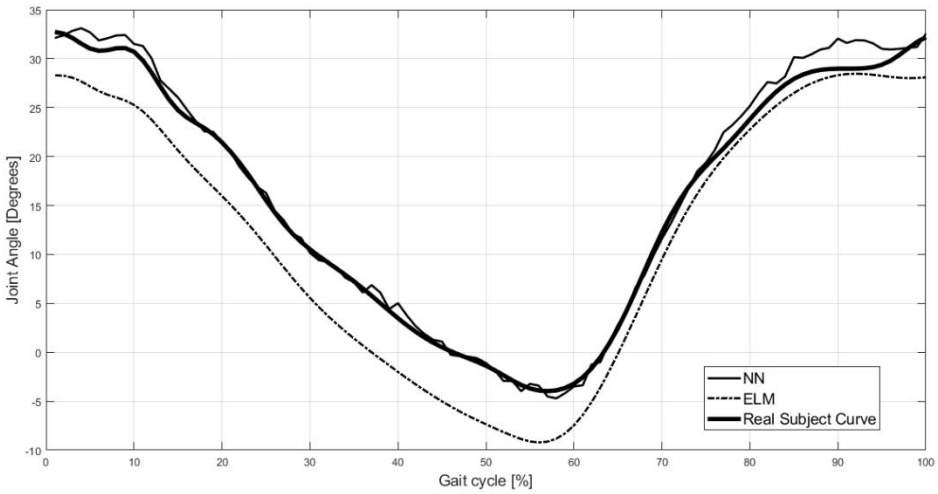

Figure 63. Young Non-Dominant Hip Test Subject 2 Results.

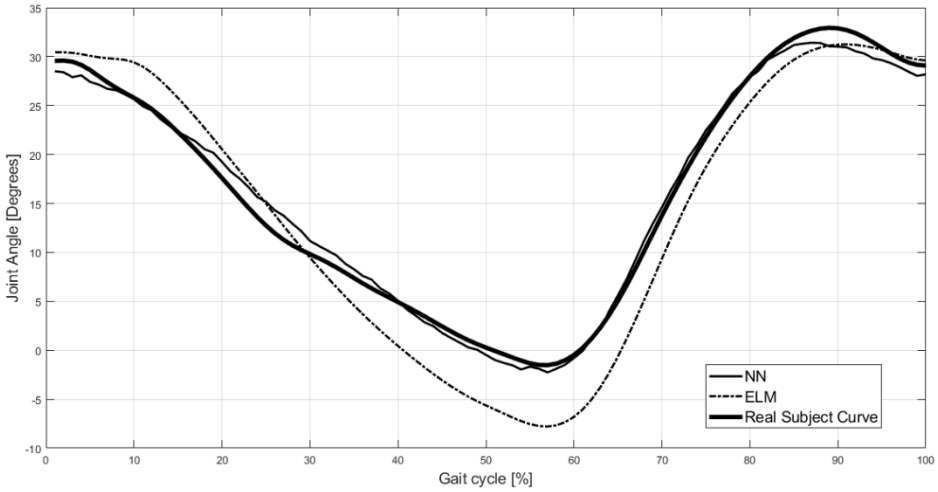

Figure 64. Young Non-Dominant Hip Test Subject 3 Results.

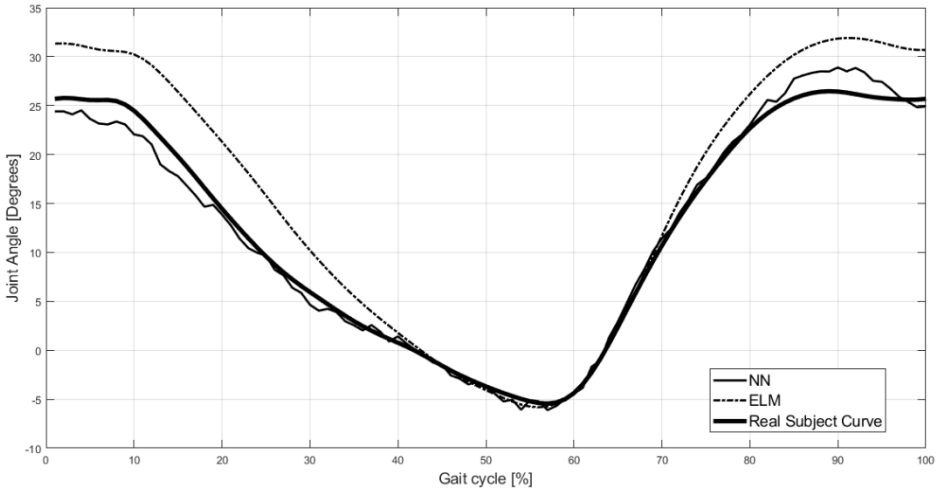

Figure 65. Young Non-Dominant Hip Test Subject 4 Results.

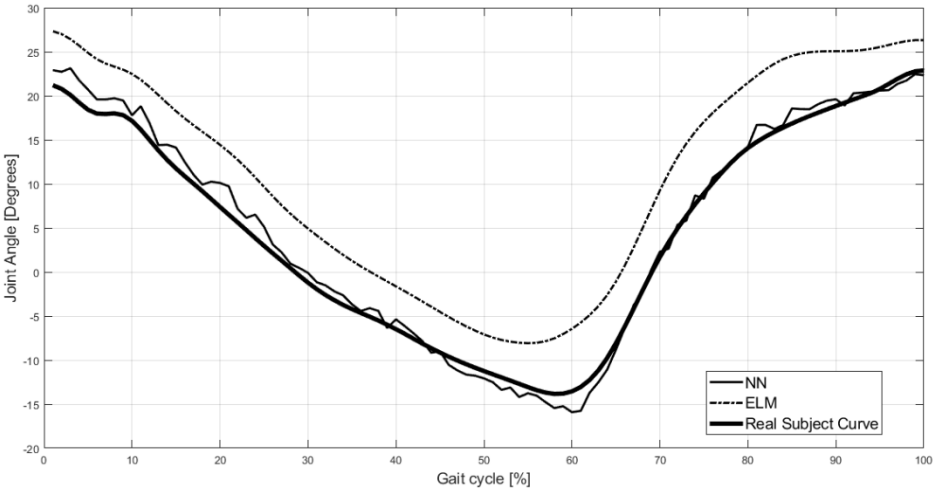

Figure 66. Young Non-Dominant Hip Test Subject 5 Results.

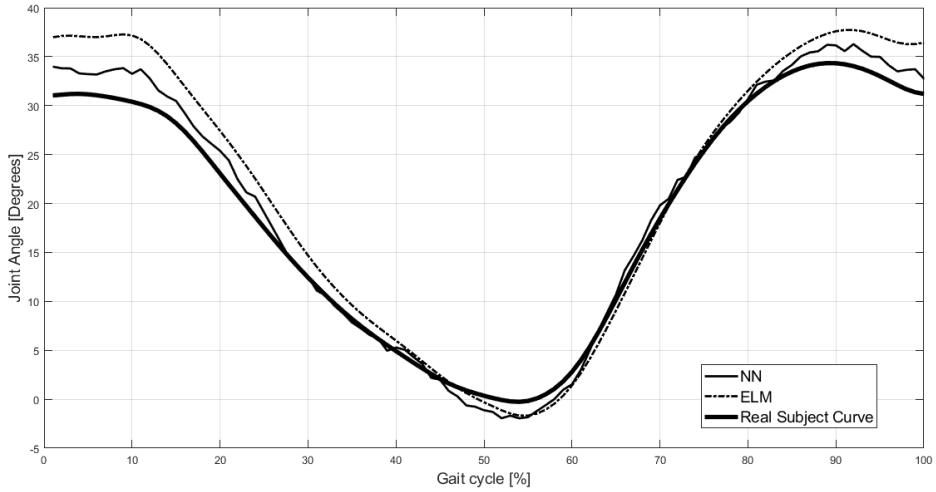

Figure 67. Young Non-Dominant Hip Test Subject 6 Results.

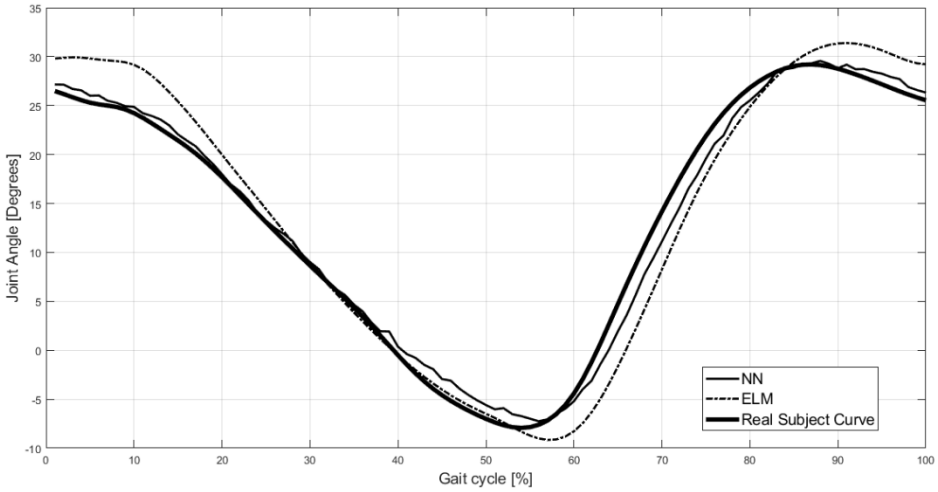

Figure 68. Young Non-Dominant Hip Test Subject 7 Results.

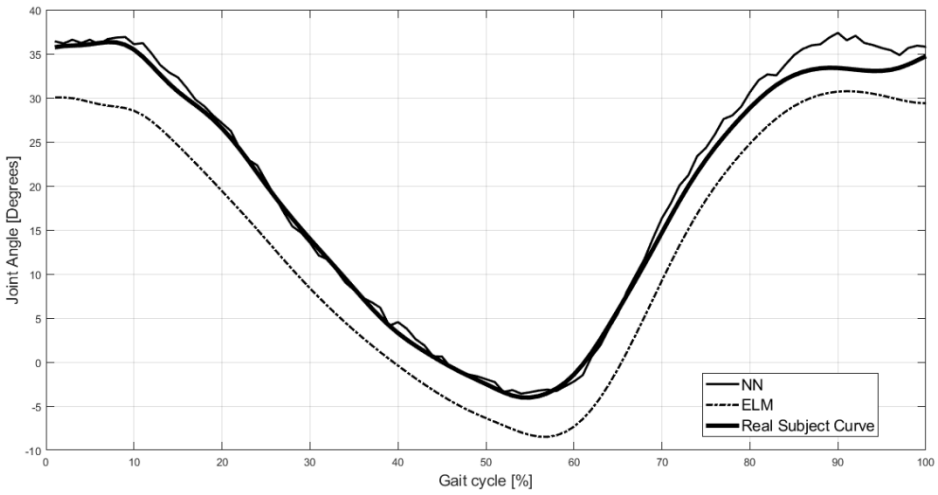

Figure 69. Young Non-Dominant Hip Test Subject 8 Results.

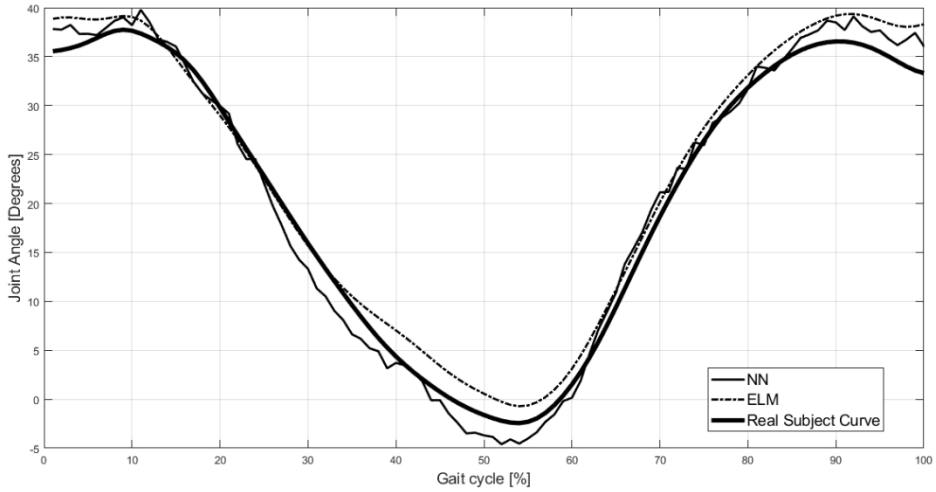

Figure 70. Young Non-Dominant Hip Test Subject 9 Results.

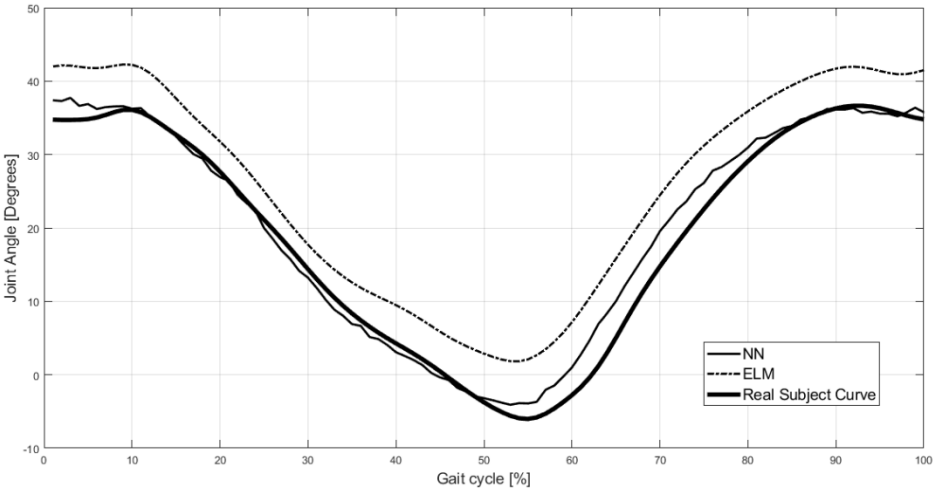

Figure 71. Young Non-Dominant Hip Test Subject 10 Results.

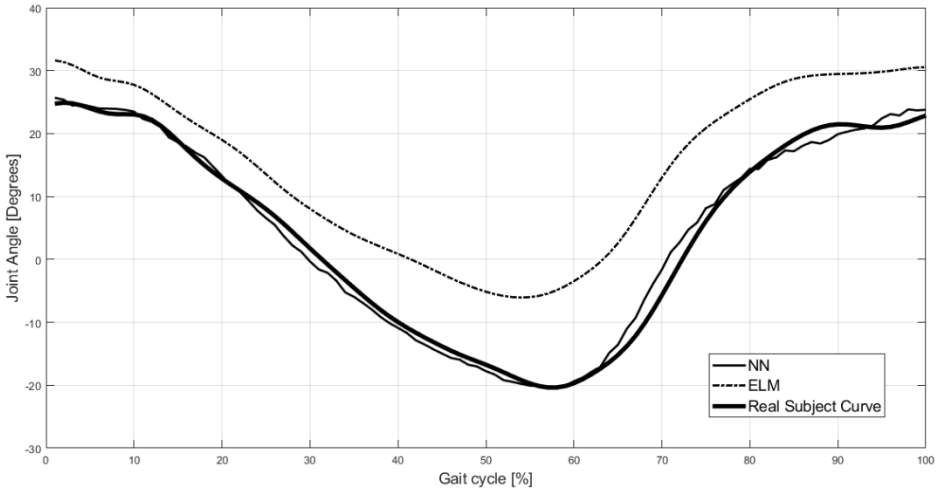

Figure 72. Young Non-Dominant Hip Test Subject 11 Results.

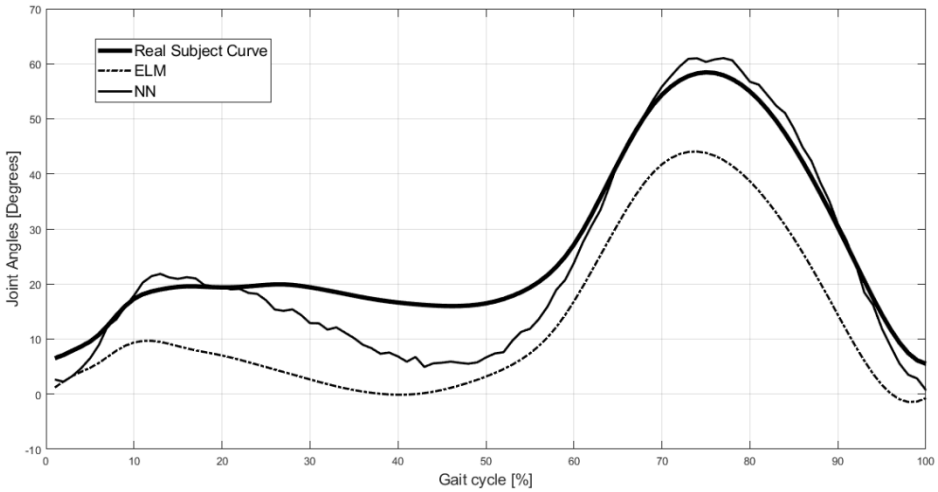

Figure 73. Old Dominant Knee Test Subject 1 Results.

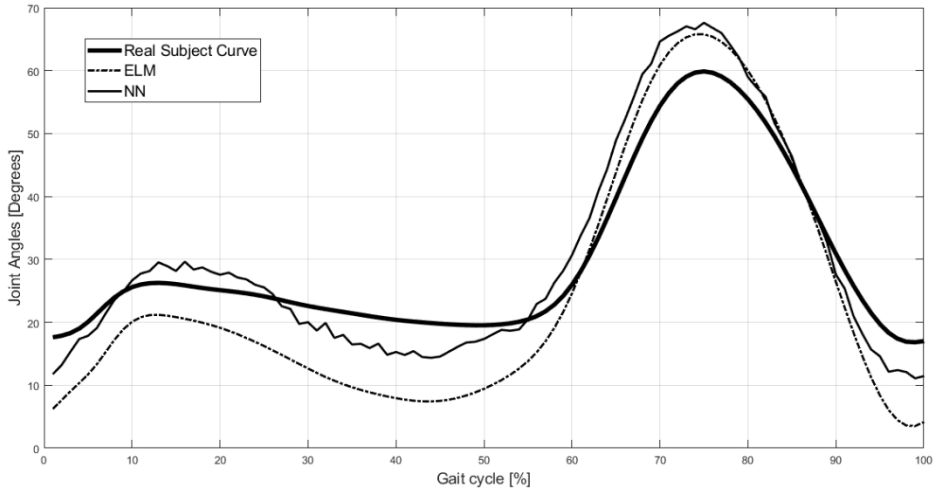

Figure 74. Old Dominant Knee Test Subject 2 Results.

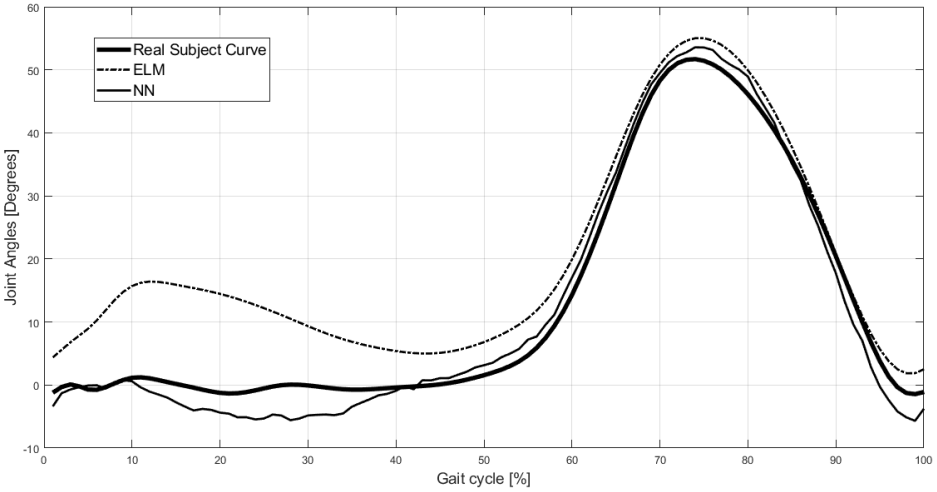

Figure 75. Old Dominant Knee Test Subject 3 Results.

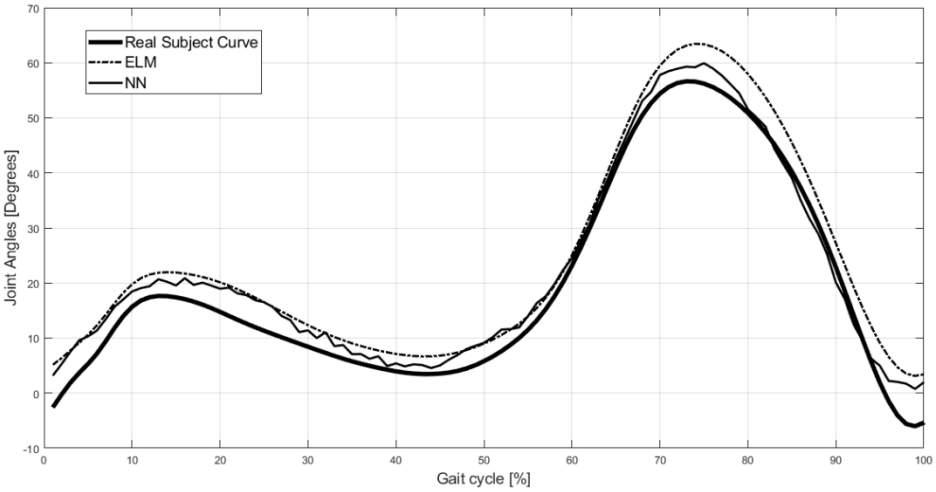

Figure 76. Old Dominant Knee Test Subject 4 Results.

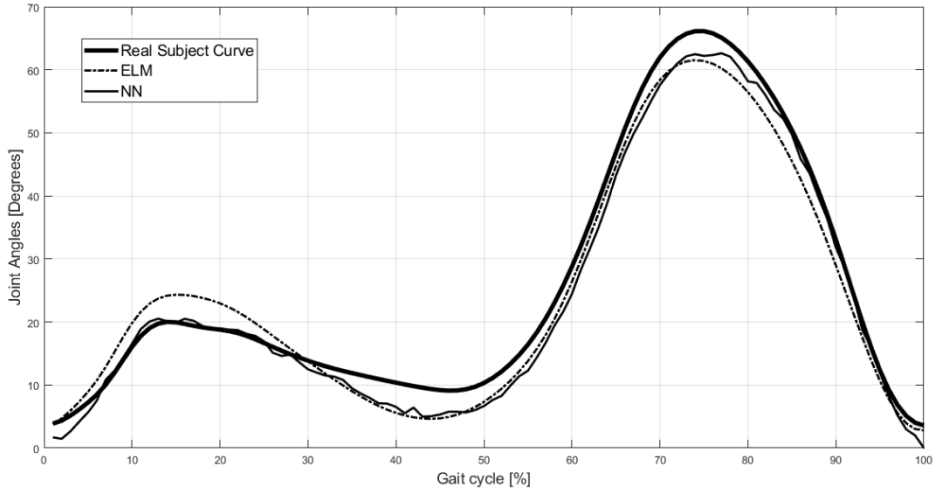

Figure 77. Old Dominant Knee Test Subject 5 Results.

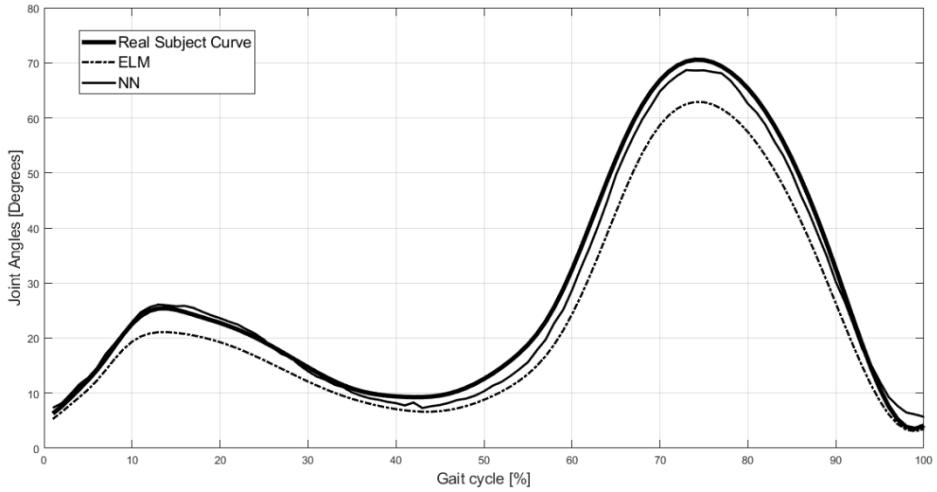

Figure 78. Old Dominant Knee Test Subject 6 Results.

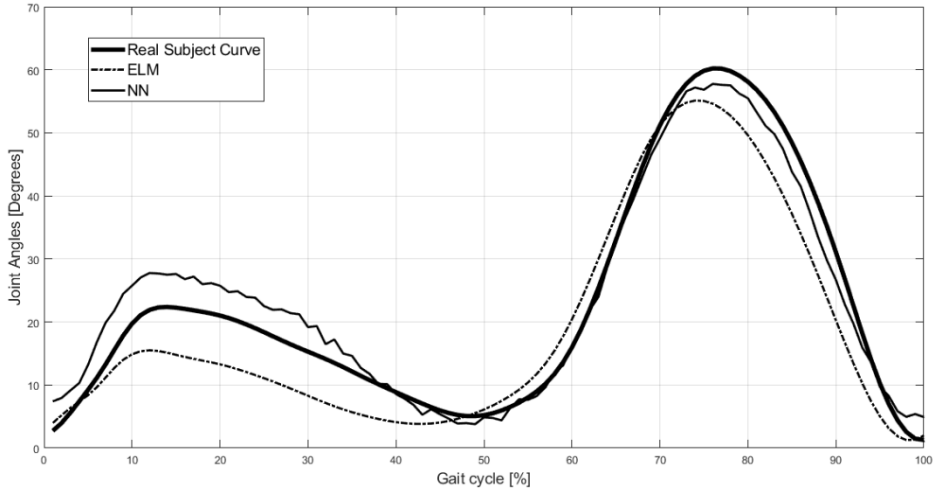

Figure 79. Old Dominant Knee Test Subject 7 Results.

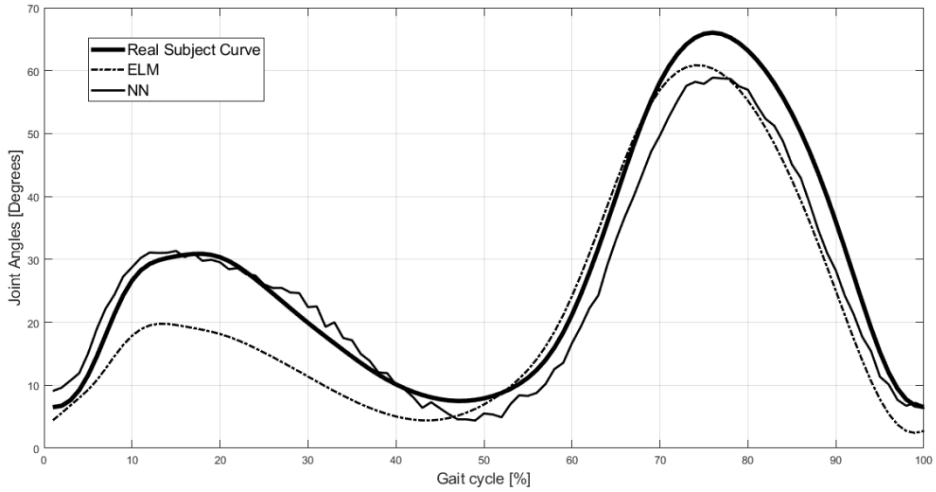

Figure 80. Old Dominant Knee Test Subject 8 Results.

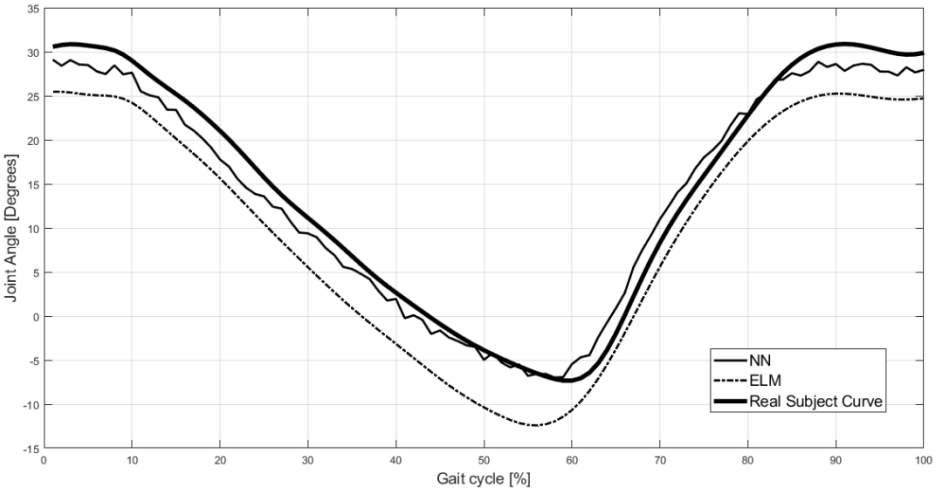

Figure 81. Old Dominant Hip Test Subject 1 Results.

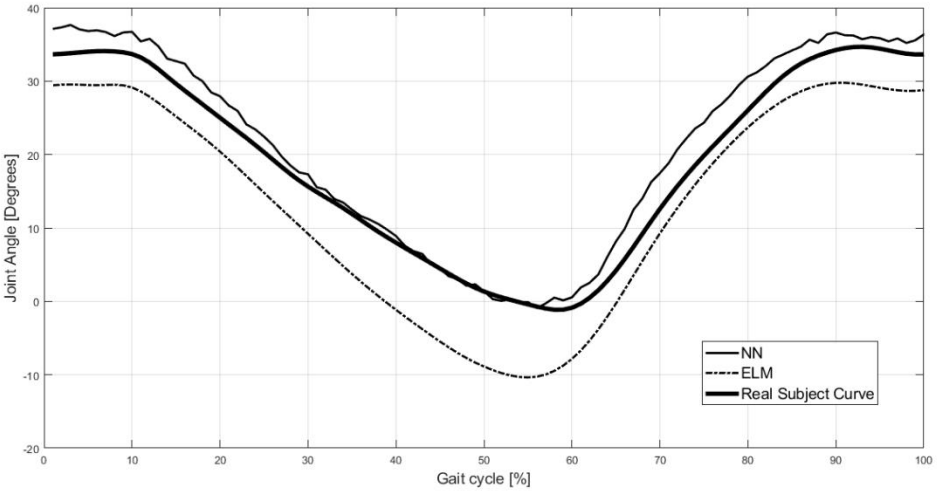

Figure 82. Old Dominant Hip Test Subject 2 Results.

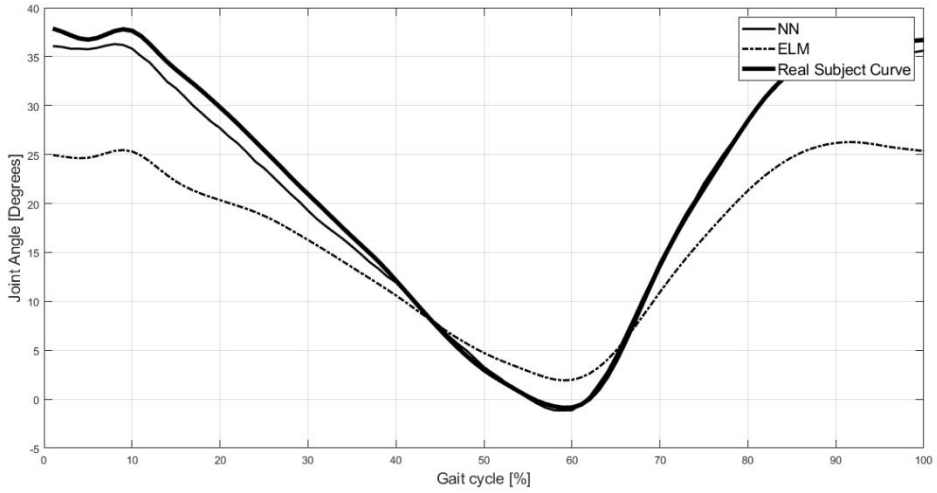

Figure 83. Old Dominant Hip Test Subject 3 Results.

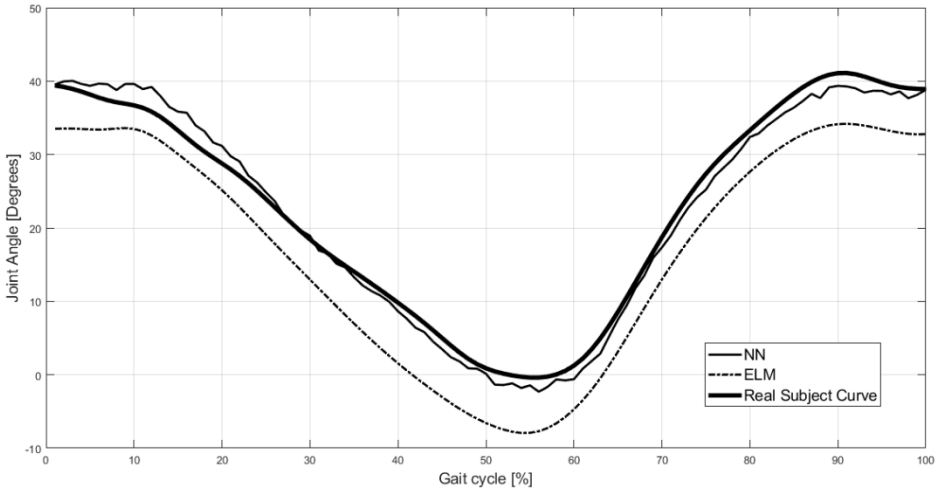

Figure 84. Old Dominant Hip Test Subject 4 Results.

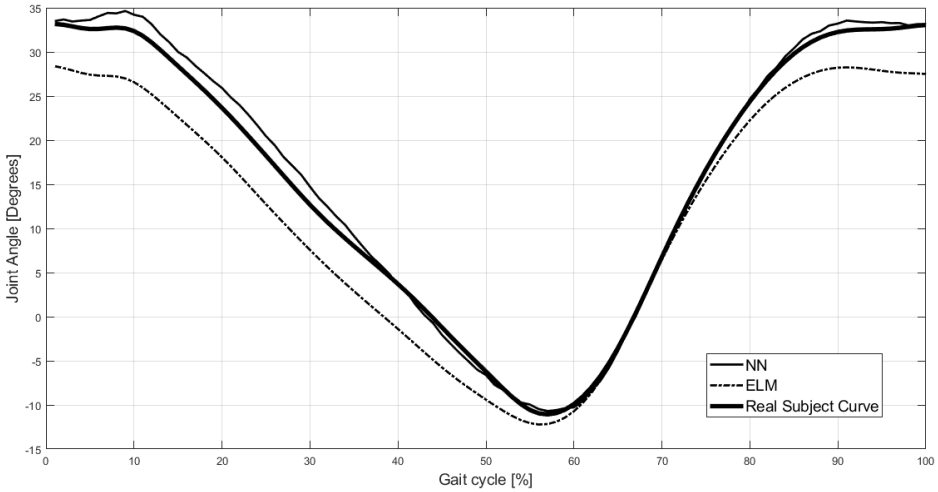

Figure 85. Old Dominant Hip Test Subject 5 Results.

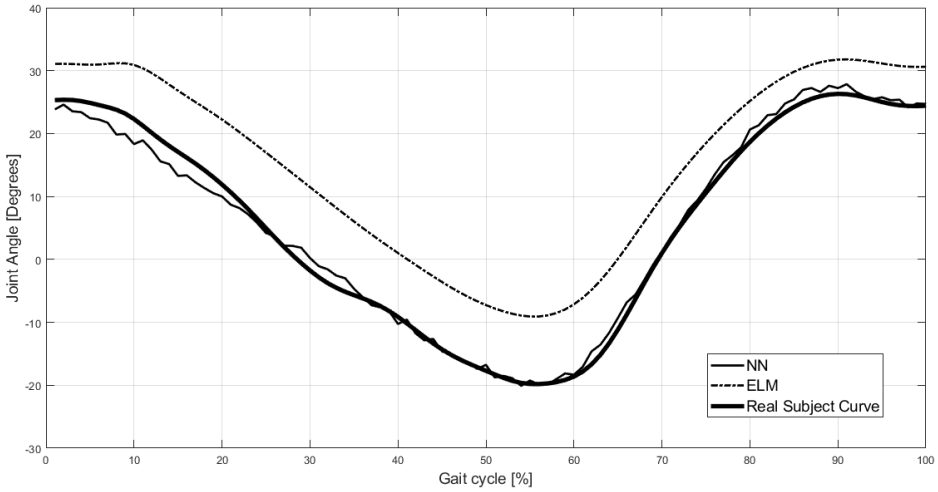

Figure 86. Old Dominant Hip Test Subject 6 Results.

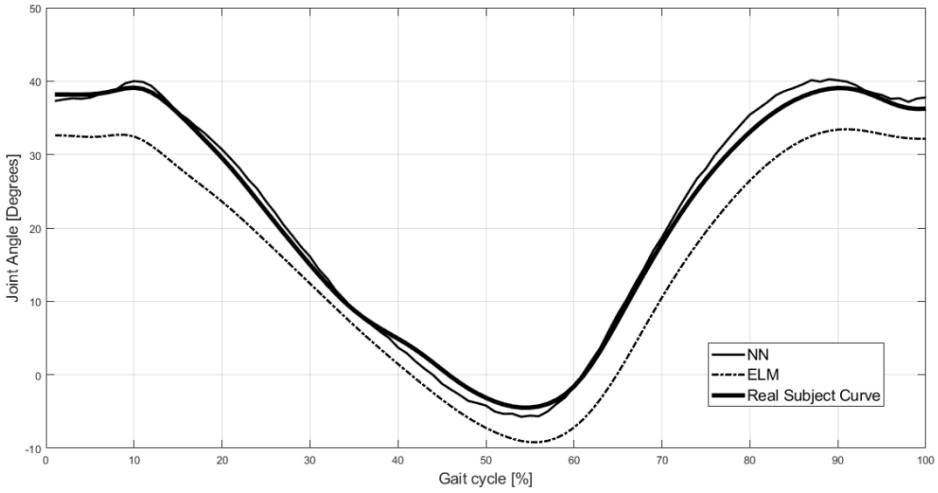

Figure 87. Old Dominant Hip Test Subject 7 Results.

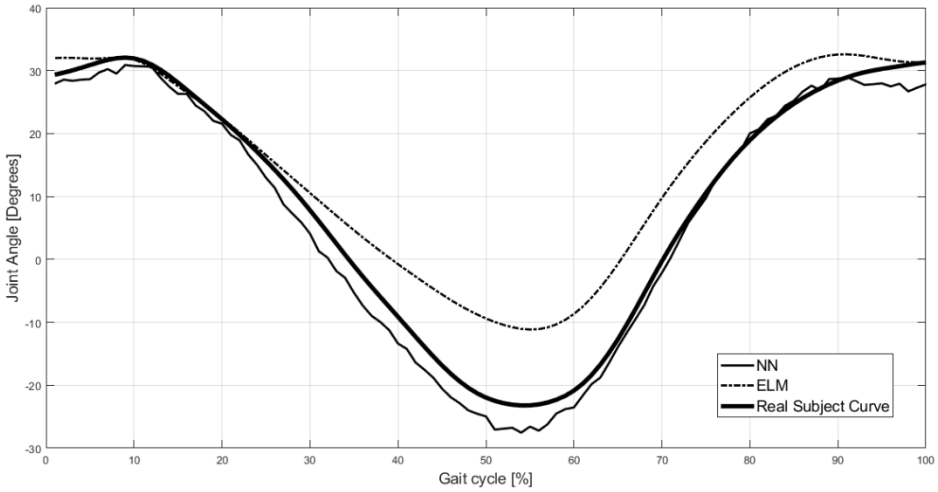

Figure 88. Old Dominant Hip Test Subject 8 Results.

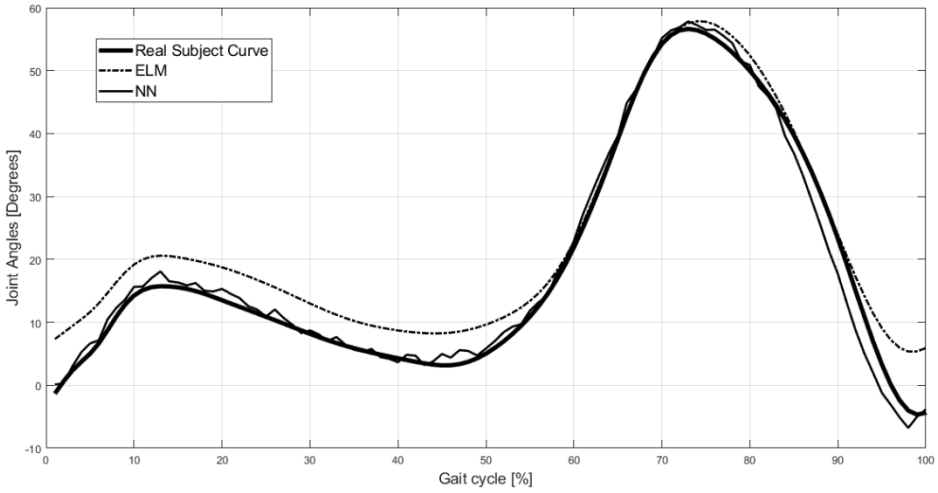

Figure 89. Old Non-Dominant Knee Test Subject 1 Results.

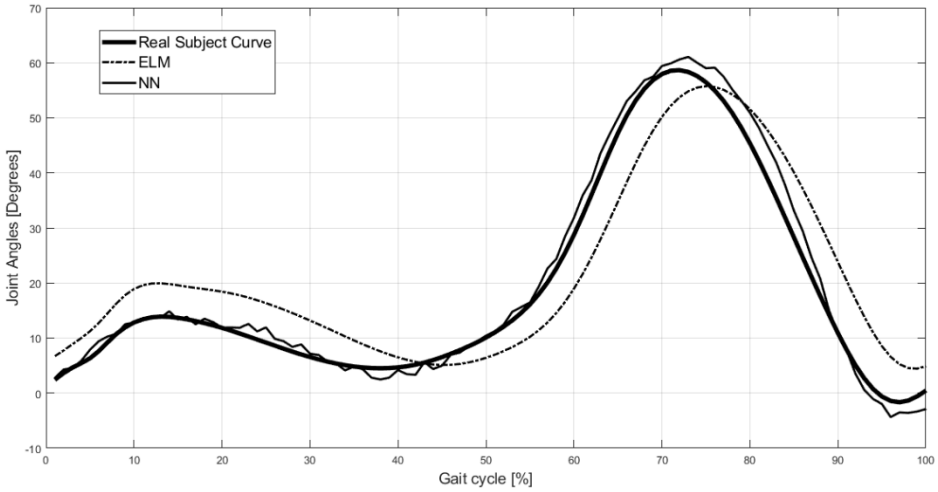

Figure 90. Old Non-Dominant Knee Test Subject 2 Results.

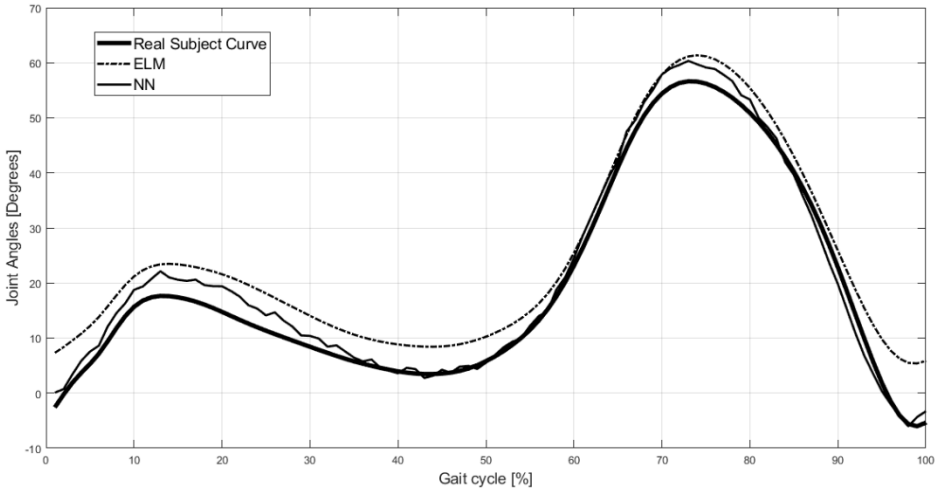

Figure 91. Old Non-Dominant Knee Test Subject 3 Results.

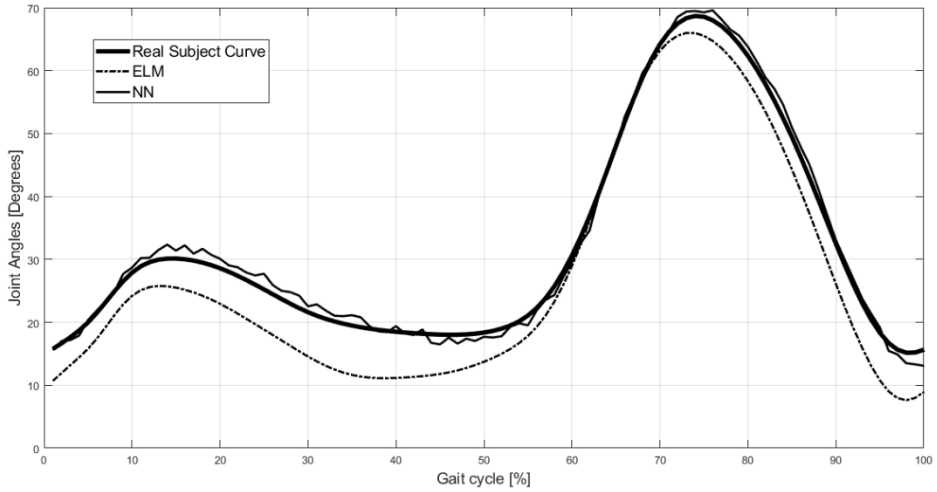

Figure 92. Old Non-Dominant Knee Test Subject 4 Results.

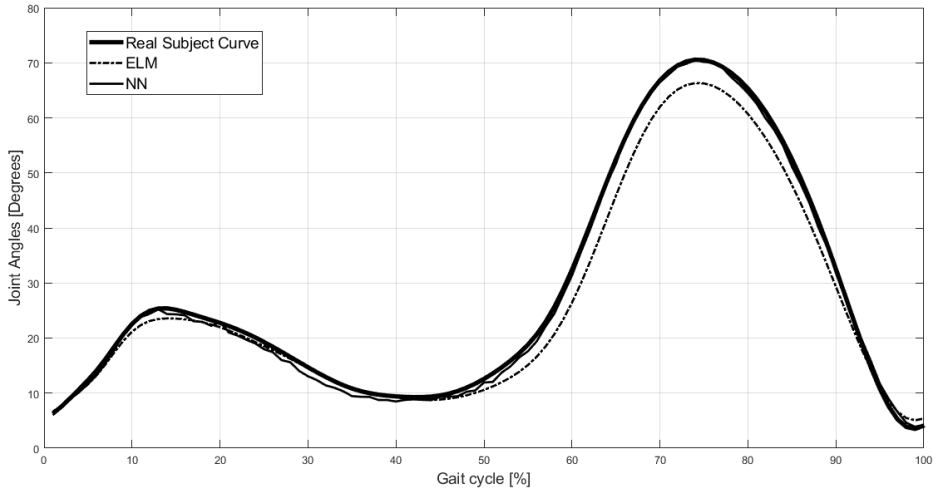

Figure 93. Old Non-Dominant Knee Test Subject 5 Results.

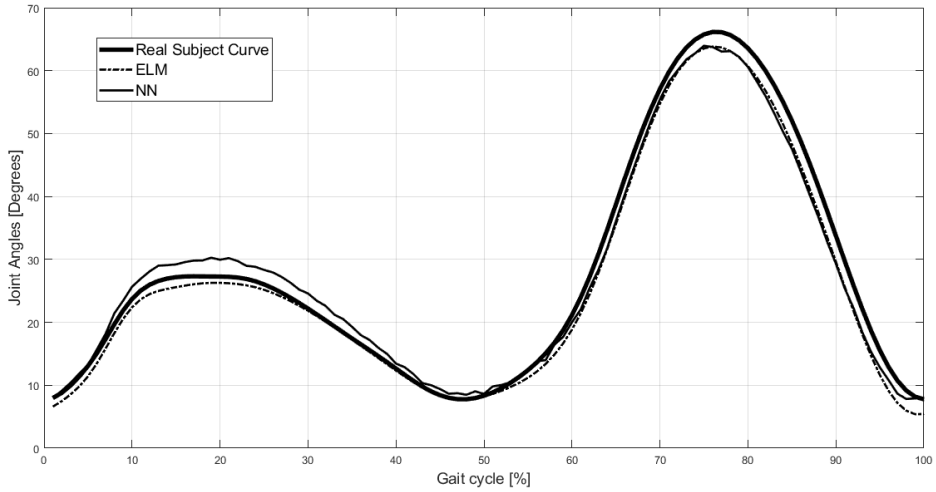

Figure 94. Old Non-Dominant Knee Test Subject 6 Results.

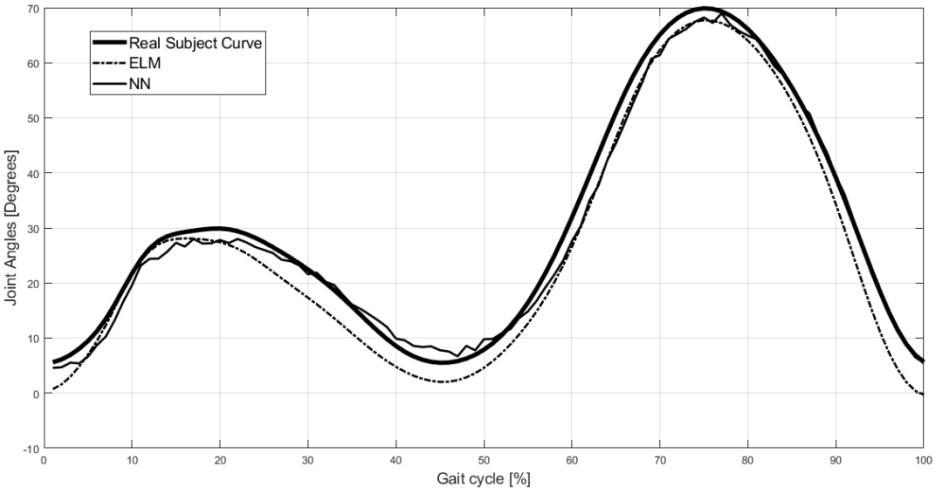

Figure 95. Old Non-Dominant Knee Test Subject 7 Results.

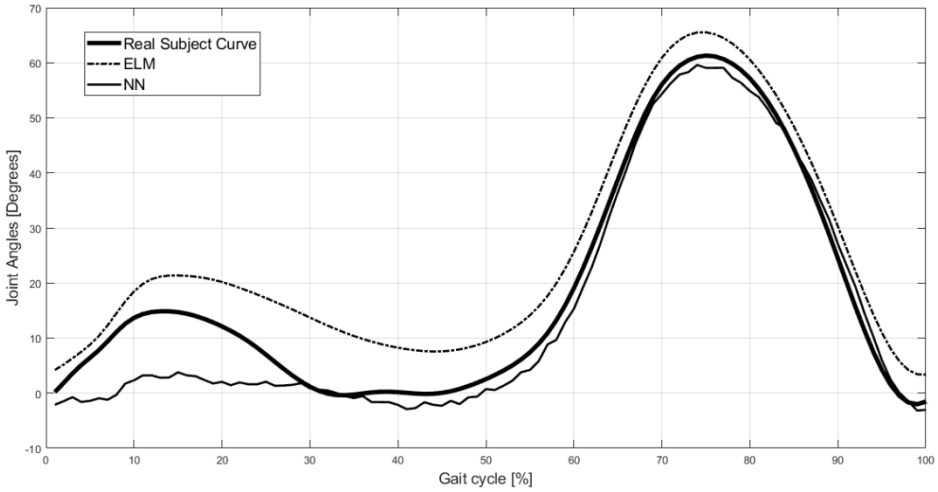

Figure 96. Old Non-Dominant Knee Test Subject 8 Results.

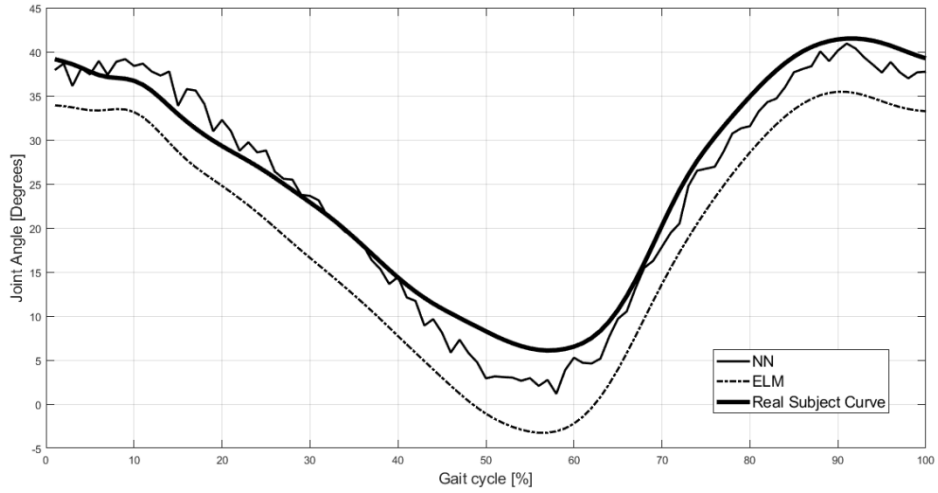

Figure 97. Old Non-Dominant Hip Test Subject 1 Results.

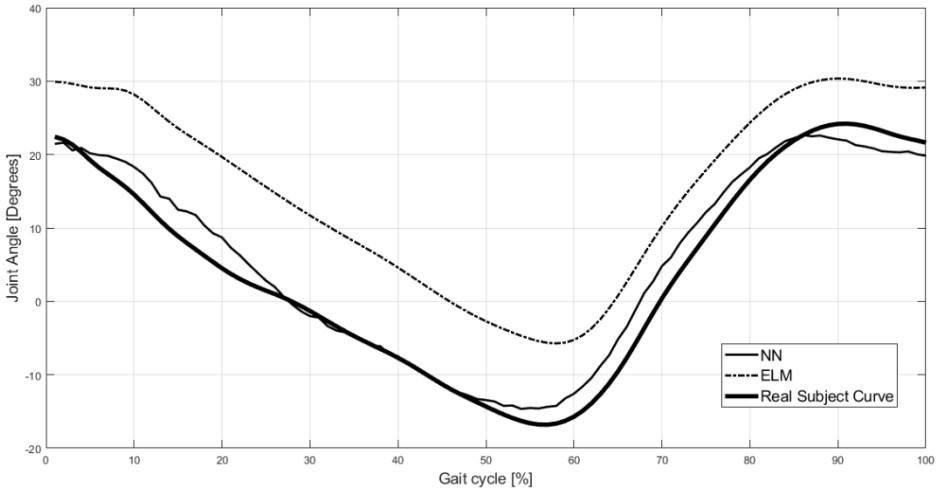

Figure 98. Old Non-Dominant Hip Test Subject 2 Results.

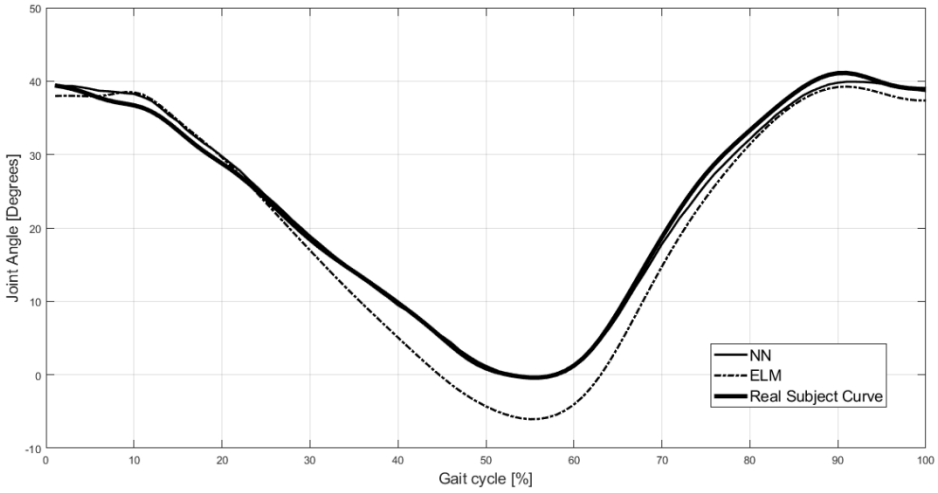

Figure 99. Old Non-Dominant Hip Test Subject 3 Results.

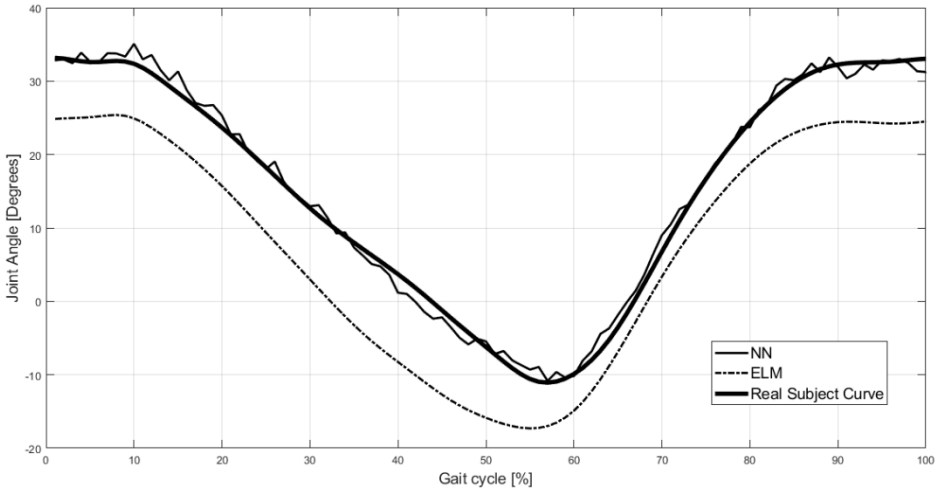

Figure 100. Old Non-Dominant Hip Test Subject 4 Results.

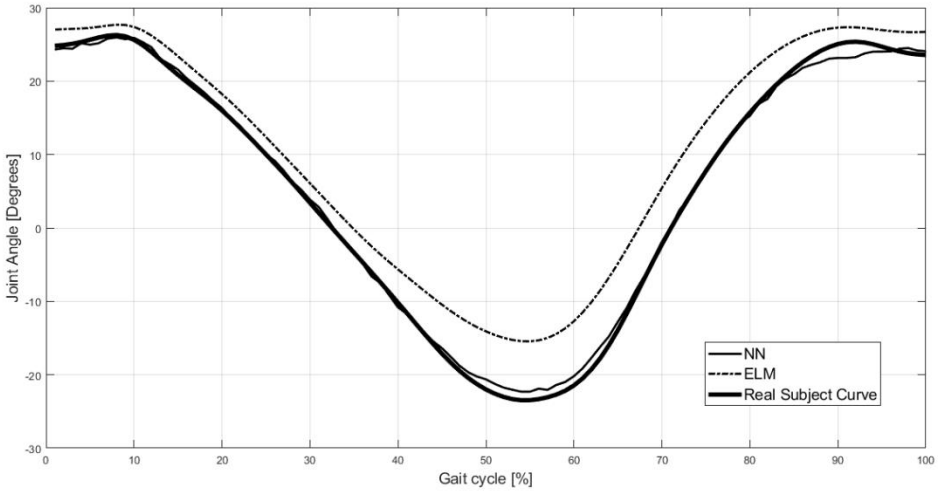

Figure 101. Old Non-Dominant Hip Test Subject 5 Results.

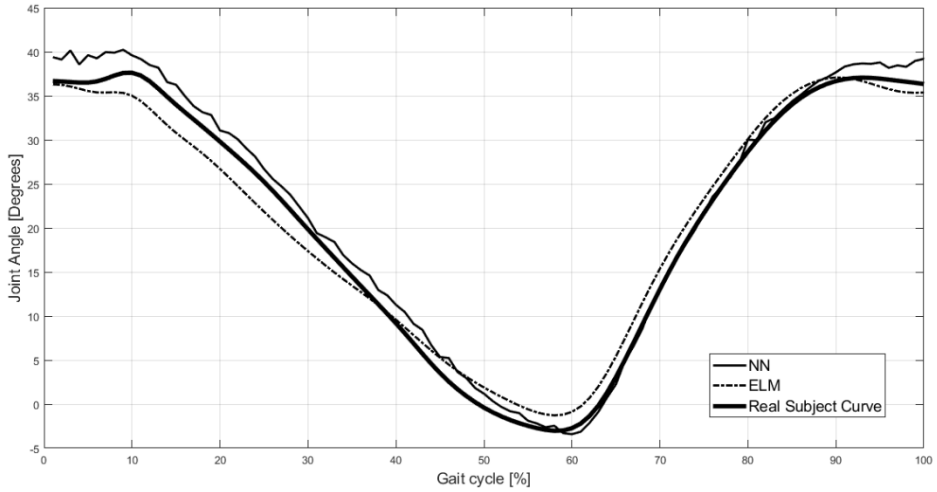

Figure 102. Old Non-Dominant Hip Test Subject 6 Results.

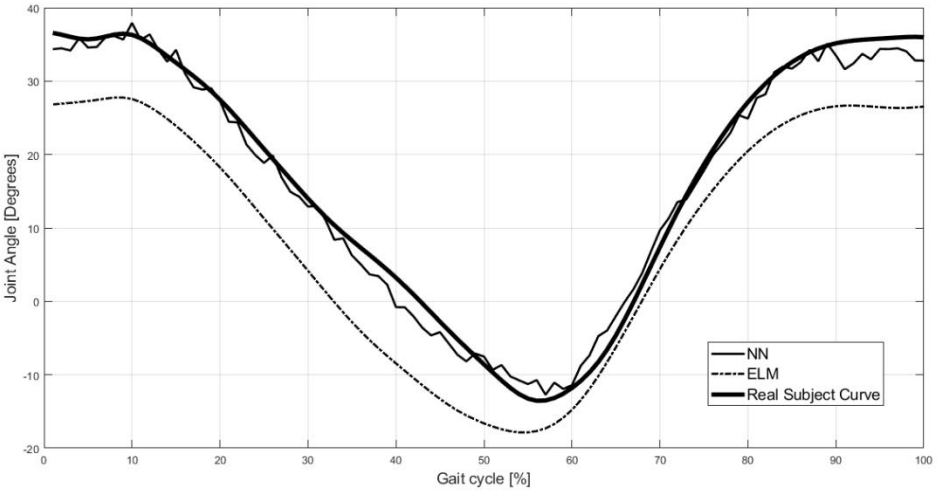

Figure 103. Old Non-Dominant Hip Test Subject 7 Results.

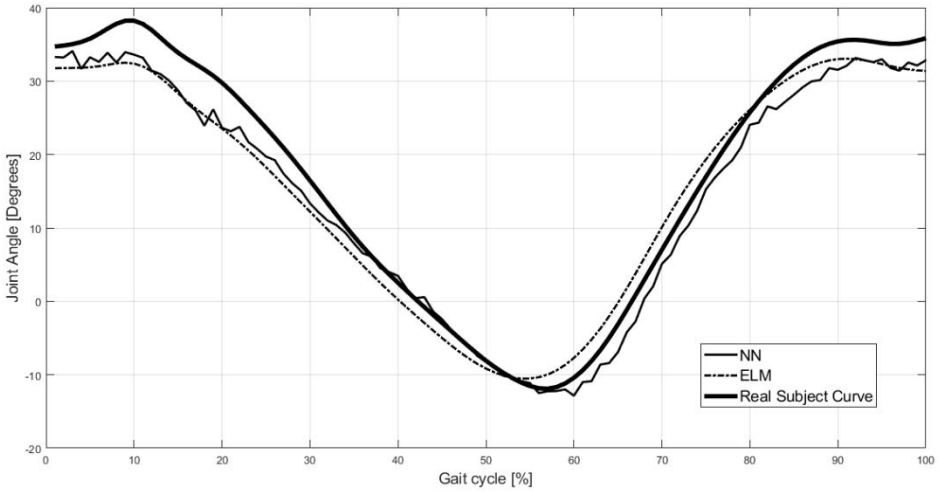

Figure 104. Old Non-Dominant Hip Test Subject 8 Results.

Annex C

Table 17. Treadmill BNN's and ELM best accuracies, young and old men dominant limb.

Limb	Method	Age Group	Train Accuracy MSE	Test Accuracy MSE	Validation Accuracy MSE
Knee	BNN	Young	**0.0002**	**0.0017**	0.0009
		Old	**0.0008**	**0.0024**	0.0009
	ELM	Young	0.0095	0.0104	-
		Old	0.0037	0.0090	-
Hip	BNN	Young	**0.0002**	**0.0044**	0.0017
		Old	**0.0006**	**0.0018**	0.0021
	ELM	Young	0.0405	0.0244	-
		Old	0.0362	0.0649	-

Table 18. Treadmill BNN's and ELM accuracies, young and old men non-dominant limb.

Limb	Method	Age Group	Train Accuracy MSE	Test Accuracy MSE	Validation Accuracy MSE
Knee	BNN	Young	**0.0008**	**0.0024**	0.0009
		Old	**0.0001**	**0.0012**	0.0019
	ELM	Young	0.0037	0.0090	-
		Old	0.0040	0.0085	-
Hip	BNN	Young	**0.0004**	**0.0041**	0.0016
		Old	**0.0003**	**0.0018**	0.0045
	ELM	Young	0.0293	0.0503	-
		Old	0.0194	0.0554	-